Ci 123 UDC 624.2/.8:534.1:533.6.07

ACTA POLYTECHNICA SCANDINAVICA

CIVIL ENGINEERING AND BUILDING CONSTRUCTION SERIES No. 123

Frequency-domain approach for calculating wind-induced vibration and aeroelastic stability characteristics of long-span bridges

RISTO KIVILUOMA

Dissertation for the degree of Doctor of Technology to be presented with due permission for public examination and debate in Auditorium R1 at Helsinki University of Technology (Espoo, Finland) on the 21st of September, 2001, at 12 o'clock noon.

ESPOO 2001

Kiviluoma, Risto. Frequency-domain approach for calculating wind-induced vibration and aeroelastic stability characteristics of long-span bridges. Acta Polytechnica Scandinavica, Civil Engineering and Building Construction Series No. 123, Helsinki 2001, 112 p. Published by the Finnish Academy of Technology. ISBN 951-666-577-2, ISSN 0355-2705, UDC 624.2/.8: 534.1:533.6.07

Keywords: aeroelasticity, vibration, cable-stayed bridges, buffeting, flutter, vortex shedding, turbulence, wind tunnel

ABSTRACT

The frequency-domain approach is applied to the aerodynamic and aeroelastic analysis of long-span bridges. Numerical models are deduced for the simultaneous buffeting and flutter analysis and for the vortex and signature turbulence induced response calculation.

The goal, considered to be achieved, is to develop numerical models capable to reliable parametric studies of detailed three-dimensional structural models of bridges.

For the models, semi-empirical approach based on aerodynamic data obtained through section model tests in a wind tunnel, is employed. The data consists of the steady aerodynamic coefficients and flutter derivatives of a deck segment to be used in the buffeting and flutter analysis. A complemental data is suggested to be extracted for the vortex and signature turbulence induced response calculation.

The simultaneous analysis model for buffeting and flutter uses theoretically complete coupled-mode approach in which most of the unintentional simplifications of earlier models are removed. It has merits for the non-iterative calculation of flutter characteristics and feasibility to efficient computer implementation.

The vortex-induced response calculation is based on the band-limited white-noise excitation model while the signature-turbulence model employs approach typical in simplified buffeting analysis of bridge girders. The vortex-induced vibration calculation model facilitates imperfect spanwise correlation and turbulence reduction effects through mutually simple mathematical formulation.

To obtain aerodynamic input parameters for the verification study, wind tunnel tests for the spring supported section model are carried out in a smooth flow. The Instrumental variable method is formulated for acceleration signals and used on evaluating flutter derivatives through coupled-motion experiments.

To verify the numerical models, the calculated responses of the Raippaluoto and Kärkinen Bridges, two cable-stayed bridges in Finland involving double I-girder steel-concrete composite deck, are compared with the on-site measurements. Here, the responses and the wind turbulence data are measured on three occasions during storm and strong winds in 1999-2000.

PREFACE

Wind-induced vibrations of long-span bridges have in the last decade become of practical interest of Finnish National Road Administration (Finnra) and some Finnish consultants owing to construction of two long-span cable-stayed bridges and increasing activity related to export projects and international competitions. The two bridges, Raippaluoto and Kärkinen, contain double I-girder steel-concrete composite deck erected with the cantilever method. Earlier experience on the aerodynamic performance of alike girders was rare necessitating the detailed study. Internationally, there is ever-growing need for refined bridge wind assessment models and codes due to engineers' dedication to design longer, lighter and more economical bridge spans. At this point, the progress is most remarkable in the Far East, but there are projects within Europe as well, including the Messina and Gibraltar Strait crossings.

The bridge aerodynamics can be considered to be a new discipline in Finnish bridge engineering. Finnra and the Laboratory of Bridge Engineering (LBE) of Helsinki University of Technology (HUT) took an effort to start the research, in which the author has been involved since 1992. This research is concentrated on developing and implementing numerical semi-empirical analysis models. In addition, elaborate wind tunnel experiments have been carried out for the Kärkinen Bridge. The research conducted has had international contributions as well, the proposed Stonecutters Bridge in Hong Kong, with its world-record cable-stayed span (1017 m), being the most recent and outstanding diligence.

The author expresses his deep gratitude to Professor Aarne Jutila for his encouragement to the research and for serving opportunity to carry out it in excellent working conditions at LBE. The author is indebted to Professor Seppo Laine from the Laboratory of Aerodynamics for his support to conduct the wind tunnel experiments and for his valuable comments on aerodynamic issues. Thanks are offered to the stuff of the Laboratory of Aerodynamics assisting in experiments. Sincere gratitude is offered to Mr Lauri Salokangas (Lab. Mgr) and Mr Heikki Salonen (Techn.) from LBE for their aid to the work. Mr Salonen showed the kind of skill on constructing the wind tunnel models that the author is particularly grateful for.

Thanks are offered to Mr Juhani Salonen (Dir) from Finnra Vaasa district for financing the on-field measurement study of the Raippaluoto Bridge and allowing the usage of data for the present study.

Special acknowledgement is made to Mr Torsten Lunabba (Dir) from Finnra for the intensive cooperation continuing since 1992. His understanding and interest on bridge aerodynamics have greatly pushed research and related consulting activities forward in Finland. The author is obliged to all other persons contributing to the study. The theoretical studies were sponsored mainly by HUT and Tekniikan Edistämissäätiö, K. and A. Lippa Foundation, which the author gratefully acknowledges.

To my daughter Sara who followed the progress of the study during her first years.

Espoo, November 2000

Risto Kiviluoma

CONTENTS

ABSTRACT 2

PREFACE 3

NOTATIONS 6

1 INTRODUCTION 13
1.1 Dynamic and aeroelastic actions of a long-span bridge 13
1.2 Background of the study 14
1.3 Aim of the study 15
1.4 Evaluation of the methods of analysis 16
1.4.1 Wind tunnel experiments of full and taut strip scale models 16
1.4.2 Quasi-steady stability models of bluff bodies 17
1.4.3 Flutter theory for bridge decks 18
1.4.4 Analytical and semi-empirical models for vortex-induced vibrations 20
1.4.5 Buffeting theory 24

2 MODEL FOR SIMULTANEOUS CALCULATION OF BUFFETING AND FLUTTER RESPONSES 26
2.1 Initial assumptions 26
2.2 Wind-induced loads subjected to deck sections 27
2.2.1 Aeroelastic loads 27
2.2.2 Steady aerodynamic loads 28
2.2.3 Buffeting loads 29
2.3 Determination of equations for spectral analysis 31
2.3.1 Expressions for the load spectral density matrix 33
2.3.2 Turbulence model for one point in space 34
2.3.3 Spatial description of turbulence 36
2.3.4 Normal-mode method of solution 39
2.4 Discussion and sample implementation of the model 42

3 CALCULATION MODEL FOR VORTEX AND SIGNATURE TURBULENCE INDUCED VIBRATIONS 45
3.1 Excitation model for vortex-induced vibrations 46
3.1.1 Excitation model for reference wind tunnel experiments 47
3.1.2 Effects of approach-flow turbulence 49
3.1.3 Effects of spanwise load correlation 55
3.2 Response calculation for vortex-induced vibrations 57
3.3 Calculation model for signature turbulence 59

4 EXPERIMENTAL STUDY WITH AN AEROELASTIC SECTION MODEL 62
4.1 Test setup and analysis procedures 63
4.1.1 Aeroelastic section model 63
4.1.2 Measuring instrumentation 65
4.1.3 Instrumental variable method for extracting flutter derivatives 65
4.2 Results and details of the tests with discussion 69
4.2.1 Flutter derivative tests 69
4.2.2 Vortex and signature turbulence induced vibration tests 74
4.2.3 Performance of the measuring instrumentation 77

5 VERIFICATION STUDY 79
5.1 Input parameters for calculation models 80
5.2 On-site measurements 82
5.2.1 Instrumentation and postprocessing procedures 82
5.2.2 Measured turbulence properties 84
5.2.3 Measured modal parameters 86
5.2.4 Performance of the measuring instrumentation 88
5.3 Computational results and comparison with the measurements 89
5.3.1 Adequacy of the input parameters 89
5.3.2 Computational results with comparison 90

6 CONCLUSIONS 98
6.1 Buffeting and flutter analysis 98
6.2 Vortex and signature turbulence induced vibration analysis 99
6.3 Experimental study with an aeroelastic section model 100
6.4 Verification study 100
6.5 New contributions of the present study and suggestions for further research . . . 101

References 103

Appendix A Correction for load lumping error due to imperfect spanwise correlation . . 109

Appendix B On-site measurements: signal filtering and postprocessing details 111

NOTATIONS

Scalars

A_i^* (i = 1, 2, 3, ..., 6)	flutter derivative associated with the aeroelastic twisting moment
B	width of the cross-section
B_m	average width of the cross-section
C_i (i = D, L or M)	steady aerodynamic drag, lift or pitching moment coefficient as it appears in the aeronautical context, i.e. the coordinate system fixed to the wind direction
C_i (i = H, V or M)	steady aerodynamic coefficient associated with the mean horizontal force, mean vertical force or mean twisting moment induced by the wind to the body
C_{HK}	steady aerodynamic coefficient related to the mean horizontal force $\bar{H}_K$
C_{VK}	unsteady aerodynamic coefficient related to the fluctuating across-wind force V_K
$C_i(\omega)$, (i = u or w)	dimensionless function specifying the exponential fall-of characteristics of coherence for u or w components of the fluctuation velocity
$C_{\eta 1}$, $C_{\eta 2}$	aerodynamic exciting coefficients associated with the vortex-induced vertical force
$C_{\theta 1}$, $C_{\theta 2}$	aerodynamic exciting coefficients associated with the vortex-induced twisting moment
$\tilde{C}_i$ (i = η or θ)	root-mean-square (RMS) exciting coefficient related to the heaving or torsional vortex-induced excitation
$C(k)$	Theodorsen's function
D_{St}	steady drag force per unit length
$G_i(n_{Li})$, (i = u or w)	dimensionless function associated with the normalized spectrums of u or w component of the fluctuation velocity
$H_i(n)$	frequency response function related to mode i
H_i (i = St, Ae or b)	horizontal component of static, aeroelastic or buffeting force per unit length
$\bar{H}_K$	mean horizontal force acting on a unit length induced by the Kármán-Bénard vortex trail
H_i^* (i = 1, 2, 3, ...,6)	flutter derivative associated with the vertical component of aeroelastic force
$H_i^{(2)}(k)$	Bessel function of third kind (= Hänkel function) of order i
H_η	dimensionless empirical constant
I_i (i = u or w)	turbulence intensity associated with u or w component of the fluctuation velocity
I_i (i = 1, 2, η or θ)	abbreviation to the specific integral equation

J	mass moment of inertia per unit length
$J_i(k)$	Bessel function of first kind of order i
J_{ij} ($i, j = A$ or B)	nodal-load correlation correction coefficient
J_{ij} ($i, j = \eta$ or θ)	coherence reduction factor
$J(n_i)$	joint acceptance function associated with mode i
K	reduced frequency defined by $K = B\omega/U$
$\bar{K}$	mean reduced frequency defined by $\bar{K} = B\omega/\bar{U}$
L_{St}	steady lift force per unit length
L_s	scale of turbulence
${}^iL_j$ ($i = x, y$ or z)	integral length scale of turbulence in x (along-wind), y (lateral transverse) or z (vertical) direction. Defined for $j = u$, v or w component of the fluctuation velocity
M_i ($i = St, Ae$ or b)	static, aeroelastic or buffeting twisting moment per unit length
M_K	fluctuating twisting moment per unit length
N	number of nodes
N_d	number of variables in the instrumental variable algorithm (= length of the data sequence)
N_m	number of mode shapes considered in analysis
N_c	degree of the polynomial curve fit
P_i^* (i = 1, 2, 3, ..., 6)	flutter derivative associated with the horizontal aeroelastic force
$R(s_A - s_B)$	normalized covariance function for the spanwise separation
R_e	Reynolds number (= Uh/ν)
$R_{ij}(\tau)$ ($i, j = u$ or w)	cross-covariance function associated with u and/or w components of the fluctuation velocity
$\tilde{R}_i(\Delta_s)$ ($i = \eta$ or θ)	variance normalized covariance function related to the across-wind or torsional excitation due to the vortex shedding
S	spectrum of nodal-load
$\tilde{S}$	approximation for nodal-load spectrum S
S_i ($i = A$ or B)	load spectral density per unit length acting on the nodal-load interference length l_i
S_{ij} ($i, j = A$ or B)	abbreviation for a specific component of S
$S_{Qi}(n)$	one-sided spectral density of the modal load of mode i
${}^jS_{Qi}(n)$	one-sided spectral density of the modal load of mode i due to the degree-of-freedom component distinguished by j
$S_{MS}(n)$	spectrum of twisting moment per unit length due to the signature turbulence
$\tilde{S}_{MS}(n)$	non-dimensional excitation spectrum associated with $S_{MS}(n)$
$S_{VS}(n)$	spectrum of across-wind force per unit length due to the signature turbulence
$\tilde{S}_{VS}(n)$	non-dimensional excitation spectrum associated with $S_{VS}(n)$
$S_{ij}(n)$ ($i, j = u$ or w)	one-sided cross-spectral density associated with u and/or w components of the fluctuation velocity
$S_{ij}(\omega)$ ($i, j = u$ or w)	cross-spectral density associated with u and/or w components of the fluctuation velocity
S_t	Strouhal number
T	averaging time of the mean wind velocity
T_s	recording time of data
U	wind velocity
$\bar{U}$	mean wind velocity
$\bar{U}_{10}$	10 min averaged wind velocity at 10 m above the zero plane

U_{Rel}	relative wind velocity
U_m	mean wind velocity at the mean height (= at the middle of two separate points in space)
$\bar{U}_{\perp}$	horizontal mean wind velocity component at the deck level perpendicular to the bridge span
V_K	fluctuating across-wind force per unit length
V_i (i = *St*, *Ae* or *b*)	vertical component of static, aeroelastic or buffeting force per unit length
$Y_i(k)$	Bessel function of second kind (= Weber's function) of order i
a_i (i = 1, 2, 3 or 4)	empirical constant
$\tilde{a}_i$ (i = 1, 2, 3 or 4)	empirical constant
a_V	constant
b	half-chord of the cross-section (= B/2 for bridge decks)
b_K	along-wind distance between the vortices in the Kármán-Bénard vortex trail
b_i (i = u or w)	dimensionless constant in the ESDU coherence model
c_B	non-dimensional variable
c_i (i = u or w)	dimensionless constant in the ESDU coherence model
c_i (i = x, y or z)	decay parameter of the exponential coherence model related to the separation in x, y or z direction
c_s	decay parameter for the coherence of signature turbulence
c_{Eq}	equivalent coherence decay coefficient
d_i (i = 1, 2, 3, ..., N_d)	polynomial coefficient due to a curve fit of C_V against α
$f(C_\eta, \dot{C}_\eta, \ddot{C}_\eta)$	dimensionless function in the lift-oscillator model
f_C	Coriolis parameter ($f_C = 2\Omega_E \sin\varphi_b$)
g_i (i = η or θ)	peak factor associated with the heaving or torsional response
$g_{(\gamma)i}$ (γ = 0, 1 or 2)	peak factor associated with the displacement (or rotation), velocity or acceleration response components denoted by i
h	height of the cross-section
h_B	atmospheric boundary layer height
h_K	distance between the vortex rows in the Kármán-Bénard vortex trail
h_m	average height of the cross-section
k	reduced frequency defined by $k = b\omega/U$
k_K	non-dimensional constant of proportionality related to the instant frequency of the vortex-induced excitation
l_i (i = i, *A* or *B*)	nodal interference length associated with the nodal-load, i.e. the length from which the spanwise distributed load is lumped to the node
l_b	length of the structural member (bridge girder or pylon leg)
m	mass per unit length
n	frequency
n_K	instant value of excitation frequency
$\bar{n}_K$	mean value of excitation frequency
n_i (i = 1, 2, 3, ..., N_m)	undamped natural frequency of mode i
n_i (i = u or w)	non-dimensional parameter in the ESDU turbulence model ($= n\,{}^{x}L_i/\bar{U}$)
n_i (i = η or θ)	undamped natural frequency of the heaving or the torsional mode of vibration
q	kinematic pressure of air (= ½ρU^2)
q_i	normal coordinate associated with mode i
q_{Rel}	kinetic pressure of air related to the relative wind velocity

$\bar{q}$	mean kinetic pressure of air (= ½ρ$\bar{U}^2$)
r_i (i = u or w)	dimensionless variable in the ESDU coherence model
s	spanwise coordinate
s_i (i = 1 or 2)	spanwise coordinate of point 1 or 2
s_i (i = A or B)	spanwise coordinate of node A or B
t	time
u_*	friction velocity
$u(t)$	along-wind component of the fluctuation velocity
$v(t)$	transverse lateral component of the fluctuation velocity
$w(t)$	transverse vertical component of the fluctuation velocity
x	global position coordinate parallel to the horizontal mean wind direction
y	global position coordinate for axis perpendicular to x and y axis (= typically the bridge spanwise position coordinate)
z	global position coordinate in the vertical direction (= height above the zero level)
z_0	surface roughness parameter (= surface roughness length)
z_{10}	constant (= 10 m)
Γ	strength of vorticity of a concentrated vortex
Δ_i (i = x, y or z)	separation along x, y or z axis
Δ_s	separation between two spanwise coordinates
Θ_u	Sears' function
Θ_w	Horlock function
Θ_{iu} (i = H, V or M)	complex-valued function specifying the aerodynamic admittance related to the u-component of fluctuation velocity and the horizontal force, vertical force or twisting moment
Θ_{iw} (i = H, V or M)	complex-valued function specifying the aerodynamic admittance related to the w-component of fluctuation velocity and the horizontal force, vertical force or twisting moment
Φ_W	wind lateral direction angle; Φ_W = 0, 90, 180 and 270 Deg for the North, East, South and West winds, respectively
Ω_E	angular rotation velocity of the Earth (= $72.9 \cdot 10^{-6}$ rad/s)
α	angle of attack
β_K	ratio between instant and mean value of the excitation frequency
β_i (i = η or θ)	ratio between excitation frequency and the natural frequency n_η or n_θ
δ_i (i = η or θ)	natural frequency (n_i) normalized bandwidth of the excitation spectrum
δ_{iSt} (i = η or θ)	natural frequency (n_i) normalized bandwidth of the excitation spectrum for the body at rest
δ_{i0} (i = η or θ)	natural frequency (n_i) normalized bandwidth of the excitation spectrum for the body at rest in smooth flow
δ_{iu} (i = η or θ)	natural frequency (n_i) normalized bandwidth of the excitation spectrum induced by turbulence for the body at rest
γ	integer variable
γ_i (i = η or θ)	non-dimensional free constant in the excitation bandwidth model
ζ_i (i = η or θ)	damping ratio of mechanical damping related to the heaving or torsional mode
ζ_i (i = 1, 2, 3, ..., N_m)	modal damping ratio of mechanical damping related to mode i

ζ_{Ai} (i = η or θ)	damping ratio of aerodynamic damping related to the heaving or torsional mode
ζ_{Ai} (i = 1, 2, 3, ..., N_m)	modal damping ratio of aerodynamic damping related to mode i
η	across-wind displacement coordinate fixed to the centre of gravity of the cross-section; positive downwards for a deck segment
η_0	complex-valued amplitude constant
η_{St}	static across-wind deflection due to the mean wind action
η_c	complex-valued vertical displacement coordinate
η_i (i = p, p+, p-)	peak amplitude, maximum positive peak amplitude or minimum negative peak amplitude of the across-wind displacement response
θ	twisting angle (rotation coordinate); positive clockwise when the wind is blowing from left to right
θ_0	complex-valued amplitude constant
θ_{St}	static twisting angle due to the mean wind action
θ_c	complex-valued rotation coordinate
θ_i (i = p, p+, p-)	peak amplitude, maximum positive peak amplitude or minimum negative amplitude of the torsional response
θ_{ij} (i, j = u or w)	phase angle associated with the turbulence coherence model
θ_m	average value of the twisting amplitudes occurring at two separate points along the span
κ	von Kármán constant (= 0.4)
λ	geometric scale of the cross-section of a scale model
λ_V	non-dimensional constant specifying the effective position of the unsteady vertical force for the quasi-steady approximation of the aeroelastic twisting moment
$\mu_{(\gamma)ij}$ (γ = 0, 1 or 2)	modal correlation coefficient associated with displacement, velocity or acceleration response of the normal coordinates q_i and q_j
ν	kinematic viscosity of air ($\nu \approx 0.316 \cdot 10^{-6}$ m^2/s...$0.149 \cdot 10^{-6}$ m^2/s for air +0 °C...+20°C in the standard atmospheric pressure of 101.3 kN/m^2)
$\nu_{(\gamma)}$ (γ = 0, 1 or 2)	zero up-crossing frequency for the displacement, velocity or acceleration response
ξ	horizontal displacement coordinate fixed to the centre of gravity of the cross-section. Positive in the along-wind direction
ξ_{St}	static horizontal deflection due to the mean wind action
ρ	density of air (≈ 1.293 kg/m^3...1.205 kg/m^3 for air +0°C...+20°C in the standard atmospheric pressure)
σ_{iCr} (i = η or θ)	critical standard deviation response for mode i
σ_{iMax} (i = η or θ)	maximum standard deviation response for mode i associated with the smooth flow in the wind tunnel
$\sigma_{(i)j}$ (i = 0, 1 or 2)	standard deviation of the displacement (i = 0), velocity (i = 1) or acceleration (i = 2) response component denoted by j
τ	time lag
$\chi_{ij}(\omega)$, (i, j = u or w)	root cross-coherence function associated with u and/or w components of fluctuation velocity acting at two separate points in space
χ_{iS} (i = V or M)	root cross-coherence function associated with the signature turbulence induced across-wind force or twisting moment
ω	circular frequency (= $2\pi n$)
ω_i (i = η or θ)	circular natural frequency of the heaving or rotation mode
ω_i (i = 1, 2, 3, ..., N_m)	undamped circular natural frequency of mode i (= $2\pi n_i$)
$\tilde{\omega}_i$ (i = η or θ)	measured circular natural frequency of mode i

φ_b	latitude of the bridge site
φ_{xi} (i = 1, 2, 3, ..., N_m)	value of the ith mode shape for the nodal degree-of-freedom x of interest
$\varepsilon(t)$	mean wind normalized u-component of the fluctuation velocity
ε_i (i = η or θ)	non-dimensional frequency detuning parameter
ε_K	non-dimensional empirical constant

Matrices and vectors

$\mathbf{A}$	system matrix of the linear vibration system
$\tilde{\mathbf{A}}$	modified system matrix related to vector $\tilde{\mathbf{Y}}_i$
$\mathbf{B}$	state transition matrix
$\mathbf{B}_c$	complex dynamic stiffness matrix
$\tilde{\mathbf{B}}$	modified transition matrix related to vector $\tilde{\mathbf{Y}}_i$
$\tilde{\mathbf{B}}_c$	modal stiffness matrix
$\mathbf{C}$	damping matrix
$\mathbf{C}_{Ae}(\omega)$	damping matrix of aerodynamic damping
$\mathbf{F}_{St}$	nodal-load vector due to the mean wind velocity
$\mathbf{F}_b$	nodal-load vector due to the buffeting loads
$\mathbf{F}_i$ (i = 1 or 2)	matrix in the autoregressive moving average model of response
$\tilde{\mathbf{F}}_i$ (i = 1 or 2)	ordinary least square approximation for matrix $\mathbf{F}_i$
$\mathbf{H}_c(\omega)$	complex frequency response matrix
$\tilde{\mathbf{H}}_c(\omega)$	modal frequency response matrix
$\mathbf{K}$	stiffness matrix
$\mathbf{K}_{Ae}(\omega)$	stiffness matrix of aeroelastic stiffness
$\mathbf{M}$	mass matrix
$\mathbf{R}$	transformation matrix
$\tilde{\mathbf{R}}$	modified transformation matrix
$\mathbf{R}_b(\tau)$	cross-covariance matrix of buffeting loads
$\mathbf{R}_x(\tau)$	cross-covariance matrix of buffeting response
$\mathbf{S}_Q(\omega)$	cross-spectral density matrix of modal buffeting loads
$\mathbf{S}_b(\omega)$	cross-spectral density matrix of buffeting loads
$\mathbf{S}_q(\omega)$	cross-spectral density matrix of the buffeting response of normal coordinates
$\mathbf{S}_x(\omega)$	cross-spectral density matrix of buffeting response
$\mathbf{W}_i$	observation error vector corresponding the time $t = i\Delta_t$
$\mathbf{X}$	vector of nodal degrees of freedom
$\mathbf{X}_{St}$	nodal response vector for static action of the mean wind velocity
$\mathbf{X}_i$	vector containing values of the coordinates η and θ corresponding the time $t = i\Delta_t$
$\mathbf{Y}_i$	state-space vector corresponding the time $t = i\Delta_t$
$\tilde{\mathbf{Y}}_i$	vector containing the acceleration data for two instants $t = i\Delta_t$ and $t = (i + 1)\Delta_t$

$\tilde{\mathbf{a}}_{ij}$ (i, j = 1, 2)	square submatrix of matrix $\tilde{\mathbf{A}}$
$\mathbf{b}_{ij}$ (i, j = 1, 2)	square submatrix of matrix $\mathbf{B}$
$\mathbf{c}_{ij}$ (i, j = 1, 2, 3, ..., N)	square submatrix of matrix $\mathbf{C}_{Ae}$
$\mathbf{f}_i$ (i = *Ae*, *St* or *b*)	nodal-load matrix for load component i

$\mathbf{k}_{ij}$ (i, j = 1, 2, 3, ..., N)	square submatrix of matrix $\mathbf{K}_{Ae}$
$\mathbf{q}(t)$	vector of normal coordinates
$\mathbf{s}_{ij}$ (i, j = 1, 2, 3, ..., N)	square submatrix of matrix $\mathbf{S}_b$

$\tilde{\mathbf{\Phi}}$	modal matrix containing the desired mode shapes for the analysis through the definition $\tilde{\mathbf{\Phi}} \equiv [\boldsymbol{\varphi}_1 \ \boldsymbol{\varphi}_2 \ \boldsymbol{\varphi}_3 \ ...]$
$\mathbf{\Psi}_i$ (i = 1, 2 or 3)	matrix containing the sampled acceleration response in a specific form
$\mathbf{\Psi}_4$	instrumental variable matrix

$\boldsymbol{\varphi}_i$	undamped still-air mode shape (eigenvector) number i
$\boldsymbol{\sigma}^2_{(\gamma)}$ (γ = 0, 1 or 2)	covariance matrix of the displacement, velocity or acceleration responses of the normal coordinates
$\boldsymbol{\mu}^2_{(\gamma)}$ (γ = 0, 1 or 2)	modal correlation coefficient matrix of the displacement, velocity or acceleration responses of the normal coordinates

Special notations

$e^{\mathbf{A}}$	exponent series of the square matrix $\mathbf{A}$ (= $\mathbf{I}$ + $\mathbf{A}$/1! + $\mathbf{A}^2$/2! + ...)
$\hat{f}(\omega)$	Fourier transform of function $f(t)$
$\dot{f}$	time derivative of function f
$\ddot{f}$	second time derivative of function f
Im(f)	imaginary part of the complex variable f
i	imaginary constant
$p(f)$	probability density of variable f
Re(f)	real part of the complex variable f
σ_i	standard deviation of the random variable denoted by subscript i
σ_i^2	variance of the random variable denoted by subscript i
×	matrix multiplication in the context of equation continuation row

Abbreviations

AIAA	American Institute of Aeronautics and Astronautics
AIEE	American Institute of Electrical Engineers
ASCE	American Society of Civil Engineers
ASME	American Society of Mechanical Engineers
DMI	Danish Maritime Institute
ESDU	Engineering Science Data Unit
FE	finite element
FFT	Fast Fourier Transform
NACA	National Advisory Committee for Aeronautics
RMS	root-mean-square

1 INTRODUCTION

1.1 Dynamic and aeroelastic actions of a long-span bridge

Long-span bridges, typically suspension and cable-stayed types, are known prone to wind-induced vibrations for various reasons. Some of the issues frequently considered in a wind resistant design can be ventured as follows:

a) Low natural frequencies of order 0.1...0.5 Hz of cable suspended spans cause wind turbulence to excite the stiffening girder with a considerable power. This phenomenon is associated with observations that the peak portion of spectrum of natural wind turbulence is concentrated to frequencies about 1/min while the magnitude of spectral density decreases rapidly with the increasing frequency. The forced movements owing to turbulence, and the associated excitation mechanism (buffeting), are stochastic in nature. A stiffening girder with typical non-streamlined ("bluff") cross-section itself produces turbulence in the fluid wake ("signature" or "local" turbulence) yielding buffeting to occur, although the approaching flow would be perfectly steady.
b) A bluff girder or pylon leg can produce a strong vortex-wake downstream the body that, as far as ideal fluid models are concerned, is associated with the aerodynamic drag force experienced by the body [72,75]. Depending on the wind speed and the cross-section's shape and size, the shedding of vortices is more or less regular with shedding periods, as first approximation, inversely proportional to the wind speed. In resonant conditions the structure's oscillation can begin to control the rhythm of vortex shedding and limited amplitude vibrations can be expected to occur in the multiple regimes of wind speed. For long-span bridge decks, the lowest of these regions falls typically about wind speed of 10 m/s. Aside the well-known vortex-trail type excitation, the more general types of aerodynamic excitation mechanisms can exist for the elongated cross-sections like bridge decks. The possible re-attachment of separated flow, the vortices generated by the local deck geometry (cavities, etc.) and the vortices generated by the movement of the body have their contribution to the periodic aerodynamic forces experienced by the bridge girder.
c) Aerodynamic forces proportional to the movement of the body (aeroelastic loads) can, to some cross-section shapes, produce self-excited divergent vibrations at high wind speeds. In mathematical models of the phenomenon, the concepts of aerodynamic damping and aeroelastic stiffness are applied frequently. To be avoided in the design is, that the absolute value of the negative aerodynamic damping force exceeds the positive mechanical damping force that produces oscillatory torsional or across-wind bending mode instability called the torsional flutter (or stall flutter, or torsional galloping) and the galloping, respectively. The starting small amplitude motion of the body, at wind speeds higher than the critical value where the instability initiates, can be considered to be undamped harmonic one. The associated critical wind speed is termed flutter velocity while the circular frequency is named the flutter frequency. Pylons

and ice-covered cables can be prone to the galloping while a stiffening girder can suffer from the torsional flutter. The aeroelastic coupling between the torsional and bending modes of the stiffening girder is possible producing considerable shifts to the natural frequencies and yielding the downstream side of the symmetrical deck to vibrate more violently than the windward one. However, the classical flutter, in which the existence of two modes is essential for the instability, is not expected to occur on conventional designs. Recently, evidence is obtained that for very long spans, of order 2 km in suspension bridges and 1 km in box-girder cable-stayed bridges, this condition is reversed and the coupling can significantly decrease the flutter velocity.

d) Stay-cables of cable-stayed bridges can be severally excited by wind because of their flexibility, small mass and small damping. In addition to the vortex and galloping induced vibrations, special types of excitation mechanisms have been reported including the wake galloping and the rain-induced vibrations. The stay vibrations can be amplified due to the oscillation of stay anchorage (i.e. the oscillations of the deck or the pylon). Large amplitude cable vibrations can be induced especially at onsets of, that the frequency of anchorage excitation is equal to the first or second natural frequency of the cable.
e) For a typical stiffening girder, twisting moment, owing to the static wind action, tends to twist the deck, and the resulting increment at the angle of attack further increases the twisting moment. At the onset of divergence wind velocity, a static torsional instability of a bridge stiffening girder initiates. Wind tunnel studies on very long-span cable-stayed bridges with shallow and wide box-girders have indicated that the risk of divergence should not be overlooked. For cable-stayed bridges, the static wind forces of stay-cables and pylons can produce significant deflections to a pylon tip which, in turn, can induce a considerable nonlinear static action due to the large compressive forces in the pylon leg.
f) The temporary stiffness-lack occurring during the construction can dispose the structure to wind effects. Probably, the most notable risks occur because of excessive buffeting responses of cantilever spans of cable-stayed bridges and flutter instabilities during construction of the first stiffening girder segments of suspension bridges [99]. Furthermore, free-standing pylons can suffer from buffeting, galloping and vortex-induced vibrations.

To distinguish between the aeroelastic and dynamic actions of wind, the former can be described as phenomenon, wherein aerodynamic forces and structural motions interact significantly. Another description applied repeatedly is that, for a body at rest, all aeroelastic actions should vanish. In the present study, divergence, galloping, torsional flutter, classical flutter and vortex-induced vibrations are treated as aeroelastic phenomena and buffeting and signature turbulence induced vibrations as dynamic ones.

1.2 Background of the study

Two frequently used basic methods for the mathematical analysis of linear vibration systems can be discerned, the time domain and the frequency domain. For loads changing arbitrarily in time, applications based on the former one yield to the solution of convolution type time integrals, while the latter involves the Fourier-transformed equations of motion with the frequency as a fundamental parameter. To express the aeroelastic loads in the time domain, the indicial aerodynamic functions [79,84] can be applied, while in the frequency domain, the flutter derivatives [78] contain the information needed. Theoretically, choice of the method is complementary, because the flutter derivatives and the indicial aerodynamic functions can be shown to perform the Fourier transform relationships between each other [28,84]. In practical situations of bridge deck analysis, the wind tunnel tests of scale models should be carried out in order to evaluate the aeroelastic loads

by reliable means. In such tests, the empirical setup for the extraction of flutter derivatives can be considered to be easier to implement than the one for the indicial functions. Many time-domain studies are based on indicial aerodynamic functions derived through the flutter derivatives.

By means of the spectral analysis of random vibration theory, the frequency-domain method can be conveniently applied to the buffeting problem owing to the stochastic nature of the problem; the statistical properties of turbulence can be characterised by the frequency dependant spectral densities and coherence functions.

Advantages of the frequency-domain method, when modelling the combined dynamic and aeroelastic actions of bridge girders, have been addressed by several authors [2,38,40,44,81,86,88] during the last decades. The flutter derivatives are functions of frequency of vibration and can be directly applied to the Fourier-transformed equations of motion. The usage of flutter derivatives in the time domain is restricted to the harmonic motion only while in the frequency domain they are valid for analysis of an arbitrary motion like that occurring in a buffeting. The Fourier-transformed equations of motion of a linear vibration system subjected to buffeting loads can be given by the formula [12,41,44,45,61]

$$(-\omega^2\mathbf{M} + i\omega\mathbf{C} + \mathbf{K})\hat{\mathbf{X}}(\omega) = [i\omega\mathbf{C}_{Ae}(\omega) + \mathbf{K}_{Ae}(\omega)]\hat{\mathbf{X}}(\omega) + \hat{\mathbf{F}}_b(\omega) \ , \qquad \textbf{(1)}$$

in which ω is the circular frequency, $\mathbf{F}_b$ is the vector of nodal buffeting loads, $\mathbf{X}$ is the vector of nodal degrees of freedom, symbol ($\hat{}$) with argument (ω) added denotes the Fourier transform and i is the imaginary unit. Here, $\mathbf{M}$, $\mathbf{C}$ and $\mathbf{K}$ are the mass, damping and stiffness matrices, respectively, related to the mechanical properties of the vibration system; $\mathbf{C}_{Ae}(\omega)$ is the aerodynamic damping matrix and $\mathbf{K}_{Ae}(\omega)$ is the aeroelastic stiffness matrix to be defined in terms of the flutter derivatives. The stability condition Eq. (1) implies is independent of the buffeting loads. On the other hand, the buffeting response is dependent upon the aeroelastic loads, especially on the aerodynamic damping.

1.3 Aim of the study

The aim of this study is to develop frequency-domain calculation models for a) buffeting, b) flutter, c) vortex-induced vibrations and d) signature turbulence induced vibrations of long-span bridges. The goal is to develop numerical models that can be used for reliable parametric studies and are feasible to integrated and efficient computer implementation. Furthermore, the constraints are specified as follows: a) crucial aerodynamic input parameters should be based on section model type wind tunnel experiments and b) the models should facilitate the analysis of detailed three-dimensional structural models of bridges. For setting the aim and constraints, the following aspects can be pointed out:

a) As addressed by several authors [85,86], the application of three-dimensional structural models is important especially in the analysis of cable-stayed bridges, as their mode shapes are generally three-dimensional on account of interacting pylon deflections. Furthermore, cables and pylons can produce considerable drag and aerodynamic damping to some mode shapes and the wind loads and vibrations of the pylons themselves are of interest.
b) The importance of vortex-induced vibrations in the context of bluff bridge cross-sections is generally overlooked probably due to the fact that the induced responses are not destructive. It seems, that there is no generally accepted theory available to predict the response based on the section model experiments or the standardised techniques to extract the design data needed.

The bulk of the models developed and empirical data presented are for bluff cylinders only, and their application to elongated cross-sections, like bridge decks, needs special consideration.

c) The phenomenon of signature turbulence induced vibrations is broadly unexplored. For the present study, the question of its importance arose in the context of the static wind tunnel tests of the Kärkinen Bridge [109] in Finland. It was found that, despite the smooth flow and rigid support system employed, significant random motions of the model took place. Not only the vibrations of static wind tunnel models have been reported earlier [24], but also the on-site measurements [7] of real bridges indicate that the phenomenon might have important effects.

d) A spring-supported section model can be considered to be an economical choice for the aerodynamic and aeroelastic analysis of a bridge. For experiments, no special requirements are needed for the wind tunnel and the same base model can be applied when determining the steady aerodynamic coefficients and aeroelastic parameters.

e) In the course of advances in the numerical fluid analysis, aerodynamic data based on section model experiments can probably be approximated through computer simulations involving the two-dimensional flow model. The possibility to predict or verify some portion of the data by means of the computational fluid dynamics can be appreciated.

f) From the bridge engineering's point of view, the aerodynamics is small, but in some circumstances an important part of the design of long-span bridges. Successful analysis models, applied prior to construction, should be capable to estimate responses for all known important excitation mechanisms of wind.

1.4 Evaluation of the methods of analysis

In the past, many bridges have been damaged due to the wind, but it was the collapse of the first Tacoma Narrows Bridge in 1940 [24, 25] that promoted bridge engineers worldwide to realise the consequences of and to start the research on aeroelastic actions of the wind. Because of the fact that the separated flows around bluff bodies, like bridge decks, are complicated to tackle by analytical means, the experimental work based on wind tunnel models has characterised the research. As pointed out by SCANLAN [83,88], the applied mathematical models, as well as wind tunnel testing techniques, have got considerable impetus from aeronautical engineering, in which the experience in analysing and suppressing aeroelastic actions on aerofoils has been gathered since 1916 [26,28].

1.4.1 Wind tunnel experiments of full and taut strip scale models

Obviously, the most reliable and generally accepted practical method to analyse the dynamic and aeroelastic actions of wind, is the full aeroelastic model wind tunnel testing technique. In the technique, the scale model of the full bridge is tested in a wind tunnel having enough space for the model. The essential model laws are owing to the basic results of the dimensional analysis and no computational efforts are essential for interpreting the results. This kind of investigations are occasionally conducted for challenging long-span bridge projects; the first ones probably in the 1940's in the United States and Great Britain related to the first Tacoma Narrows Bridge and the early design proposals of the Severn Bridge, respectively. The former model duplicated the observed oscillations promoting the acceptance of this empirical concept [92]. The full model can be applied to study many special questions like the inclined winds during construction [87] and large deflection effects on the response. As discussed by IRWIN [35], a full bridge model is not always the most sensitive instrument for studying the vortex-induced vibrations. It is typically built in small scale where the modelling of fine details of the bridge is cumbersome. Furthermore, for long-span suspension bridges, the lock-in flow speeds fall to very low values due to Froude's

number scaling (gravitational scaling). As a consequence, some unwanted Reynolds number (air viscosity and inertia scaling) effects can take place.

In many cases, the full model testing technique has economical and other limitations. A newer "taut strip" model technique [19, 98] has served as alternative to this empirical concept. In it, only the stiffening girder of the bridge is modelled with dynamic properties controllable by the taut wires inside the model. Furthermore, the similarity law concerning Froude's number can be relaxed allowing higher flow speeds to be used in experiments.

The considerable effect that turbulence might have to stability characteristics of the full or the taut strip wind tunnel models has been pointed out by DAVENPORT *et al*. [17,18], among others. In general, to get the most reliable estimate for the prototype bridge response, the turbulence conditions on the bridge site should also be modelled in the wind tunnel. To produce turbulence, one can apply grids and active (motor-controlled) devices in short wind tunnels and various upstream roughness elements in long boundary layer wind tunnels.

1.4.2 Quasi-steady stability models of bluff bodies

PARKINSON *et al.* [67,68] and NOVAK [62,64] have proposed the galloping theory based on the wind-tunnel experiments of simplest kind, that is, on the steady aerodynamic coefficients of the cross-section. In their approach, and in the quasi-steady formulation of aeroelastic loads in general, no distinction is made between the inclination of relative wind velocity U_{Rel} (*Fig. 1*), accounting the velocity of the body and the angle of attack α, specifying the steady wind direction with respect to the body at rest. In the heaving oscillations, the angle of attack is then $\alpha \approx \dot{\eta}/U$, where U is the wind velocity, η is the across-wind displacement and the dot designates a time derivative. The formulation for aeroelastic across-wind force per unit length V_{Ae} is given by

$$V_{Ae} = q_{Rel} B C_V \ , \tag{2}$$

where

$$\begin{cases} q_{Rel} \approx q \equiv \dfrac{1}{2}\rho U^2 \\ C_V = \displaystyle\sum_{i=1}^{N_c} \left(\frac{\dot{\eta}}{U} \right)^i d_i \ . \end{cases} \tag{3}$$

Here, B is the width of the cross-section, ρ is the density of air; q_{Rel} and q are the kinetic pressures of air associated with the relative wind velocity and wind velocity, respectively. Coefficient d_i ($i = 1, 2, ..., N_c$) is the constant due to a polynomial fit of the steady aerodynamic coefficient C_V against the angle of attack with N_c being the degree of polynomial. The steady vertical force V_{St} is related to the steady lift L_{St} and the steady drag D_{St} applied in the aeronautical practise as illustrated in *Fig. 1*. The associated steady aerodynamic coefficients are given by formula $C_V = -(C_L \cos\alpha + C_D \sin\alpha)$, where C_D and C_L are the steady aerodynamic drag and lift coefficients, respectively.

The excitation model of Eqs (2) and (3), when applied in conjunction to the single-degree-of-freedom oscillator model, yields to a nonlinear vibration system in which the nonlinearity is owing to the damping term. By assuming that the amplitude is nearly constant in the period of one vibration cycle, PARKINSON *et al*. [67,68] and NOVAK [62,64] were able to treat the amplitude dependence of the stability and the hysteresis (or bifurcation) found in experiments by analytical means. The

term hysteresis is used to describe that the maximum vibration amplitude of the wind tunnel model can differ when the flow speed is decreased to or increased to critical value.

For small amplitudes, Eqs (2) and (3) impose a negative aerodynamic damping, if the Glauert-Den Hartog criterion [29,30,95] for instability is met, i.e. $C_D + dC_L/d\alpha < 0$. Since the drag coefficient is positive in sign, the slope of the lift coefficient characterises the stability.

Alike theory has been proposed for rotational oscillations. Here, a negative slope of the steady moment coefficient initiates the torsional galloping. The angle of attack, related to the relative wind velocity, varies in different locations at the cross-section; its value should be determined against some specific point at the cross-section (point $\lambda_V B$ in *Fig. 1b*). The windward edge (λ_V = -½) has been applied for bluff cross-sections [6] while the chord leeward quarter point (λ_V = ¼) is the analytical result for thin aerofoils or flat plates [26].

As far as bridge decks are concerned, the inconsistency of the two quasi-steady "negative slope" theories has been shown, among others, by FARQUHARSON [24]. It is now generally accepted, that the applicability of the quasi-steady stability models is characterised by the reduced velocity $U/(hn)$, in which n is the vibration frequency and h is the height of the cross-section. For example, Eqs (2) and (3) to be applicable for bluff cylinders, the reduced velocity should be $U/(hn) > 12$, say. This kind of constraint can be interpreted by two ways, i.e. the significant oscillations of the structure should be "slow" (n is small) or the wind speed should be far above the range where flow unsteadiness, in particularly due to the vortex shedding, become dominant [57].

As far as the frequency-domain analysis methods and small amplitudes are concerned, the aerodynamic damping and aeroelastic stiffness matrices, or part of them, in the equations of motion (1) can be constructed by means of the quasi-steady formulation using the steady aerodynamic coefficients. This approach suffers from inconsistency in the torsional damping formulation for bridge decks but can be applied to other load components and structural members.

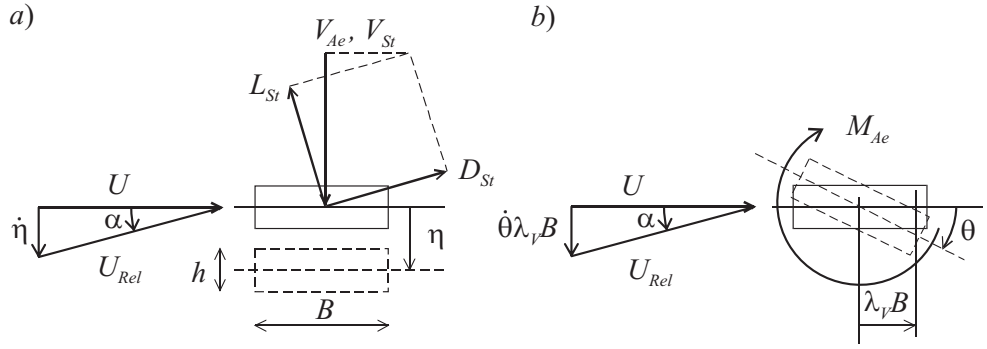

Fig. 1 Quasi-steady formulation of aeroelastic loads: a) the heaving and b) the rotation (or torsion).

The effects of upstream turbulence on galloping have been studied, e.g. by NOVAK *et al*. [63,65] and KWOK *et al*. [47]. Their approach suggests, that the significant modifications found for scale models in wind tunnel experiments, can be modelled through the changes in steady aerodynamic coefficients.

1.4.3 Flutter theory for bridge decks

In the context of aerodynamic design of the new Tacoma Narrows Bridge, BLEICH [4] proposed in the late 1940's the analogue for the aeroelastic actions of the bridge span and the aeroplane wing flutter. His flutter theory, proposed for the analysis of truss-stiffened girders, was based on THEODORSEN's [100] potential flow solution for the harmonically oscillating thin aerofoil or flat

plate. Neglecting the small virtual mass terms BLEICH [4] established the aeroelastic vertical force and moment acting per unit length of the fluttering plate-like deck in the form

$$\begin{cases} V_{Ae} = -2\pi\rho bU^2\left\{ C(k)\dfrac{b\dot{\eta}_c}{U} + [1 + C(k)]\dfrac{b\dot{\theta}_c}{2U} + C(k)\theta_c \right\} \\ M_{Ae} = \pi\rho b^2U^2\left\{ C(k)\dfrac{b\dot{\eta}_c}{U} + [1 - C(k)]\dfrac{b\dot{\theta}_c}{2U} + C(k)\theta_c \right\} , \end{cases} \tag{4}$$

in which C(k) is Theodorsen's function, M_{Ae} is the aeroelastic twisting moment per unit length and $b = B/2$ is the deck half chord. Here, the harmonic motion is understood to be described by the complex coordinates $\eta_c = \eta_0 e^{i\omega t}$ and $\theta_c = \theta_0 e^{i\omega t}$, where ω is the circular frequency of the oscillatory motion, t is the time and where the amplitude constants (η_0 and θ_0) are also complex. Theodorsen's function is a complex-valued function of the reduced frequency $k = b\omega/U$. Its value can be expressed in the closed form [26,100] applying tabulated functions by

$$C(k) = \frac{J_1(k) - iY_1(k)}{J_1(k) - iY_1(k) + iJ_0(k) + Y_0(k)} \equiv \frac{H_1^{(2)}(k)}{H_1^{(2)}(k) + iH_0^{(2)}(k)} , \tag{5}$$

where $J_i(k)$, $Y_i(k)$ and $H_i^{(2)}(k)$ are the (order $i = 0$ or 1) Bessel functions of first kind, second kind (Weber's function) and third kind (Hänkel function), respectively.

SCANLAN and TOMKO [78], among others, have contributed the flutter theory by replacing the terms containing Theodorsen's function, by the empirically determined flutter derivatives and by developing methods to extract the flutter derivatives by section model experiments in wind tunnel. In this case too, the experimental method was borrowed from the aeronautical practise. There are two basic techniques for the experimental extraction: the free-vibration and the forced (motor controlled) vibration tests. The former technique is most often applied to the bridge analysis owing to simplicity of the wind tunnel setup. In the latter technique, also water can be applied as a test medium. Utilizing the former technique, SABZEVARI *et al*. [73] and SCANLAN *et al*. [79] were able to show a significant difference between aeroelastic loads that the flat plate and the bridge deck can have. Section models representing streamlined decks of some modern bridges, including the Severn Bridge [105] and the Great Belt East Bridge [71], are analysed satisfactorily for flutter by applying the theoretical flutter derivatives based on Theodorsen's solution. Furthermore, the solution has been adopted for verification purposes in many studies.

According to SCANLAN [88], the aeroelastic loads of a bridge cross-section undergoing small amplitude sinusoidal motion are expressed by the formulae

$$\begin{cases} H_{Ae} = qB(KP_1^*\dfrac{\dot{\xi}}{U} + KP_2^*\dfrac{B\dot{\theta}}{U} + K^2P_3^*\theta + K^2P_4^*\dfrac{\xi}{B}) \\ V_{Ae} = qB(KH_1^*\dfrac{\dot{\eta}}{U} + KH_2^*\dfrac{B\dot{\theta}}{U} + K^2H_3^*\theta + K^2H_4^*\dfrac{\eta}{B}) \\ M_{Ae} = qB^2(KA_1^*\dfrac{\dot{\eta}}{U} + KA_2^*\dfrac{B\dot{\theta}}{U} + K^2A_3^*\theta + K^2A_4^*\dfrac{\eta}{B}) , \end{cases} \tag{6}$$

in which ξ is the horizontal displacement coordinate, θ is the rotation coordinate, H_{Ae} is the horizontal aeroelastic force per unit length; P_i^*, H_i^* and A_i^* (i = 1, 2, 3 or 4) are the flutter derivatives. The flutter derivatives are assumed to be dependent upon the reduced frequency $K = B\omega/U$. In Eqs (6), only the real-valued variables are considered in contradict to Eqs (4). These two equations

have the equal physical purpose for specifying the in-phase (aeroelastic stiffness) and the out-of-phase (arodynamic damping) force or moment components within a harmonic motion.

The bridge deck flutter derivative data, as measured by means of a scale model in a wind tunnel, is theoretically contaminated by implications of the dissimilar scaling, like that associated with the Reynolds number. There exists at least one study, OKAUCHI *et al*. [66], in which the results obtained through the large scale section model tested in the natural wind are compared with the wind tunnel test results. Good agreement between the two results was concluded. This supports the generally accepted view that section models of bridge decks can be designed to reasonable geometric scale so that severe implications due to scaling problems are not likely to occur.

The spanwise correlation of aeroelastic loads for bridge girders is typically assumed to be perfect. SCANLAN *et al*. [86] and SCANLAN [89], however, have proposed models to account for the loss of spanwise correlation.

SCANLAN *at al*. [80] and SARKAR *et al*. [76], among others, have made attempts to measure the effects of approach-flow turbulence on the flutter derivatives. Their experiments indicate that turbulence has no significant effect on the flutter derivatives themselves. It is suggested by SCANLAN *et al*. [86] and SCANLAN [89] that turbulence can modify the spanwise correlation of aeroelastic loads and thus the aeroelestic stability characteristics.

If the turbulent upstream flow is considered in the flutter analysis, the wind velocity in Eqs (6) should be modified to take into account the fluctuations in the horizontal wind velocity. If the mean wind velocity is near the flutter onset, the flutter velocity is exceeded in short duration gusts. It is problematic to state, whether or not the gust is steady long enough to build up a catastrophic motion. The problem, and the long-span bridge wind analysis in general, have been treated by LIN [52], BUCHER *et al*. [8,9,10], LIN *et al.* [53,54] and WALL *at al.* [104] by applying time-domain methods and the theory of stochastic differential equations. Owing to this approach, they introduced additional assumptions for the buffeting excitation process and were able to treat the turbulence effects on bridge flutter by analytical means.

1.4.4 Analytical and semi-empirical models for vortex-induced vibrations

The well-known law of linear dependence between the shedding frequency n_K of vortices and the steady flow velocity is associated with the study of STROUHAL [96] and is expressed by equation

$$n_K = S_t \frac{U}{h} , \qquad \textbf{(7)}$$

where S_t is the Strouhal number. This number is generally known to be a slowly varying function of the Reynolds number $R_e = Uh/\nu$, in which ν is the kinematic viscosity of fluid. Strouhal numbers are typically about 0.2 and 0.1, for circular cylinders and bridge decks, respectively.

An analytical study concerning the stability of the vortex patterns in a wake of a stationary cylindrical body was carried out by VON KÁRMÁN and RUBACH [42] in 1911. Based on two-dimensional potential flow theory and assuming that the fluid is irrotational except in concentrated vortices, it was shown, that the vortex pattern is stable, if the vortices are organized in unsymmetrical double row pattern (*Fig. 2*). This stable configuration of vortices possesses the relations $h_K/b_K = \pi^{-1}\operatorname{arccosh}\sqrt{2} \approx 0.281$ and $|\Gamma| = \sqrt{8}\, u_K b_K$, where Γ is the strength of vorticity of a concentrated vortex, u_K is the velocity of the vortices, b_K is the distance between the vortices in a row and h_K is the distance between the rows. Furthermore, it was shown that the vortex trail induces almost steady drag force to the body given by the formula [42]

$$\bar{H}_K = qhC_{HK} \ , \tag{8}$$

in which $\bar{H}_K$ is the mean value of the induced horizontal force per unit length and the associated force coefficient C_{HK} is expressed as

$$C_{HK} = \frac{2\Gamma}{U^2 h}\frac{h_K}{b_K}(U - 2u_K) + \frac{\Gamma^2}{\pi U^2 h\, b_K} \ . \tag{9}$$

Some attempts have been made to obtain analytical expressions for the fluctuating lift force experienced by the bluff cylinder owing to the ideal Kármán-Bénard vortex trail (*Fig. 2*). Considering infinite vortex trail and circular cross-section, CHEN [11] found that

$$V_K = \rho u_K \Gamma = qhC_{VK} \ , \tag{10}$$

where

$$C_{VK} = \left(\frac{\Gamma}{Ub_K}\right)^2 \frac{b_K}{h} \tanh\frac{\pi h_K}{b_K} \ . \tag{11}$$

Here, V_K is the fluctuating across-wind force per unit length and C_{VK} is the associated aerodynamic exciting coefficient. The study does not establish the time-dependence of the unsteady exciting coefficient, but SALLET [75] has been able to suggest that the dependence should be sinusoidal with a frequency given by Strouhal's relation. The aeroelastic actions can be considered in Eqs (9) and (11) by noting that the spacing between the vortex row h_K, and thus the induced forces, can alter, if the cross-section performs across-wind oscillations. In general, analytical formulations for the aerodynamic exciting coefficients are dependent on the approximations assumed for the near-wake behind the body [11].

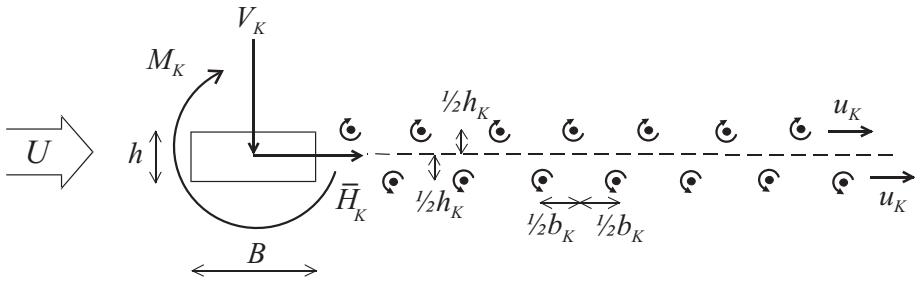

Fig. 2 A sketch of unsymmetrical double row pattern of vortices known as the Kármán-Bénard (or von Kármán) vortex trail. Here, the vortex-induced twisting moment per unit length M_K, omitted in the analysis of cylindrical bodies, is illustrated for completeness.

Considerable efforts have been made to determine experimental values for aerodynamic exciting coefficients of cylindrical bodies in varying Reynolds number regimes. Generally, the experimental data shows such a scatter that uniform relationship is not established [11].

In some references, like the textbook of DEN HARTOG [30], the catastrophic torsional motion

of the first Tacoma Narrows Bridge has been associated with the vortex-induced vibrations; although the term flutter is the most widely accepted term describing the governing mechanism in the civil engineering terminology [83]. In early section model investigations involving a spring-supported rigid "H-shaped" section, the shape closely presenting the first Tacoma Narrows Bridge cross-section, it was found that [26]:

a) While the model is at rest, the vortex shedding is controlled by the wind, i.e. by Strouhal's law.
b) In a certain discrete wind speed regime, the frequency of vortex shedding will coincide with or be a multiple of one of the natural frequencies of the model. Such coincidence occurs in self-excited vibrations of the model.
c) At finite range of wind speeds beyond the resonance condition, the oscillations of the structure and not the wind speed controls the vortex shedding. In general, this lock-in phenomenon can cause the maximum amplitude to occur in higher wind speeds than expected by the resonance condition.

More recent observations comprise:

d) The low-speed excitation found for H-shaped elongated cross-sections are not associated with the von Kármán type vortex trail but to the motion-dependent vortices generated by the leading edge. The fluid cavity behind the leading edge and the sharp trailing edge is assumed to be responsible for the formation of such vortices. The leading edge vortices can shed from upper and lower side of the edge mutually independently, but behind the body they can interact to form the von Kármán vortex trail of "special type" [59].
e) The spanwise correlation of excitation on three dimensional cylindrical bodies increases with increasing amplitude [70,101,106].
f) There can exist a limiting amplitude that the vibration amplitudes do not exceed even if the damping and mass is reduced [37].
g) The approach-flow turbulence can decrease the correlation of lift force and the structure's maximum amplitude. NAKAMURA *et al.* [58] and NAKAMURA [60] have concluded that the phenomenon occurs especially in the large-scale turbulence in which the integral length scale of turbulence is of order width of the cross-section.
h) The response reduction effect of large-scale turbulence tends to vanish at large amplitude motion [107].
i) With the increasing flow speed, the critical Reynolds number value can exist where the regular vortex shedding becomes disorganized and random. With the further increased flow speed beyond the associated transition range, the vortex shedding can again become regular [27]. For circular cylinders, the Strouhal number and other vortex-related parameters can be strongly dependent on the Reynolds number. Furthermore, the transition range approximately comes about to the range of primary interest in structural design.
j) Excitation mechanisms of bridge decks belong to the group of Kármán-vortex, motion-induced or their combination, depending on the slenderness ratio (B/h) of the cross-section. Most bridge girders belong to the motion-induced group. For them, a lock-in start wind velocity is dependent upon the slenderness ratio rather than the Strouhal number [56,94].

The list of important experimental observations, mainly those related to responses of circular cylinders, is compiled in more complete form by SARPKAYA [77]. The above list does not only show the complexity that can be inherent in the rigorous analysis of bridge decks, but also suggests alternating mathematical models feasible for the analysis.

A mathematical model based on nonlinear oscillators, the lift-oscillator model, has been

proposed by HARTLEN and CURRIE [31] with further contributions by many investigators listed in Refs [77,95]. In the lift-oscillator model, the fluid itself is assumed to form an oscillator that can produce aerodynamic damping forces to the structure. The equations of motion of the elastically supported rigid section model are given by

$$\begin{cases} m(\ddot{\eta} + 2\omega_\eta\zeta_\eta\dot{\eta} + \omega_\eta^2\eta) = qhC_\eta \\ C_\eta + f(C_\eta, \dot{C}_\eta, \ddot{C}_\eta) = a_V\dot{\eta} \ , \end{cases} \tag{12}$$

where m is a the mass per unit length, ω_η is the circular natural frequency of the heaving mode and ζ_η is the damping ratio. Here, a_V is the empirical constant and $f(C_\eta, \dot{C}_\eta, \ddot{C}_\eta)$ is a non-dimensional function of the aerodynamic exciting coefficient C_η and its time derivatives. Several alternatives for this function have been proposed by various authors, but in general, the associated differential equation results harmonic oscillation for the aerodynamic exciting coefficient for a body at rest ($\dot{\eta} \equiv 0$). The justification of the lift-oscillator model has, by its vital parts, been based on experiments. The model has its roots in mechanics and in electricity rather than in the equations of fluid motion [77]. Some further, but not complete [77], justification can be obtained by the Iwan-Blevins oscillator model [6,36] that takes the form similar to Eqs (12) despite the slightly more analytical approach adopted. For its versatility, the lift-oscillator model has been successfully applied on characterising many of the phenomena found in experiments. These include the lock-in, sub-harmonic resonances and hysteresis.

The problem of vortex-induced vibrations of cylindrical structures has been treated by the frequency-domain (spectral) approach by BLEVINS *et al*. [5], VICKERY *et al*. [102,103], WOOTTON [107] and others. In the correlation model of BLEVINS and BURTON [5], the vortex-induced aerodynamic forces are presented by a narrow-band stationary random process. The aeroelastic action of the line-like structure is considered in a sense that the exiting coefficients and spanwise correlation of fluctuating across-wind force are assumed to be dependent upon the vibration amplitude.

With couple of expectations, the vortex-shedding models for bridge decks are semi-empirical in nature, i.e. the models contain free parameters that are to be determined through the section model or other type of experiments [82]. Obviously, in the context of aeroelastic section models, the conventional harmonic force model is the most widely applied method to predict a prototype bridge response. It is discussed by IRWIN [35] that, if the damping ratio is similar and the spanwise load correlation reduction effect is accounted for, the model roughly yields to the result that the observed non-dimensional amplitudes are similar to the prototype bridge.

The model of SCANLAN [82], employing the fundamental van Der Pol type nonlinear oscillator, has received attention in bridge analysis. In the lock-in condition, this model neglects the harmonic excitation force because of its unimportance compared with the aerodynamic damping force. The lock-in dynamics of an aeroelastic section model is assumed to be governed by the formula

$$m(\ddot{\eta} + 2\omega_\eta\zeta_\eta\dot{\eta} + \omega_\eta^2\eta) = qh\left(1 - \varepsilon_K\frac{\eta^2}{h^2}\right)H_\eta\dot{\eta} \ , \tag{13}$$

in which ε_K and H_η are the empirical non-dimensional constants. Neglecting the effects of flow three-dimensionality, the extension of model for predicting the maximum response of the prototype bridge is straightforward [82,95]. EHSAN and BOSCH have contributed the model by deducing refined models for the load correlation. Furthermore, the improved identification technique to extract the free parameters and the verification study are given by EHSAN and SCANLAN [21].

SCANLAN [90] has also proposed a linear model for analysis of bridges that is in many senses

similar to the flutter model, except that the harmonic force is added to represent the vortex-induced aerodynamic excitation in the lock-in conditions. The free parameters incorporated are derived by matching the rate of growth and limiting amplitude characteristics found in section model experiments. Here, the model is released from an initially displaced position by a similar manner as in free-vibration flutter derivatives extraction [78].

It can be expected that the possible interaction between the vortex-induced vibration and galloping, as inspected by CORLESS and PARKINSON [13] among others, has minor interest in the analysis of bridges since the galloping onset wind velocity should be beyond the design wind speed in successful designs.

1.4.5 Buffeting theory

The importance of bridge buffeting was pointed out by DAVENPORT [14,15,16] in the 1960's. His calculation model was based on the frequency-domain approach, the spectral analysis of random vibration theory. In the model, the variances of vibration amplitudes are the primary quantities to be solved rather than deterministic response time histories. With the knowledge of the probability distribution of loading, the peak response at the specific time interval can be calculated by the mathematical means. An alike statistical concept has been proposed earlier for the aeroplane buffeting problem by LIEPMANN [51]. In the model, the response is approximated by superimposing uncoupled single-degree-of-freedom mode responses. The variance of normal coordinate σ_{qi}^2 associated with the *i*th mode is expressed by the equation

$$\sigma_{qi}^2 = \int_0^\infty |H_i(n)|^2 S_{Qi}(n) dn \approx \sigma_{Bi}^2 + \sigma_{Ri}^2 , \tag{14}$$

in which $S_{Qi}(n)$ is the one-sided spectral density of the modal load and $H_i(n)$ is the modal frequency response function. Here, the "background response" σ_{Bi}^2 and the "resonant response" σ_{Ri}^2 are given by

$$\begin{cases} \sigma_{Bi}^2 = \dfrac{1}{\tilde{K}_i^2} \displaystyle\int_0^\infty S_{Qi}(n) dn \\ \sigma_{Ri}^2 = \dfrac{\pi}{4(\zeta_i + \zeta_{Ai})\tilde{K}_i^2} n_i S_{Qi}(n_i) dn , \end{cases} \tag{15}$$

where n_i is the natural frequency, ζ_i is the modal damping ratio due to the mechanical damping, ζ_{Ai} is the modal damping ratio due to the aerodynamic damping and $\tilde{K}_i$ is the generalized stiffness of the *i*th mode. An application of reasonable scaled turbulence in section model experiments, makes it possible to predict the prototype bridge buffeting directly from the measured response of the scale model by means of Eq. (14). The approach of LAROSE [108] combines Davenport's buffeting theory and the wind tunnel test results in this manner. Obviously, this model also accounts for the signature turbulence induced vibrations.

As far as numerical models are concerned, the assumption of uncoupled modes is not feasible in all cases. It might yield error in circumstances where two or more modes have natural frequencies close to each other and/or where coupling on account of aeroelastic loads is significant. In general, the mode shapes of cable-stayed bridges can exhibit such behaviour. Rigorous frequency-domain coupled-mode approaches have been developed by several authors including Refs [38,40,41,45,69].

For such models, the simplified equations based on Eq. (14) can still serve the purpose of useful verification tool.

The primary problem in deducing reliable buffeting estimates is the determination of the spectral density of modal load. One should have knowledge at least of a) mode shapes of the girder, b) turbulence spectrums, c) spanwise coherence characteristics of the turbulence and d) steady aerodynamic coefficients of the deck section. Furthermore, as discussed by DAVENPORT [16], the correction factor termed aerodynamic admittance is usually needed to reckon with the inadequateness of the quasi-steady aerodynamic theory, i.e. the disparity between the actual load spectrum and the spectrum determined by means of the steady aerodynamic coefficients. Aerodynamic admittance functions are commonly assumed dependent upon the reduced frequency. Outside the vortex-shedding lock-in regimes, the value of aerodynamic admittance is close to unity in the very low-frequency range and reduces towards zero with the increasing frequency. From this viewpoint, the effects of certain aerodynamic admittance functions are conservatively neglected in some studies including those that deal with suspension bridges with very low fundamental natural frequencies [40,41]. On the other hand, the field measurements of cable-stayed bridges [3] and typical suspension bridges have indicated that this correction is essential for the reliable response estimation.

2 MODEL FOR SIMULTANEOUS CALCULATION OF BUFFETING AND FLUTTER RESPONSES

2.1 Initial assumptions

There are numerous assumptions that should be considered in order to deduce mathematical models for the fluid-structure interaction problem. For the analysis of bridges they are well established and the most important ones for the present aims can be listed as follows:

a) For the superposition principle of aerodynamic forces to hold, vibration amplitudes of a bridge deck are assumed to be small (lower than ±3 Deg in torsion, say).
b) The aeroelastic loads and the associated flutter derivatives are assumed to be functions of the mean reduced frequency and static twisting angle of the deck. The spanwise correlation of aeroelastic loads is assumed to be perfect.
c) The aerodynamic strip hypothesis is valid, i.e. the aerodynamic forces acting on a deck section (strip) are not influenced by the flow conditions at the strip vicinity.
d) The spatial correlation of fluid velocity fluctuations and the buffeting load they induce are considered to be identical.
e) The dynamical system is representable by means of the linear equations of motion around the equilibrium position. The equilibrium position is dependent upon the mean wind velocity.
f) Winds considered are assumed to be strong, the mean values of order 10 m/s or higher, for the referred turbulence models to be valid.
g) The buffeting excitation is assumed to be a stationary ergodic random process, i.e. the conditions of rapid change at mean wind velocity (rising and settling phases of storms) are not considered.
h) The horizontal across-wind component of turbulence spectrum $S_{vv}(n)$ is assumed to have unimportant effects on the structural response and is neglected for the computational efficiency.
i) Lateral wind velocity components perpendicular to bridge spans are assumed to produce dominant wind actions to bridge decks.

Generally, none of the assumptions mentioned above are found to be restrictive in the sense, that they should be relaxed in analysis of typical long-span bridges, with expectations:

j) In analysis of a bridge construction stage, the strip hypothesis may yield error, if the effects of the finite aspect ratio of the girder are not accounted for.
k) Winds parallel to bridge span can cause notable buffeting during the cantilever construction of cable-stayed bridges [87].
l) Conservative models for coherence decay characteristics can be assumed to account for possible increase of load correlation vs. fluctuation velocity correlations [1,19,38,86].

The assumptions are not intended to be fully accepted in all cases, but in the present development it is believed that their implications are small or negligible in comparison to uncertainties in the structural and aerodynamic data.

2.2 Wind-induced loads subjected to deck sections

Benefiting the superposition principle of aerodynamic forces, the vector representing wind-induced loads can be divided into the aeroelastic $\mathbf{f}_{Ae}$, steady $\mathbf{f}_{St}$ and buffeting $\mathbf{f}_b$ parts by formula

$$\mathbf{f}_i(t) = \mathbf{f}_{Ae} + \mathbf{f}_{St} + \mathbf{f}_b \ , \tag{16}$$

in which $\mathbf{f}_i(t)$ is the aerodynamic load vector of node *i.* The sign conventions employed are illustrated in *Fig. 3*.

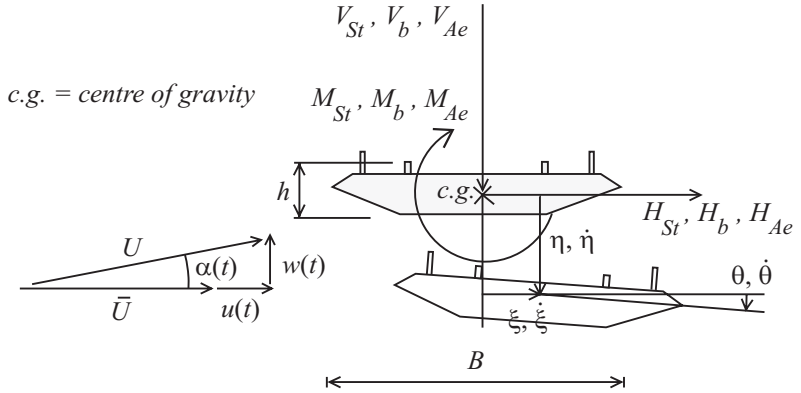

Fig. 3 Sign conventions for the simultaneous buffeting and flutter analysis.

2.2.1 Aeroelastic loads

The vector representing aeroelastic nodal-loads is obtained by inserting the mean wind velocity to Eqs (6). By completing the expressions of aeroelastic loads to contain all the 18 flutter derivatives, the result can be written as

$$\mathbf{f}_{Ae} = \bar{q}Bl\bar{K}\begin{Bmatrix} P_1^*\frac{\dot{\xi}}{\bar{U}} + P_2^*\frac{B\dot{\theta}}{\bar{U}} + \bar{K}P_3^*\theta + \bar{K}P_4^*\frac{\xi}{B} + P_5^*\frac{\dot{\eta}}{\bar{U}} + \bar{K}P_6^*\frac{\eta}{B} \\ H_1^*\frac{\dot{\eta}}{\bar{U}} + H_2^*\frac{B\dot{\theta}}{\bar{U}} + \bar{K}H_3^*\theta + \bar{K}H_4^*\frac{\eta}{B} + H_5^*\frac{\dot{\xi}}{\bar{U}} + \bar{K}H_6^*\frac{\xi}{B} \\ B\left(A_1^*\frac{\dot{\eta}}{\bar{U}} + A_2^*\frac{B\dot{\theta}}{\bar{U}} + \bar{K}A_3^*\theta + \bar{K}A_4^*\frac{\eta}{B} + A_5^*\frac{\dot{\xi}}{\bar{U}} + \bar{K}A_6^*\frac{\xi}{B}\right) \end{Bmatrix}, \tag{17}$$

where $\bar{q} = \frac{1}{2}\rho\bar{U}^2$ is the mean kinetic pressure of air, $\bar{K} = B\omega/\bar{U}$ is the mean reduced frequency and l is the nodal interference length, i.e. the length from which spanwise distributed load is subjected to the node. Here, in comparison to Eqs (6), the flutter derivatives with subscripts 5 and 6 are the complementary terms. These terms, and the horizontal terms in general, have recently received attention in the analysis of very long-span bridges [40,41]. Eq. (17) can be split into the form

$$\mathbf{f}_{Ae} = \mathbf{c}_{ii}\dot{\mathbf{x}}_i + \mathbf{k}_{ii}\mathbf{x}_i \,, \tag{18}$$

in which $\mathbf{x}_i$ is the nodal degree-of-freedom vector of node i with components given in order ξ, η and θ. Here, matrices $\mathbf{c}_{ii}$ and $\mathbf{k}_{ii}$ are given by the formulae

$$\mathbf{c}_{ii} = \frac{\bar{q}Bl\bar{K}}{\bar{U}}\begin{bmatrix} P_1^* & P_5^* & BP_2^* \\ H_5^* & H_1^* & BH_2^* \\ BA_5^* & BA_1^* & B^2A_2^* \end{bmatrix}, \tag{19}$$

and

$$\mathbf{k}_{ii} = \bar{q}l\bar{K}^2\begin{bmatrix} P_4^* & P_6^* & BP_3^* \\ H_6^* & H_4^* & BH_3^* \\ BA_6^* & BA_4^* & B^2A_3^* \end{bmatrix}. \tag{20}$$

The aerodynamic damping matrix and the aeroelastic stiffness matrix in Eq. (1) can be formed through Eqs (19) and (20). The other elements of matrices except those on the diagonal bands are zeros.

2.2.2 Steady aerodynamic loads

By means of the steady aerodynamic coefficients, the static nodal-load vector can be given as

$$\mathbf{f}_{St} \equiv \bar{q}Bl\begin{Bmatrix} C_H \\ C_V \\ BC_M \end{Bmatrix}, \tag{21}$$

where C_H is the steady aerodynamic coefficient associated with the horizontal force and C_M is the steady aerodynamic coefficient for the twisting moment. The steady aerodynamic coefficients and their relation to the steady angle of attack are to be determined via wind tunnel experiments involving a rigid section model. Here, time-averaged forces are measured typically by means of a balance constraining the model or by integration over the measured surface pressures.

In order to evaluate the mean wind velocity at alternating heights, the logarithmic law is assumed as [22,49]

$$\bar{U} = \frac{u_*}{\kappa}\left(\ln\frac{z}{z_0} + 34.5\frac{f_C z}{u_*}\right), \qquad (f_C = 2\Omega_E \sin\varphi_b), \tag{22}$$

where z_0 is the surface roughness parameter, κ is the von Kármán constant, u_* is the friction velocity, f_C is the Coriolis parameter, Ω_E is the angular rotation velocity of the Earth and φ_b is the latitude of bridge site. The constants involved in Eq. (22) are taken as $\kappa = 0.4$ and $\Omega_E = 72.9 \cdot 10^{-6}$ rad/s. The friction velocity is given by the formula [49]

$$u_* = \frac{\kappa}{\ln\dfrac{z_{10}}{z_0}} \left(\bar{U}_{10} - 34.5\frac{f_C z_{10}}{\kappa} \right) , \tag{23}$$

in which $z_{10} = 10$ m is the reference height (10 m above the ground zero level) and $\bar{U}_{10}$ is the mean wind velocity at that height. The logarithmic law of Eq. (22) can be expected to be valid in the lowest 200 m of the atmospheric boundary layer [49]. Due to fact that the friction velocity is found approximately constant up to the height of 30 m [22,49] the possibility of choosing another reference height than 10 m can be utilized in measurements.

2.2.3 Buffeting loads

In consistent to *Fig. 3*, the horizontal component of wind velocity at instant t can be presented as $U = \bar{U} + u(t)$, where $u(t)$ is the longitudinal component of the fluctuating velocity. For the horizontal mean wind velocity the vertical wind velocity component is characterized by the corresponding transverse fluctuating velocity component $w(t)$. The approximation for the angle of attack $\alpha(t) \approx w(t)/\bar{U}$ and the linear expression for the steady aerodynamic coefficient $C_i(\alpha) \approx C_i + \alpha(t) dC_i/d\alpha$, ($i = H$, V or M), yield the common quasi-steady approximation for the buffeting nodal-load vector

$$\mathbf{f}_b \approx \bar{q}Bl\frac{2u(t)}{\bar{U}} \begin{Bmatrix} C_H \\ C_V \\ BC_M \end{Bmatrix} + \bar{q}Bl\frac{w(t)}{\bar{U}} \begin{Bmatrix} \dfrac{dC_H}{d\alpha} \\ \dfrac{dC_V}{d\alpha} \\ B\dfrac{dC_M}{d\alpha} \end{Bmatrix} . \tag{24}$$

Here, the second-order terms containing fluctuation velocity components squared are neglected. For the special cases of vertically inclined mean wind velocities, the steady aerodynamic coefficients in Eq. (24) can be replaced correspondingly. Eq. (24) is generally known to be valid as the first approximation only, because of the frequency dependence of buffeting loads at high values of the reduced frequency. The inadequacy can be examined through the frequency response related to a sinusoidally acting vertical or horizontal component of the fluctuating velocity. By inserting the corrective transfer function separately to both components, the Fourier transform of the buffeting nodal-load vectors is expressed as

$$\hat{\mathbf{f}}_b = \bar{q}Bl\frac{2\hat{u}(\omega)}{\bar{U}} \begin{Bmatrix} C_H\Theta_{Hu}(\omega) \\ C_V\Theta_{Vu}(\omega) \\ BC_M\Theta_{Mu}(\omega) \end{Bmatrix} + \bar{q}Bl\frac{\hat{w}(\omega)}{\bar{U}} \begin{Bmatrix} \dfrac{dC_H}{d\alpha}\Theta_{Hw}(\omega) \\ \dfrac{dC_V}{d\alpha}\Theta_{Vw}(\omega) \\ B\dfrac{dC_M}{d\alpha}\Theta_{Mw}(\omega) \end{Bmatrix} , \tag{25}$$

where $\Theta_{iu}(\omega)$ and $\Theta_{iw}(\omega)$, with ($i = H$, V or M), are the complex-valued correction functions associated with the horizontal and vertical components of the fluctuation velocity, respectively. The non-zero imaginary parts of the correction functions incorporate the fact that the aerodynamic load lags behind the wind speed fluctuations.

Analytical expressions for the correction functions are not established, except for the potential flow solution of a thin aerofoil. For the thin aerofoil (or a flat plate), functions $\Theta_{Vw}(\omega)$ and $\Theta_{Mw}(\omega)$ take the value of Sears' function denoted by symbol Θ_w [26]. Furthermore, the correction functions $\Theta_{Vu}(\omega)$ or $\Theta_{Mu}(\omega)$ are solved by HORLOCK [32]. The associated function, that functions $\Theta_{Vu}(\omega)$ and $\Theta_{Mu}(\omega)$ coalesce, will be termed the Horlock function herein and will be denoted by symbol Θ_u. Sears' and Horlock functions are illustrated in *Fig. 4*. Their exact values [26,32] can be shown to be related to Theodorsen's function as

$$\begin{cases} \Theta_w(k) = C(k)[J_0(k) - \mathrm{i}J_1(k)] + \mathrm{i}J_1(k) \\ \Theta_u(k) = \dfrac{C(k)}{2}[J_0(k) - \mathrm{i}J_1(k)] + \dfrac{J_0(k)}{2} + \mathrm{i}J_1(k) \ . \end{cases} \tag{26}$$

The Horlock function in *Fig. 4* and in Eqs (26) is taken as half of the value appearing in the original reference for the scaling factor 2 included in Eqs (25). It can be observed from *Fig. 4* that as the reduced frequency approaches infinity the arguments of the functions change rapidly while the modulus approach zero. On account of Eqs (4) and (26) it can be expected that there exist relations between the flutter derivatives and the aerodynamic admittances, like those suggested by SCANLAN in Ref. [88].

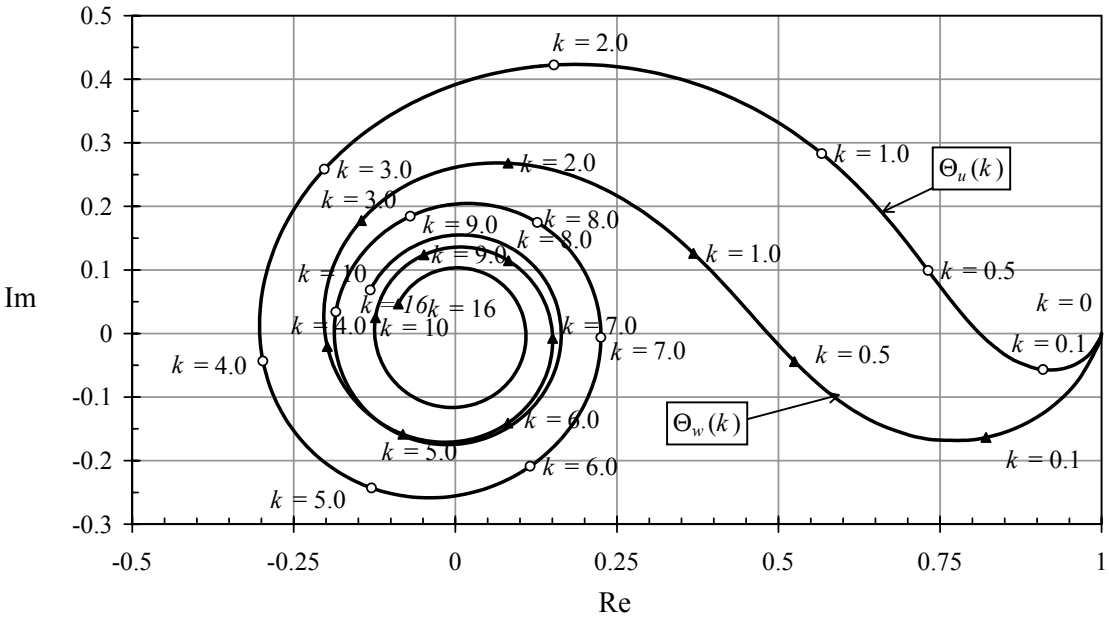

Fig. 4 The real (Re) and imaginary (Im) components of the complex-valued Sears' and Horlock functions.

Of primary interest in buffeting analysis is the absolute value of correction functions squared, referred as aerodynamic admittance functions. The aerodynamic admittance functions corresponding to Sears' and Horlock functions are illustrated in *Fig. 5*. Also shown are the real and imaginary parts of the complex products $\Theta_u \Theta_w^*$ and $\Theta_u^* \Theta_w$. These products appear in the spectral formulation of buffeting loads. The Sears-type admittance function has found successful applications in the

buffeting analysis of bridges while the Horlock-type admittance is not widely examined. There is some debate concerning the applicability of Sears' function to all kinds of bridge cross-sections and to every load component [3,40]. It is apparent in *Fig. 5* that, as far as the analytical aerodynamic admittance functions are concerned, the reduction effect in typical resonance frequency range of long-span bridges imposed to strong winds is around 40...60 %. Furthermore, the imaginary parts of cross-products $\Theta_u\,\Theta_w^*$ and $\Theta_u^*\Theta_w$ are small in comparison to the real parts. The response reduction effect of the aerodynamic admittance functions can be of order that it should be taken into account in the rigorous buffeting analysis of long-span bridges. The reduction effect for the fluctuation velocity *u*-component is significantly smaller than for the *w*-component. Therefore, the assumption of Sears-type admittance to both components, as applied occasionally in literature, seems to be unjustified from the theoretical point of view.

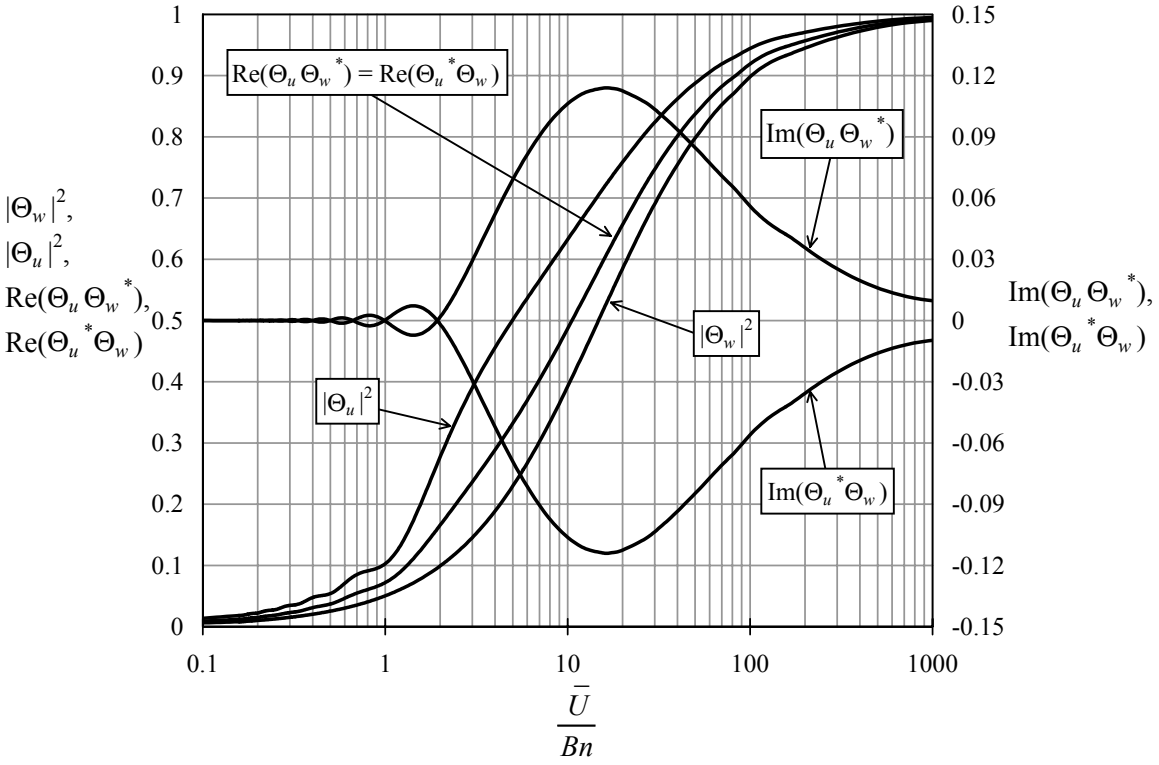

Fig. 5 Analytical aerodynamic admittance functions and associated cross-products for a flat plate plotted against the mean reduced velocity.

2.3 Determination of equations for spectral analysis

Considering a global element model, it is convenient to express all cross-covariance functions, related to the statistical dependence of nodal buffeting loads and associated nodal responses, systematically by means of cross-covariance matrices. The cross-covariance matrices for the buffeting loads and the associated response, respectively, can be defined as

$$\begin{cases} \mathbf{R}_b(\tau) = \lim\limits_{T\to\infty}\dfrac{1}{T}\displaystyle\int_{-T/2}^{T/2}\mathbf{F}_b(t)\,\mathbf{F}_b^T(t+\tau)dt \\ \mathbf{R}_x(\tau) = \lim\limits_{T\to\infty}\dfrac{1}{T}\displaystyle\int_{-T/2}^{T/2}\mathbf{X}(t)\,\mathbf{X}^T(t+\tau)dt\ , \end{cases} \qquad \textbf{(27)}$$

where T is the time period, τ is the time lag and superscript (T) denotes transpose. The cross-covariances in Eqs (27) can be transformed into the frequency domain by performing the Fourier transformation to each element. The cross-spectral density matrix $\mathbf{S}_i(\omega)$ and the associated cross-covariance matrix $\mathbf{R}_i(\tau)$ are related through the Wiener-Khintchine equations

$$\begin{cases} \mathbf{S}_i(\omega) = \int_{-\infty}^{\infty} \mathbf{R}_i(\tau) e^{-i\omega\tau} d\tau , & (i = b \text{ or } x) \\ \mathbf{R}_i(\tau) = \dfrac{1}{2\pi} \int_{-\infty}^{\infty} \mathbf{S}_i(\omega) e^{i\omega\tau} d\omega . \end{cases} \tag{28}$$

Here, since the constant $1/(2\pi)$ is added into the inverse transform, the response variance σ_i^2 is obtained by integrating over the frequency range using the formula

$$\sigma_i^2 = \int_{-\infty}^{\infty} S_{ii}(\omega) d\omega , \tag{29}$$

in which $S_{ii}(\omega)$ is the diagonal element of interest in the response cross-spectral density matrix.

The frequency-domain equations of motion (1) can be rewritten into the form

$$\mathbf{B}_c(\omega)\hat{\mathbf{X}}(\omega) = \hat{\mathbf{F}}_b(\omega) , \tag{30}$$

in which the aeroelastically influenced complex dynamic stiffness matrix $\mathbf{B}_c(\omega)$ is given by

$$\mathbf{B}_c(\omega) = -\omega^2\mathbf{M} + i\omega(\mathbf{C} - \mathbf{C}_{Ae}) + \mathbf{K} - \mathbf{K}_{Ae} . \tag{31}$$

The solution of Eq. (30) is obtained as

$$\hat{\mathbf{X}}(\omega) = \mathbf{H}_c(\omega)\hat{\mathbf{F}}_b(\omega) , \tag{32}$$

where $\mathbf{H}_c(\omega)$ is the complex frequency response matrix obtained through the matrix inversion of the complex dynamic stiffness matrix; $\mathbf{H}_c(\omega) = \mathbf{B}_c(\omega)^{-1}$. By inserting Eq. (32) to Eqs (27) and through taking the Fourier transform by means of Eqs (28) one gets the fundamental relation between the cross-spectral density matrices

$$\mathbf{S}_x(\omega) = \mathbf{H}_c(\omega)\mathbf{S}_b(\omega)\mathbf{H}_c(\omega)^{T*} . \tag{33}$$

In this general form, the multimode buffeting analysis is formulated by several authors [12,38,40,41,45]. The advantage achieved is that the resulting Eq. (33) accounts for the coupling terms due to the aeroelastic loads as well as due to the buffeting loads.

The flutter velocity and frequency can be detected on the condition that the complex dynamic stiffness matrix becomes singular. The typical approach in such analysis is to employ the state-space expansion to convert the problem to a first-order linear differential equation system. The complex-valued eigenvectors and eigenvalues of the resulting system matrix specify the singularity points of the system matrix and the flutter characteristics. Since the system matrix is dependent on an initially unknown flutter frequency, an iterative approach is required to find the flutter frequency that matches the eigenvalues at fixed wind speed. The iteration can be assisted by choosing initially

a flutter prone mode shape and the associated eigenfrequency. CHEN *et al*. [12] have demonstrated the non-iterative alternative for this concept by approximating the flutter derivatives by the rational functions. Other approaches to improve computation efficiency, with allowing some proximity to the analysis, include the pK-F method applied to bridges by NAMINI *et al*. [61].

In the present model, an alternate approach is employed. The flutter velocity and frequency are detected by the visual inspection of the response spectral density charts plotted for gradually incremented wind velocities. Around the singularity point, the height of a spectral peak approaches infinity as the width of the peak approaches zero. Illustrations of such behaviour are given by GARRICK *et al*. [28] and the author [45,46], among others. Historically, this kind of inspection of the structure's response around the critical wind velocity has been applied in the flight flutter testing of aeroplanes since 1935 [28]. From the theoretical point of view there is no difference between the present approach and the state-space approach. Instead of evaluating the complex-valued eigenvectors and eigenvalues of the system matrix, the present model involves inverses of the complex dynamic stiffness matrix. Iterative processes are avoided as the inverses are taken with fixed values of frequency and wind speed.

2.3.1 Expressions for the load spectral density matrix

In general, the fluctuating velocity components are known to be statistically dependent on each others. It follows that the statistical dependence is also transferred to the buffeting nodal-loads through Eqs (25) causing the load cross-spectral density matrix to become non-diagonal. Considering two nodes, denoted by subscripts *i* and *j*, the formal application of Eqs (25), (27) and (28) yields

$$\mathbf{S}_b(\omega) = \begin{bmatrix} \mathbf{s}_{12} & \mathbf{s}_{12} & \cdots & \mathbf{s}_{1N} \\ \mathbf{s}_{21} & \mathbf{s}_{22} & \cdots & \mathbf{s}_{2N} \\ \vdots & \vdots & \ddots & \vdots \\ \mathbf{s}_{N1} & \mathbf{s}_{N2} & \cdots & \mathbf{s}_{NN} \end{bmatrix}, \tag{34}$$

where the sub-matrices of size 3 x 3 are given by

$$\mathbf{s}_{ij} = \left(\frac{\bar{q}Bl}{\bar{U}}\right)_i \left(\frac{\bar{q}Bl}{\bar{U}}\right)_j \begin{bmatrix} 2C_H\Theta_{Hu}(\omega) & \dfrac{dC_H}{d\alpha}\Theta_{Hw}(\omega) \\ 2C_V\Theta_{Vu}(\omega) & \dfrac{dC_V}{d\alpha}\Theta_{Vw}(\omega) \\ 2BC_M\Theta_{Mu}(\omega) & B\dfrac{dC_M}{d\alpha}\Theta_{Mw}(\omega) \end{bmatrix}_i \begin{bmatrix} S_{uu}(\omega)J_{uu} & S_{uw}(\omega)J_{uw} \\ S_{wu}(\omega)J_{wu} & S_{ww}(\omega)J_{ww} \end{bmatrix}_{ij} \times$$

$$\times \begin{bmatrix} 2C_H\Theta^*_{Hu}(\omega) & 2C_V\Theta^*_{Vu}(\omega) & 2BC_M\Theta^*_{Mu}(\omega) \\ \dfrac{dC_H}{d\alpha}\Theta^*_{Hw}(\omega) & \dfrac{dC_V}{d\alpha}\Theta^*_{Vw}(\omega) & B\dfrac{dC_M}{d\alpha}\Theta^*_{Mw}(\omega) \end{bmatrix}_j . \tag{35}$$

Here, $S_{kl}(\omega)$, (k, $l = u$ or w) is the turbulence cross-spectral density associated with two nodes (i.e. at two points in space). Furthermore, coefficient J_{kl} is introduced for correcting the effects of

imperfect correlation of buffeting loads along the nodal interference length, i.e. for reducing the error deduced through lumping buffeting loads to the finite number of nodes. The coefficient will be termed the nodal-load correlation correction coefficient. For sufficient small interference lengths vs. correlation spanwise decay characteristics it can be taken as unity. The expression for the nodal-load correlation correction coefficient can be solved in closed form for the typical exponential correlation decay vs. separation (Appendix A). For other types of correlation models, the equivalent exponential decay is applied in the present study.

To complete the formation of the load cross-spectral density matrix, two types of meteorological data, to be treated subsequently, are required: a) the spectral densities at one point in space and b) the spatial model for evaluating the cross-spectral densities related to two separate points in space.

2.3.2 Turbulence model for one point in space

Considerable work has been carried out in order to establish universal curves that characterise spectral densities $S_{uu}(\omega)$ and $S_{ww}(\omega)$ in strong winds. Such curves can be presented in a non-dimensional form as a function of the dimensionless parameter $\omega L_s / \bar{U}$, in which L_s is the length scale of turbulence. Obviously, the length scales most typically employed in the wind engineering purposes are the integral length scales of turbulence and the height above the ground. In the present study, turbulence is modelled by the modified von Kármán model presented in the ESDU data sheets [22]. The spectrums are given in a one-sided form by the formula

$$\frac{nS_{ii}(n)}{\sigma_i^2} = G_i(n_i) , \qquad \left(n_i = \frac{n\,{}^{x}L_i}{\bar{U}} \right), \tag{36}$$

in which the subscript i refers to the u or w components of fluctuating velocity, σ_i^2 is the variance of the fluctuating velocity component, $G_i(n_i)$ is the non-dimensional function and ${}^{x}L_i$ is the integral length scale of turbulence (integrated in along-wind direction). The integral length scales in the modified von Kármán model are dependent on the mean wind velocity, reflecting trends that the height of the boundary layer and the size of the large scale eddies increase with the wind speed, when observed relatively far from the ground. Close to the ground, the length scales are independent of the wind velocity but dependent upon the surface roughness, so that the length scales decrease with the increasing terrain roughness. Function $G_i(n_i)$ satisfies the conditions

$$\int_0^\infty \frac{1}{n} G_i(n) dn = \int_0^\infty \frac{1}{n_i} G_i(n_i) dn_i = 1 , \qquad (i = u \text{ or } w). \tag{37}$$

The integral length scales in the modified von Kármán model are to be determined adopting Taylor's hypothesis of "frozen gust" [49] (along the direction of mean wind, time and distance variables are interchangeable), i.e. the expression for the integral length scale is

$${}^{x}L_i = \frac{\bar{U}}{\sigma_i^2} \int_0^\infty R_{ii}(\tau)\, d\tau , \qquad (i = u \text{ or } w). \tag{38}$$

Eqs (28) and (38) imply the constraint for the spectral density at zero frequency $S_{ii}(0)$ and the integral length scale by [95]

$$ {}^{x}L_i = \frac{\bar{U}}{4} \frac{S_{ii}(0)}{\sigma_i^2}, \qquad (i = u \text{ or } w). \tag{39} $$

This equation can be utilized in the determination of integral length scales directly from the measured spectrums.

The magnitude of velocity fluctuations is characterised by the non-dimensional quantity termed the turbulence intensity. Turbulence intensity component I_i is defined as

$$ I_i = \frac{\sigma_i}{\bar{U}}, \qquad (i = u \text{ or } w), \tag{40} $$

where σ_i is the standard deviation of fluctuation velocity component (= $\sqrt{\sigma_i^2}$). Here, as well as in the spectrum measurements, the averaging time is typically one hour because of the properties of wind gustiness [49].

The modified von Kármán model is given with respect to equilibrium conditions, i.e. for upwind fetch of uniform terrain of some 30 km, ideally 600 km [22]. In other circumstances local values for the integral length scales, turbulence intensities and roughness parameters are instructed to be applied.

For the present aims, the choice of the turbulence model is argued as follows:

a) It is expected that the model can give a realistic presentation of turbulence at wider range of wind velocities in comparison to structural designs spectrums tuned for the high design winds.
b) The model provides a proven method to calculate the spectral density component $S_{ww}(n)$, that in most cases possesses the greatest importance in the bridge deck buffeting analysis, with the data obtained in the along-wind direction. This data, on the other hand, can be measured, in minium, by single anemometer located at the bridge site.

Cross-spectrums $S_{uw}(\omega)$ and $S_{wu}(\omega)$ have recently received attention [38] in the analysis of bridges. In many studies these are neglected. This relaxation seems to be artificial from the theoretical point of view, because bridges are relatively close to the ground, where the turbulence is known to be anisotropic. Furthermore, the mathematical theory of boundary layer flow presumes that for turbulence to exist, the cross-spectrum and the related Reynolds stresses cannot vanish.

The general behaviour of the real part (co-spectrum) of cross-spectrums $S_{uw}(\omega)$ and $S_{wu}(\omega)$ in the boundary layer turbulence is known from experiments. In the low-frequency range, associated with the large-scale eddies, the co-spectrum is negative in sign. This results from the fact that the mean wind velocity increases upwards resulting the downwards moving air (i.e. $w(t) < 0$) to have greater component in the mean wind direction than the air moving upwards (i.e. $w(t) > 0$). Towards higher frequencies and smaller wavelengths, the co-spectrum falls to zero, as turbulence becomes isotropic.

The imaginary part of the cross-spectrum between the u and w velocity components (quadrature-spectrum) contributes nothing to a structural response because its effect cancels out [23]. This feature follows form the stationarity assumption resulting $S_{uw}(\omega) = S_{wu}(\omega)^*$, i.e. the imaginary parts have the equal magnitudes but the opposite signs. In the subsequent analysis the quadrature-spectrum is ignored, but the co-spectrum is retained. The cross-spectrum is assumed to take the form [38,40,41]

$$\frac{nS_{uw}(n)}{u_*^2} = \frac{nS_{wu}(n)}{u_*^2} = -\frac{14\,\frac{nz}{\bar{U}}}{(1+9.6\frac{nz}{\bar{U}})^{2.4}} \,. \tag{41}$$

Published models for the cross-spectrum that cover the whole frequency range, and to which Eq. (41) can be compared with, seem to be rare.

JAIN *et al*. [38] reported two studies where the bridge buffeting responses have been underestimated 7 % and 25% due to exclusion of the cross-spectrums. By inspecting Eqs (35) and (41), one can suggest that if C_i and $dC_i/d\alpha$ have the equal signs the buffeting response will be decreased due to the action of cross-spectrum and vice versa.

2.3.3 Spatial description of turbulence

The cross-spectrum between two points in space is generally complex-valued despite that the one-point spectrum in either of the points is real-valued. The non-zero imaginary part accounts for the possibility that, if a disturbance in fluid is observed in one point, the same disturbance is obtained in the other point at some later time [23]. The absolute value of the two-point cross-spectrum is generally expressed by means of the root cross-coherence function $\chi_{kl}(\omega)$ as

$$|S_{kl}(\omega)|_{ij} = \sqrt{|S_{kl}(\omega)|_i |S_{kl}(\omega)|_j}\ \chi_{kl}(\omega)\ , \qquad (k,\ l = u \text{ or } w). \tag{42}$$

Here, the subscripts i and j refer to the points i and j in space, respectively. The empirical exponential decay law is widely applied in wind engineering applications. By this law the coherence function for the given component of the fluctuation velocity is expressed as

$$\chi_{kk}(\omega) = e^{C_{kk}(\omega)}\ , \qquad (k = u \text{ or } w), \tag{43}$$

where $C_{kk}(\omega)$ is the non-dimensional function. The well-known expression for function $C_{kk}(\omega)$ is given by [95]

$$C_{kk}(\omega) = -\frac{\omega}{\pi(\bar{U}_i + \bar{U}_j)} \sqrt{c_x^2\Delta_x^2 + c_y^2\Delta_y^2 + c_z^2\Delta_z^2}\ , \qquad (k = u \text{ or } w), \tag{44}$$

where c_l and Δ_l are the decay coefficient and the separation in the direction of $l = x, y$ or z coordinate, respectively. Here, the global Cartesian coordinate system for the structure is fixed x-axis parallel to the direction of horizontal mean wind velocity and z-axis parallel to the vertical direction. For spanwise separations the square-root expression in Eq. (44) simplifies into the form $c_y|\Delta_y|$. If an empirical coherence data at the bridge site is available, Eq. (44) provides simple relation for the interpolation of decay coefficients. The model of Eqs (43) and (44) will be termed the conventional exponential coherence model herein.

Some investigators, including JANCAUSKAS and SANKARAN [39], have found that, if one is deducing coherence models applicable to varying turbulence environments, the integral length scales of turbulence can be favoured to make the decay function $C_{kk}(\omega)$ non-dimensional. Furthermore, on the frequency range close to zero, Eq. (44) imposes that velocity fluctuations at two distinct points in space are completely correlated, which seems not to be the case in the atmosphere [23]. This property has recently obtained attention in the design of very long-span

bridges as it might cause the background part of the buffeting response to be overestimated. An attempt is made in the ESDU coherence model [23] to account for this defect. MANN *et al*. [55] represent experimental results related to the Great-Belt Bridge coherence measurements from which advantages of the model can be observed. In the ESDU coherence model, the relation between the coherence decay and the integral length scales of turbulence is invoked. The coherence functions can be derived through the "sequential calculus" as

$$\begin{cases} C_{uu}(\omega) = -1.15\left[(0.747 r_u)^2 + c_u^2 \dfrac{\omega^2}{U_m^2}(\Delta_y^2 + \Delta_z^2)\right]^{0.75} \\ C_{ww}(\omega) = -0.65\left[(0.747 r_w)^2 + c_w^2 \dfrac{\omega^2}{U_m^2}(\Delta_y^2 + \Delta_z^2)\right]^{0.65} \\ c_i = \dfrac{1.6 r_i^{0.13}}{\left[(0.747 r_i)^2 + \dfrac{\omega^2}{\bar{U}_m^2}(\Delta_y^2 + \Delta_z^2)\right]^{b_i}}, \quad (\text{or } c_i = 1.0, \text{ whichever is greater}) \\ b_i = 0.175 r_i^{0.2} \\ r_i = \dfrac{\Delta_y^2 + \Delta_z^2}{2\sqrt{({}^{y}L_i \Delta_y)^2 + ({}^{z}L_i \Delta_z)^2}}, \quad (i = u \text{ or } w), \end{cases} \tag{45}$$

where $\bar{U}_m$ is the mean wind velocity at the mean height, i.e. at the average height of the two points considered. Furthermore, ${}^{y}L_u$, ${}^{z}L_u$, ${}^{y}L_w$ and ${}^{z}L_w$ are the integral length scales to be determined at the mean height. Expressions for these length scales reduce to the functions of the single length scale ${}^{x}L_u$ by

$$\begin{cases} {}^{y}L_u = (0.5 - 0.23\, e^{-c_B})\ {}^{x}L_u \\ {}^{z}L_u = (0.5 - 0.34\, e^{-c_B})\ {}^{x}L_u \\ {}^{y}L_w = (0.5 - 0.23\, e^{-c_B}) \left(\dfrac{I_w}{I_u}\right)^3 {}^{x}L_u \\ {}^{z}L_w = (1.0 - 0.68\, e^{-c_B}) \left(\dfrac{I_w}{I_u}\right)^3 {}^{x}L_u \\ c_B = 35\left(\dfrac{z}{h_B}\right)^{1.7} \\ \dfrac{I_w}{I_u} = 1 - 0.45 \cos^4\left(\dfrac{\pi}{2}\dfrac{z}{h_B}\right) \\ h_B = \dfrac{u_*}{6 f_C}, \end{cases} \tag{46}$$

where h_B is the boundary layer height. There is also the assumed relation between turbulence intensity components I_w and I_u shown in this equation.

The coherence models mentioned are compared in *Fig. 6* for the mean wind velocity of 30 m/s at the level of 30 m above the ground. The frequencies applied are 0.4 Hz and 0.002 Hz in order to illustrate the behaviour in the resonance and in the background frequency band, respectively.

Apparent in the figure is that the best fit between the ESDU coherence model and the conventional exponential law at 0.4 Hz is obtained through the decay parameter value about six. The value is quite typical in analysis. The trend at 0.002 Hz is quite dissimilar illustrating the imposed reduction of the background response. Furthermore, the *w*-component is significantly smaller than the *u*-component in the low-frequency range. This reflects to the bridge buffeting assessments as the *w*-component typically dominates the vertical response.

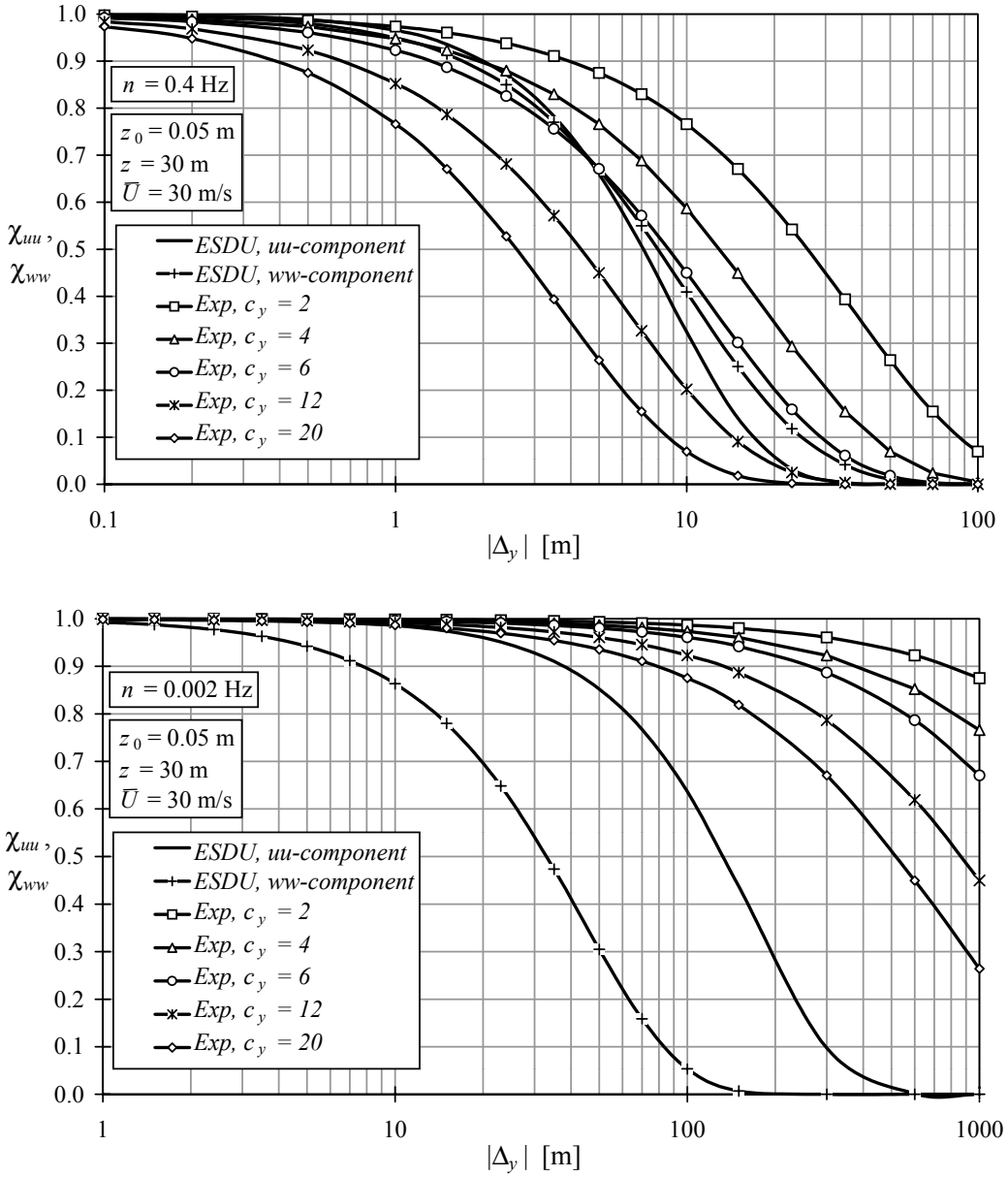

Fig. 6 Comparison between the ESDU and the conventional exponential (Exp) coherence models in typical resonance frequency and low frequency bands.

In the present study, the ESDU coherence model is used in the buffeting calculations. The choice is made for its inherent ability to reduce the number of open parameters to single parameter ${}^{x}L_{u}$ that is also required for the one-point spectrum model.

Also needed in the analysis is the root cross-coherence function between the *u* and *w* components of the fluctuation velocity. For this coherence function there seems to be lack of data

in literature. For the present model simple approximation, applied also by KATSUCHI *et al*. [41] and JONES *et al*. [40], is employed by

$$\chi_{uw}(\omega) = \chi_{wu}(\omega) = \sqrt{\chi_{uu}(\omega)\ \chi_{ww}(\omega)}\ . \tag{47}$$

With an established coherence function the real part ${}^{C}S_{kk}(\omega)$ and the imaginary part ${}^{Q}S_{kk}(\omega)$ of the cross-spectral density functions, associated with two points referred by subscripts *i* and *j*, can be expressed by the formula

$$\begin{cases} {}^{C}S_{kl}(\omega) = \sqrt{|S_{kl}(\omega)|_i |S_{kl}(\omega)|_j}\ \chi_{kl}(\omega)\ \cos\theta_{kl}\ , \\ {}^{Q}S_{kl}(\omega) = \sqrt{|S_{kl}(\omega)|_i |S_{kl}(\omega)|_j}\ \chi_{kl}(\omega)\ \sin\theta_{kl}\ , \end{cases} \qquad (k,\ l = u \text{ or } w) \tag{48}$$

in which θ_{kl} is the phase angle. The observed phase angles vary randomly in the atmosphere except for the vertical and along-wind separations [23]. Furthermore, the only imaginary component that might have practical importance for winds perpendicular to bridge spans, and which is found to be significantly non-zero, is the one related to the vertical separation and the *u*-component of the fluctuating velocity. Therefore, in analysis of horizontal structures, like bridge girders, the effects of the imaginary components can be ignored.

In the present model, all the phase angles are assumed to be zero, except phase angles θ_{uw} and θ_{wu} as they should account for the possible negative signs of the real part of the one-point cross-spectrums $S_{uw}(n)$ and $S_{uw}(n)$. When applying Eq. (41), however, the real parts are always negative resulting the approximation $\theta_{uw} = \theta_{wu} = \pi$ valid for the whole frequency range. It follows that the load spectral density matrix of the model is symmetric and real-valued.

2.3.4 Normal-mode method of solution

In order to solve Eq. (33) for structural models containing large number of unknowns, the normal-mode method can be invoked. The response is calculated by means of the normal coordinates by

$$\mathbf{X} = \tilde{\mathbf{\Phi}}\mathbf{q}\ , \tag{49}$$

where $\tilde{\mathbf{\Phi}}$ is the reduced modal matrix comprising the prescribed number of first eigenvectors $\boldsymbol{\varphi}_i$ (mode shapes) and $\mathbf{q}$ is the vector of normal coordinates $q_i(t)$. The eigenvalues and associated eigenvectors are calculated through the generalized eigenvalue problem

$$\mathbf{K}\boldsymbol{\varphi}_i = \omega_i^2 \mathbf{M}\boldsymbol{\varphi}_i\ , \tag{50}$$

in which ω_i is the *i*th undamped circular natural frequency. The scaling of eigenvectors is arbitrary. In the subsequent analysis they are assumed to be normalized with respect to the modal mass. Several numerical iteration schemes are available for solving the generalized eigenvalue problem, and some of them can be found in the commercial finite element (FE) programs for structural analysis. For the present development, however, it is not of primary interest, how the modal data actually is deduced, but the normalization is important as the normalized modes contain information of the structure's mass. When the normal coordinates are substituted into the equations of motion (1), and the terms are multiplied left by matrix $\tilde{\mathbf{\Phi}}^T$, the result can be expressed in the form containing reduced size matrices by

$$\tilde{\mathbf{B}}_c(\omega)\hat{\mathbf{q}}(\omega) = \tilde{\mathbf{\Phi}}^T\hat{\mathbf{F}}_b(\omega) \ , \tag{51}$$

where the modal stiffness matrix is

$$\tilde{\mathbf{B}}_c(\omega) = -\omega^2\tilde{\mathbf{I}} + \mathrm{i}\omega\tilde{\mathbf{\Phi}}^T\mathbf{C}\tilde{\mathbf{\Phi}} + \tilde{\mathbf{K}} - \tilde{\mathbf{\Phi}}^T\left[\mathrm{i}\omega\mathbf{C}_{Ae}(\omega) + \mathbf{K}_{Ae}(\omega)\right]\tilde{\mathbf{\Phi}} \ . \tag{52}$$

Here, $\tilde{\mathbf{I}}$ is the unit matrix and $\tilde{\mathbf{K}}$ is the diagonal matrix of the eigenvalues ω_i^2. In the elementary case of proportional mechanical damping, matrix product $\tilde{\mathbf{\Phi}}^T\mathbf{C}\tilde{\mathbf{\Phi}}$ in Eq. (52) yields also the diagonal matrix with terms given by $2\omega_i\zeta_i$. This approach is adopted in the present study; the mechanical damping is given by means of the modal damping ratios. An easy extension to general viscous damping models, including those due to the external dampers, can be disclosed. The solution of Eq. (51) is obtained as

$$\hat{\mathbf{q}}(\omega) = \tilde{\mathbf{B}}_c^{-1}(\omega)\tilde{\mathbf{\Phi}}^T\hat{\mathbf{F}}_b(\omega) \equiv \tilde{\mathbf{H}}_c(\omega)\tilde{\mathbf{\Phi}}^T\hat{\mathbf{F}}_b(\omega) \ , \tag{53}$$

where the modal frequency response matrix $\tilde{\mathbf{H}}_c(\omega)$ is obtained through an inverse of the modal stiffness matrix. By taking into account Eq. (49), the solution in the nodal coordinate system can be given as

$$\hat{\mathbf{X}}(\omega) = \tilde{\mathbf{\Phi}}\tilde{\mathbf{H}}_c(\omega)\tilde{\mathbf{\Phi}}^T\hat{\mathbf{F}}_b(\omega) \ . \tag{54}$$

Here, product $\tilde{\mathbf{\Phi}}\tilde{\mathbf{H}}_c(\omega)\tilde{\mathbf{\Phi}}^T$ can be interpreted to be the normal-mode approximation of complex frequency response matrix $\mathbf{H}_c(\omega)$ of Eq. (32). By means of this approximation Eq. (33) takes the form [12,44,45]

$$\mathbf{S}_x(\omega) = \tilde{\mathbf{\Phi}}\tilde{\mathbf{H}}_c(\omega)\mathbf{S}_Q(\omega)\tilde{\mathbf{H}}_c(\omega)^{T*}\tilde{\mathbf{\Phi}}^T \ , \tag{55}$$

in which the cross-spectral density matrix of modal buffeting load is given as

$$\mathbf{S}_Q(\omega) = \tilde{\mathbf{\Phi}}^T\mathbf{S}_b(\omega)\tilde{\mathbf{\Phi}} \ . \tag{56}$$

The variances of desired degree-of-freedom can be calculated by integrating over the frequency range applying Eqs (29) and (55).

Eq. (55) can be further developed into the form that might be more useful from the analysis point of view. The covariances of normal coordinates can be expressed in a matrix form and are calculated by integrating the elements of matrix $\mathbf{S}_q$ over the frequency range via the formula

$$\mathbf{\sigma}^2_{(0)} = \int_{-\infty}^{\infty}\mathbf{S}_q(\omega)\,d\omega \ , \tag{57}$$

in which $\mathbf{\sigma}^2_{(0)}$ is the covariance matrix of normal coordinates and the cross-spectral density matrix of normal coordinates is

$$\mathbf{S}_q(\omega) = \tilde{\mathbf{H}}_c(\omega)\mathbf{S}_Q(\omega)\tilde{\mathbf{H}}_c(\omega)^{T*} \ . \tag{58}$$

Similarly, the covariance matrices of modal velocity response $\mathbf{\sigma}^2_{(1)}$, modal acceleration response $\mathbf{\sigma}^2_{(2)}$ and modal responses related to higher time derivatives, are given by

$$\boldsymbol{\sigma}^2_{(\gamma)} = \int_{-\infty}^{\infty} \omega^{2\gamma}\, \mathbf{S}_q(\omega)\, d\omega \ , \qquad (\gamma = 1,\ 2,\ 3,\ ...). \tag{59}$$

The covariance matrices of Eqs (57) and (59) are to be expressed by means of the modal correlation coefficients that can be defined as

$$\mu_{(\gamma)ij} = \frac{\sigma^2_{(\gamma)ij}}{\sqrt{\sigma^2_{(\gamma)ii}\sigma^2_{(\gamma)jj}}} \ , \qquad (\gamma = 0,\ 1,\ 2,\ ...). \tag{60}$$

Here, the subscripts *i* and *j* denote the matrix index referring to the mode number and $\sigma^2_{(\gamma)\,ij}$ signifies the element of the covariance matrix. Finally, the response variance $\sigma^2_{(\gamma)x}$ of the degree-of-freedom of interest, denoted by subscript *x,* is given by

$$\sigma^2_{(\gamma)x} = \sum_{i}^{N_m}\sum_{j}^{N_m} \pm \mu_{(\gamma)ij}\sigma_{(\gamma)xi}\sigma_{(\gamma)xj} \ , \qquad (\gamma = 0,\ 1,\ 2,\ ...), \tag{61}$$

where N_m is the number of mode shapes considered in the analysis and the uncorrelated standard deviation response of the *i*th mode is given by

$$\sigma_{(\gamma)xi} = \sqrt{\varphi^2_{xi}\sigma^2_{(\gamma)ii}} \ , \qquad (\gamma = 0,\ 1,\ 2,\ ...). \tag{62}$$

The sign of the summation term in Eq. (61) is given by the sign of product $\varphi_{xi}\varphi_{xj}$, i.e. by the function signum($\varphi_{xi}\varphi_{xj}$). The advantage gained is that standard deviation responses of individual mode shapes involved in Eq. (61) can be utilized in calculation of the stress resultants caused by vibrations of the structure. Furthermore, the statistical dependence between the modal responses can be inspected from the magnitudes of the modal correlation coefficients.

From the bridge design point of view, the peak response amplitude is of interest. As far as the buffeting problem of long-span bridges is concerned, the peak amplitude can be obtained by multiplying the standard deviation response by a factor of order 3.5 to 4.0. The present model employs a rigorous calculation of peak factors applying the well-known expression given by DAVENPORT [14]. The peak factor $g_{(\gamma)}$ for a response component is taken as

$$g_{(\gamma)} = \sqrt{2\ln[\nu_{(\gamma)}T]} + \frac{0.5772}{\sqrt{2\ln[\nu_{(\gamma)}T]}} \ , \qquad (\gamma = 0,\ 1 \text{ or } 2), \tag{63}$$

where T is the averaging time of mean wind velocity (= 600 s or 1 h) and $\nu_{(\gamma)}$ is the zero up-crossing frequency. The zero up-crossing frequency is dependent on the details of the response spectrum of the nodal degree-of-freedom of interest and its magnitude alters slightly depending on, whether the deflection ($\gamma = 0$), velocity ($\gamma = 1$) or acceleration response ($\gamma = 2$) is concerned. The zero up-crossing frequency is given by Rice's formula

$$\nu_{(\gamma)} = \frac{1}{2\pi}\frac{\sigma_{(\gamma+1)x}}{\sigma_{(\gamma)x}} \ , \qquad (\gamma = 0,\ 1 \text{ or } 2). \tag{64}$$

The normal-mode method allows approximative calculation of the response for the static nodal-loads of Eq. (21). By neglecting the contribution of aeroelastic stiffness, the resulting nodal response

vector $\mathbf{X}_{St}$ can be written into the form

$$\mathbf{X}_{St} = \sum_{i=1}^{N_m} \frac{1}{\omega_i^2} \, \boldsymbol{\varphi}_i{}^T \mathbf{F}_{St} \boldsymbol{\varphi}_i \ , \qquad \textbf{(65)}$$

in which $\mathbf{F}_{St}$ is the vector of static nodal-loads. Since in the present model the wind speeds are to be analysed in ascending order (starting from the lowest value of interest and approaching the flutter velocity), the updated values of static angle of attacks can be easily applied in the analysis. Here, the approximative divergence analysis can be carried out simultaneously. In general, there can exist more than one equilibrium path as the deck can diverge by either positive or negative rotation. The simple linear approximation for the steady aerodynamic coefficient vs. angle of attack is assumed in the present study.

2.4 Discussion and sample implementation of the model

The present approach overcomes the labourious iteration of the flutter frequency due to the typical state-space expansion of system matrix involving the complex eigenvalue analysis [12,38]. For the flutter frequency and velocity to be identifiable from the response spectrums, the analysis should be carried out applying a sufficient frequency separation and a wind speed increment. The model employs the limited number of "still air" mode shapes in the analysis that is not guaranteed to be the best approximation under the influence of aeroelastic stiffness terms. It is discussed by SCANLAN [81] and SCANLAN *et al*. [86] that, as far as bridges are concerned, the implied error can be assumed to be small as the aeroelastic loads have not been found to change the natural mode shapes considerable; although there can exist shifts at eigenvalues (i.e. at natural frequencies). Furthermore, the possible errors can be inspected and simply eliminated by adding more mode shapes into the analysis. The present model accounts for special issues problematic to the line-like structural representation of bridges [34]. These include the mean wind induced static deflection effects on the modal coupling and the excursion of centre of rotation of a bridge stiffening girder. It allows one to inspect the buffeting and mean wind response up to the flutter velocity to detect that assumptions taken are justified and to obtain source data for inspecting that the bridge can resist the estimated oscillations.

The present approach does not provide features to examine the nature of instability in detail. The phase shift and relative magnitudes between the vertical bending and torsional modes at the coupled flutter, cannot be evaluated. For that kind of purposes, the multimode flutter models [12,38], based on the complex eigenvalue analysis, can be favoured.

The present numerical model allows certain modifications that speed up the calculation and reduce computer's base memory requirements. Significant memory and runtime savings can be achieved by removing zero multiplications from the matrix operations. It follows that the matrices applied should contain elements only for those nodes that are subjected to external loads and the response is intended to be calculated. The mode shape data employed can be based on as detailed model as desired. This is because a pre-processor program can be implemented to pick up the essential data from the original file containing the complete mode shape data.

The present calculation model, with the aforementioned modifications, is implemented with the standard FORTRAN-77 language for the computer code "BWIND-3" developed by the author. The flow chart of the code is shown in *Fig. 7*. The simultaneous buffeting and flutter analysis portion comprises five separate program units to be executed in order. External files are applied for the data interchange between the units.

The program calculates the static mean wind response using the modal approximation (the BWIND0 unit). The response can be fed back to update the steady aerodynamic coefficients and the associated nodal-loads with changing angle of attacks. Form the algorithmic point of view, this is implemented by simply dividing each velocity increment to a great number of sub-intervals. This feature is mainly included for the divergence analysis; the estimation of the divergence onset wind velocity with typical static FE-codes is in many cases problematic, as the load magnitude changes due to the structure's deflections or rotations.

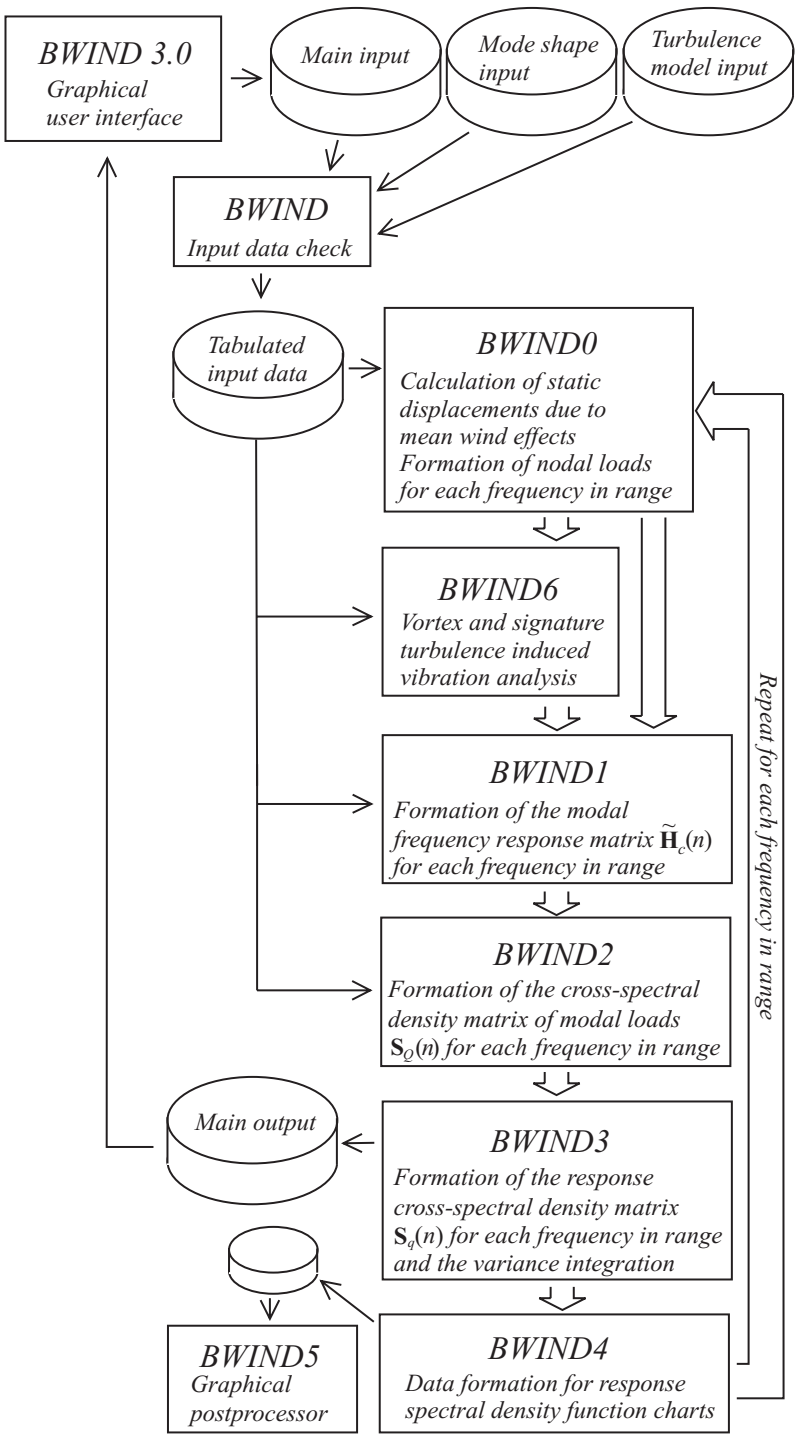

Fig. 7 Flow chart of the computer code BWIND-3 illustrating a tested implementation of the present numerical model.

The mode shapes and the turbulence model are to be inputted by the means of separate files. The purpose of the former file is to provide interface to the FE-codes applied in the modal analysis and the latter file to provide possibility to store and retrieve alternating turbulence models including those measured on bridge sites. Continuous functions are interpolated linearly between the data points specified in the input; the integral length scales of turbulence in two directions as they can be dependent on both the wind speed and height. The aerodynamic admittances are inputted by means of complex-valued functions containing the modulus and argument data vs. reduced wind velocity.

The BWIND-3 implementation reduces the computer's base memory and disk space requirements on a very affordable level. The runtime required for full analysis is dependent mainly on four quantities: a) number of loaded nodes, b) number of mode shapes, c) number of frequencies considered in the analysis and d) number of wind speeds analysed. The procedures involved require extensive floating point operations related to matrix algebra. Therefore, an application of computer with powerful computational capabilities can reduce the runtime significantly - from several hours to half an hour or less, say. Most of the run time is spent in the program unit BWIND2 (*Fig. 7*) that forms the cross-spectral density matric of modal buffeting loads. The coherence model applied has considerable effects in this context. For example, the ESDU coherence model is unfavourable as it requires calculation of the mean wind speed and the integral length scales at the mean height through complicated expressions.

3 CALCULATION MODEL FOR VORTEX AND SIGNATURE TURBULENCE INDUCED VIBRATIONS

The calculation models, presented herein for the vortex and signature turbulence induced vibration analysis, are semi-empirical in nature employing wind tunnel tests for aerodynamic input parameters. Among the various types of wind tunnel models and testing techniques available, the spring-supported section model to be tested in a smooth flow is chosen. Furthermore, only the flow speed and response time histories are assumed to be measured in experiments from which the essential input parameters have to be deduced. The primary purpose of the model is to predict the prototype bridge response by means of the measured responses of the section model. The approach taken can be reasoned as follows:

a) The smooth flow test provides a logical framework for estimating base values for design parameters related to the vortex-induced vibrations as the smooth flow usually yields the most severe response.
b) The aeroelastic section model, if properly scaled for the similarity requirements, directly accounts for the aeroelastic actions.
c) Considering practical applications, it can be emphasized that the wind tunnel experiments can be carried out by the same scale model, wind tunnel, measuring instrumentation and test rig which are used on the flutter derivatives extraction.

In the prototype bridge response assessments, special correction factors for the load correlation and turbulence effects might be required. The similarity requirements retained for the reference section model of the present development are as follows:

d) The cross-section geometry.
e) Reduced velocity $U/(hn_i)$.
f) Normalized mass $m/(\rho h^2)$ and mass moment of inertia $J/(\rho h^4)$.

The similarity requirement for the damping ratio is relaxed in order to make the scale model damping low enough to ensure that the response amplitudes are of order the aeroelastic actions are conservatively accounted for. This might imply inconsistency to the determination of lock-in range, since it has been found to be dependent upon the mechanical damping [77,91]. The data of SCANLAN [90] for the bluff bridge sections, obtained through smooth flow tests, indicates that the lock-in velocity range become narrower with the increasing damping ratio; but the effect is not drastic. On the other hand, the lock-in range can also be dependent on the amplitude [77], i.e. the lock-in range widens when the amplitude increases. It is assumed that these phenomena roughly cancel out the effects of each other and the implications of the dissimilar damping are omitted.

From the strict formal point of view, the similarity requirement for the mass and mass moment of inertia restricts application of the model to structural members similar to the ones the section

model is prepared for. The vortex-induced response amplitude is generally known to be dependent upon the combined damping and mass parameter [91] termed the Scruton number. It is possible that the mass scaling can be relaxed without severe implications. This possibility is not, however, pursued further here.

In the testing technique assigned, the physical details of the aerodynamic excitation process remain widely unexplored. What is identifiable from the process is the part that significantly affects the vibration response, i.e. the part of the excitation having frequency content at or close to a natural frequency of the section model. For the present aims, this is not thought to restrict severally the usefulness of the model because the prototype bridge can be assumed to act in the same manner. The excitation frequency content that is outside the natural frequency ranges has minor influence on the response and is not of primary interest.

Generally, for wind tunnel experiments involving scaled models, the similarity requirement for the Reynolds number (R_e) is not met. Considering large structures, like bridge decks, this might yield error to analysis, since there may exist the transition range where the vortex shedding is disorganized and random. The established transition range for a circular cylinder is $0.3 \cdot 10^6 < R_e < 3.5 \cdot 10^6$, approximately [91]. This suggests the most pessimistic scenario, in which wind tunnel experiments (conducted typically for $R_e < 0.3 \cdot 10^6$) account for the different phenomenon that the prototype bridge undergoes (around $R_e > 1.7 \cdot 10^6$). The scenario is exploited owing to the fact, that there exist bridge girders, whose severe vortex-induced vibrations are successfully reduced using the countermeasures designed through the section model experiments. In general, the Reynolds number effects on the sharp corner bluff bodies, involving the fixed separation points, are omitted. This omission is also done in the present development. It follows that the fluid excitation mechanism, whether or not it originates from the vortex trail, is assumed to be primary dependent on the reduced velocity in the low amplitude range.

It is not straightforward to distinguish between the vortex and signature turbulence induced structural response as they both originate from the fluid wake effects. Some authors [35] consider the vortex-induced vibration as a special case of the signature turbulence. In the present model, the peak factor, in addition to the visual inspection of the response curves, is used for distinguishing between the dominant excitation mechanisms. This inexact definition is considered to be appropriate because of the low damping and the relatively large vibration amplitude of the reference section model. The peak factor is applied as a measure of the ratio between the peak amplitude and the standard deviation response occurring during the specific interval of time. As far as the slightly damped wind tunnel models are concerned, the magnitude of peak factors at lock-in can be expected to be close to value $\sqrt{2}$ of the ideal harmonic motion. Elsewhere, the signature turbulence is assumed to be the dominant excitation mechanism. For the signature turbulence induced responses, the peak values of order 4 can be expected, owing to the buffeting analogue.

3.1 Excitation model for vortex-induced vibrations

Providing that the maximum response amplitude in smooth flow is of primary interest, the harmonically excited linear single-degree-of-freedom oscillator seems to form the simplest, and still reasonably accurate, bases for the analysis. In bridge design, this oscillator model deviates from the others in a sense, that its parameters give conception of the magnitude of excitation force applied and allows comparison with the tabulated data in literature. Considering the imperfect spanwise load correlation, turbulence and Reynolds number effects, the model can be further extended in the framework of spectral analysis.

Based on the wind tunnel tests of aeroelastic section models representing bridge decks, various researchers have observed that there can exist multiple regimes of wind speed, in which vortex-

induced vibration amplitudes are marked. A number of these regimes seems to be dependent on the height to width ratio of the cross-section [56,94]. Furthermore, the frequency of motion coalesces the natural frequencies of section model. In the present model, the aforementioned behaviour is taken into account by assuming that the amplitude of harmonic load is a continuos function of wind speed.

3.1.1 Excitation model for reference wind tunnel experiments

Considering the smooth flow and slightly damped aeroelastic section model, distinguishable lock-in regimes can be expected to be observable. In these regimes, the steady-state vortex-induced response can be assumed to contain only one or two significant harmonic components. The possible appearance of two significant harmonic components is associated with the beating phenomenon occurring, if the components have frequencies close to each other. Simple excitation model, capable to reproduce the reference section model actions, can be given by

$$\begin{cases} V_K = qh\left\{C_{\eta 1}\cos(2\pi n_\eta t) + C_{\eta 2}\cos[2\pi n_\eta(1+\varepsilon_\eta)t]\right\} \\ M_K = qh^2\left\{C_{\theta 1}\cos(2\pi n_\theta t) + C_{\theta 2}\cos[2\pi n_\theta(1+\varepsilon_\theta)t]\right\} \end{cases}, \tag{66}$$

where n_i ($i = \eta$ or θ) is the natural frequency of the section model, ε_i ($i = \eta$ or θ) is the non-dimensional detuning parameter and C_{ij} ($i = \eta$ or θ and $j = 1$ or 2) is the aerodynamic exciting coefficient. In accordance with the wind-induced loads presented in Chapter 2, the reference point of the fluctuating across-wind force per unit length V_K and fluctuating twisting moment per unit length M_K is chosen into the centre of gravity of the cross-section. As far as no excessive beating is observed, coefficients $C_{\eta 2}$ and $C_{\theta 2}$ can be omitted. The excitation model of Eqs (66) can be interpreted in a manner, that the excitation may include components due to the motion-induced vortices and due to the regular vortex trail.

The aerodynamic exciting coefficients are generally evaluated through aeroelastic section model experiments by assuming resonant conditions. For resonance there is 90 Deg phase shift between the harmonic displacement response and the harmonic force that initiates it. As it is discussed by BLEVINS and BURTON [5], this out-of-phase component is the only component that can extract energy from fluid to the linear oscillator. It is the component that specifies the peak amplitude of the structure. If the beating is absent, and if there is no remarkable mass or stiffness coupling between the heaving and torsional modes, the wind tunnel model resonant response and the aerodynamic exciting coefficients are related by

$$\begin{cases} \dfrac{\eta_p}{h} = \dfrac{1}{16\pi^2\zeta_\eta}\left(\dfrac{\rho h^2}{m}\right)\left(\dfrac{U}{hn_\eta}\right)^2 C_{\eta 1} \\ \theta_p = \dfrac{1}{16\pi^2\zeta_\theta}\left(\dfrac{\rho h^4}{J}\right)\left(\dfrac{U}{hn_\theta}\right)^2 C_{\theta 1} \end{cases}, \tag{67}$$

where ζ_θ is the damping ratio of the torsional mode and J is the mass moment of inertia per unit length; η_p and θ_p are the amplitudes of heaving and torsional modes, respectively. For the present model the relations of Eqs (67) are generalized to take into account the general type of motion of the section model and the stochastic excitation models. In analogue to Eqs (67), the steady-state response of the section model is expressed by the formulae

$$\begin{cases} \dfrac{\sigma_\eta}{h} = \dfrac{1}{16\pi^2\zeta_\eta}\left(\dfrac{\rho h^2}{m}\right)\left(\dfrac{U}{hn_\eta}\right)^2 \tilde{C}_\eta \\ \sigma_\theta = \dfrac{1}{16\pi^2\zeta_\theta}\left(\dfrac{\rho h^4}{J}\right)\left(\dfrac{U}{hn_\theta}\right)^2 \tilde{C}_\theta \end{cases}, \tag{68}$$

in which σ_i ($i = \eta$ or θ) is the response standard deviation and the dimensionless coefficient $\tilde{C}_i$ ($i = \eta$ or θ) is termed as the root-mean-square (RMS) exciting coefficient. It can be noted that, if the section model response contains only one significant harmonic component, the RMS exciting coefficients are related to aerodynamic exciting coefficients as $C_{i1} = \sqrt{2}\,\tilde{C}_i$.

The RMS exciting coefficients, as defined in Eqs (68), are the primary quantities to be extracted through experiments. In addition, the experimental data comprises the peak factors g_η and g_θ defined by

$$\begin{cases} g_\eta = \dfrac{\eta_{p+} - \eta_{p-}}{2\sigma_\eta} \\ g_\theta = \dfrac{\theta_{p+} - \theta_{p-}}{2\sigma_\theta} \end{cases}, \tag{69}$$

where η_{p+}, θ_{p+} and η_{p-}, θ_{p-} are the peak positive and negative amplitudes, respectively.

As the RMS exciting coefficients are calculated from the response of the scale model, two alternatives exist for their definition; their value can be fixed by taking into account or omitting the aerodynamic damping and aeroelastic stiffness. VICKERY and BASU [103] give examples of these quantities for the circular cylinder. From their data it is evident that around the lock-in, these two parameters are sensitive to the wind velocity and their plots against flow speed contain sudden jumps. In the present model, without expecting significant implied error, the aerodynamic damping and aeroelastic stiffness are taken as zeros when evaluating or applying the RMS exciting coefficients. This approach is reasoned as follows:

a) At small or medium amplitude motions of the aeroelastic section models, the aerodynamic damping and aeroelastic stiffness are generally found to be primary dependent upon the reduced velocity. It follows that the aerodynamic damping and aeroelastic stiffness can be considered to be similar to the prototype structure in the amplitude ranges that are of main interest in bridge design.
b) For a large amplitude motion, the structural oscillations tuned to a natural frequency characterise the excitation process. In such circumstances the load spectrum has a peak at the natural frequency. The associated almost harmonic excitation force and the (linear of nonlinear) aerodynamic damping force are both 90 Deg out-of-phase with respect to the displacement response. Therefore, these components can be equated to the external harmonic force extracted from the experiments.
c) The aeroelastic stiffness might slightly change the lock-in frequency, but its effects on response amplitudes can be considered to be negligible.

This approach was pursued one step further by SARPKAYA [77] who stated that vortex-induced vibration models should be based on the mechanical damping defined in the vacuum rather than in still air.

3.1.2 Effects of approach-flow turbulence

In the present model, only the longitudinal component of fluctuation velocity is considered. For convenience, the instant longitudinal component of the flow velocity is defined by the formula

$$\begin{cases} U = \bar{U}[1 + \varepsilon(t)] \\ \varepsilon(t) \equiv \dfrac{u(t)}{\bar{U}} \end{cases}, \tag{70}$$

where $\varepsilon(t)$ is the non-dimensional representation of the longitudinal component of fluctuation velocity. It has a zero mean value due to its definition. The random process $\varepsilon(t)$, as it characterises the fluctuations in the natural wind velocity, can be well assumed Gaussian distributed. The probability density of the process is given by

$$p[\varepsilon(t)] = \frac{1}{\sqrt{2\pi}\, I_u} e^{-\frac{1}{2}\left[\frac{\varepsilon(t)}{I_u}\right]^2}, \tag{71}$$

where symbol p denotes the probability density of the symbol inside the brackets.

It is assumed that the instant frequency of excitation component is directly proportional to the wind speed. Letting k_K denote the non-dimensional constant of proportionality and by defining frequency ratio β_K as

$$\beta_K(t) \equiv \frac{n_K(t)}{\bar{n}_K}, \tag{72}$$

where $n_K(t)$ and $\bar{n}_K$ are the instant and mean value of the excitation frequency, respectively, it follows that

$$\beta_K(t) = k_K \frac{\bar{U}}{h\bar{n}_K}[1 + \varepsilon(t)] . \tag{73}$$

This equation can be interpreted as an extension of the classical Strouhal's law with coefficient k_K representing the Strouhal number. In the present model, however, no distinction is made whether the excitation is owing to the vortex trail governed by the Strouhal law, motion-induced vortices or more general form of fluid instability.

Eq. (73) transforms random variable $\varepsilon(t)$ to new random variable $\beta_K(t)$ by a single-valued function with an existing single-valued inverse transform. Taking into account the associated relation between the probability densities of the transformed and original random variables [49]

$$p[\beta_K(t)] = p[\varepsilon(t)] \left|\frac{d\varepsilon(t)}{d\beta_K(t)}\right|, \tag{74}$$

it follows that the probability density of the frequency content of the exciting force (*Fig. 8*) is given by

$$p[\beta_K(t)] = \frac{1}{\sqrt{2\pi}\, I_u} \; e^{-\frac{1}{2}\left[\frac{\beta_K(t) - 1}{I_u}\right]^2} . \qquad \textbf{(75)}$$

If the amplitude of the exciting force is approximately constant, the spectral density of excitation force would take the shape alike the probability density function, i.e. the excitation spectrum contains a peak at the mean frequency $\overline{n}_K$. The probability density distribution of Eq. (75) implies then one of the key hypotheses of the model, borrowed from the work of VICKERY and BASU [103]. Namely, the effect of longitudinal component of turbulence intensity is to widen the excitation spectrum bandwidth above the theoretical one associated with the harmonic force.

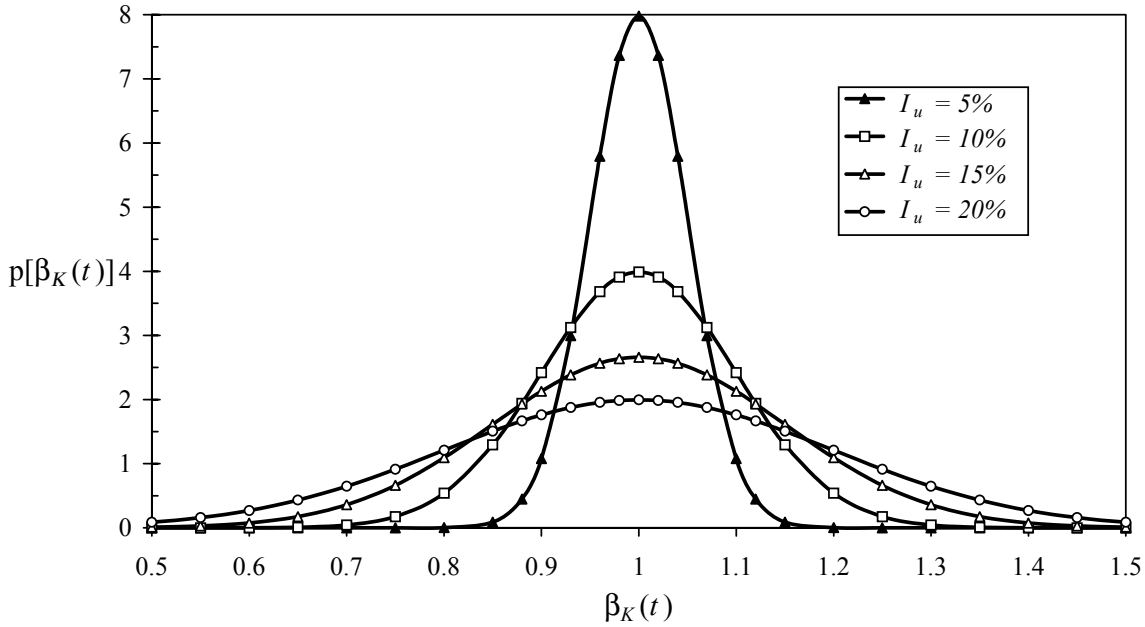

Fig. 8 Assumed probability density for the frequency of vortex-induced excitation for a body at rest immersed in a turbulent flow.

Therefore, for a turbulent flow the frequency-domain approach, the spectral analysis, provides the preferred basis of analysis. The main problem at hand is to provide a reasonable estimate for the spectral density of excitation. The resonant and/or lock-in conditions $\overline{n}_K \approx n_\eta$ or $\overline{n}_K \approx n_\theta$ are those of interest in the present development. When extending the model for oscillating bodies, considerable uncertainty in deducing the shape of excitation spectral density curve exists. In the present study, the band-limited white noise model is applied for its mathematical simplicity. In this model, equivalent values of excitation spectrum producing consistent response estimates, can be invoked. The implied error due to the shape of spectrum is assumed to be unimportant in comparison to other uncertainties in analysis. Concentrating the analysis on lock-in regimes, the body being at rest can be interpreted to undergo infinitesimal amplitude motion at the natural frequency n_i ($i = \eta$ or θ). Here, the heaving and torsional modes are distinguished with the subscripts η and θ, respectively. In order to relate the bandwidth of the present excitation spectrum to the theoretical bell-shaped Gaussian spectrum, a relation is introduced as

$$\delta_{iu} = k_{iu} I_u \,, \qquad (i = \eta \text{ or } \theta), \tag{76}$$

where δ_{iu} is the turbulence-induced excitation spectrum bandwidth, normalized with respect to natural frequency n_i, and k_{iu} is the non-dimensional constant of proportionality. The value of the proportionality constant can be inspected through Eq. (75). For example, if the excitation bandwidth and the bandwidth of the probability density function squared are assumed to be equal, it holds that $k_{iu} \approx 1.665$. Here, the value $k_{\eta u} = 1.414$ has been applied for cylindrical bodies by VICKERY and BASU [103]. Eq. (76) yields zero bandwidth for smooth flow, which is not in agreement with the experimental evidence. Therefore, the normalized bandwidth for the body at rest is given in the form

$$\delta_{iSt} = \sqrt{\delta_{i0}^2 + \delta_{iu}^{\,2}} \,, \qquad (i = \eta \text{ or } \theta), \tag{77}$$

as suggested by VICKERY and BASU [103]. Here, δ_{iSt} and δ_{i0} are the normalized bandwidth for the turbulent and the smooth flow, respectively. Values $\delta_{\eta 0} = 0.05...0.1$ for the circular cylinders are reported by VICKERY and BASU [103]. The experiments of VICKERY and CLARK [102] for the tapered stacks impose the value $\delta_{\eta 0} = 0.08$.

In the present model, the dependence of the excitation spectrum characteristics on vibration amplitude is to be modelled through the amplitude dependence of the bandwidth. With the increasing vibration amplitude, the excitation is expected to become more correlated and the bandwidth of excitation spectrum to become narrower than they are for the body at rest. If the vibration amplitude reaches a specific limiting value, the body motion might distort the regular excitation [5,37]. Considering turbulent flows it has been suggested that the amplitude reduction effect of approach-flow turbulence will vanish as the amplitudes become large [107]. Suitable relations satisfying the constraints discussed above, can be given, e.g. with the family of curves

$$\delta_i = (\delta_{i0} - \delta_{iMin}) \left| \frac{\sigma_i}{\sigma_{iCr}} - 1 \right|^{\gamma_i} + \delta_{iMin} \,, \qquad (i = \eta \text{ or } \theta), \tag{78}$$

in which δ_i is the natural-requency-normalized bandwidth and σ_{iCr} is the critical standard deviation response where the normalized excitation spectrum bandwidth has the minimum value denoted by symbol δ_{iMin}. While more reliable relations could be developed via wind tunnel experiments, a simple parabolic one ($\gamma_i = 2$) is applied in the present development (*Fig. 9*). In general, the decay characteristics can be depended upon the turbulence level [21,77]. Without additional assumptions, the relation of Eq. (78) is valid for bandwidth induced by the approach-flow turbulence as well as for the smooth-flow bandwidth. The implications of this parabolic approximation are in some respects the same as the ones owing to the parabolic exciting coefficient vs. amplitude relation dealt by BLEVINS and BURTON [5]. The primary purpose of the free parameters (σ_{iCr}, γ_i and δ_{iMin}) is to provide fittingness to the experimental data. The physical interpretation can be given also as:

a) Parameter σ_{iCr} establishes the largest standard deviation response in which the vortex excitation remains correlated. Response magnitudes higher than that will distort the vortex formation and reduce the correlation. Expressions for the theoretical maximum amplitude for cylindrical structures are deduced, among others, by IWAN [37].
b) Parameter δ_{iMin} accounts for the effects of dissimilar Reynolds number in wind tunnel experiments. For the full-scale structures, the excitation bandwidth can become wider, if the vortex excitation falls to the supercritical [27] range.

c) Exponent parameter γ_i accounts for the manner how the excitation bandwidth δ_{i0} approaches the one observed in experiment. This parameter is applied in consistent to other two free parameters and the measured peak factors extracted in wind tunnel experiments. Here, the peak factors are assumed to be related to the excitation bandwidth.

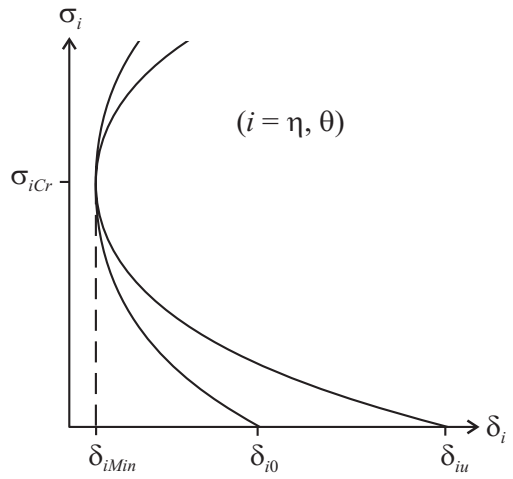

Fig. 9 Assumed parabolic amplitude dependence of the excitation bandwidth.

The excitation model, to be completed, requires expressions for the variances of vortex-induced across-wind force and twisting moment. A hypothesis is made that the variances are independent of the approach-flow turbulence. This implies that the effect of approach-flow turbulence causes the excitation force to contain wider spread of frequencies, while keeping the force variance, and the turbulent kinetic energy inducing it, invariant. The normalized excitation variances for the reference wind tunnel experiments are then given by

$$\begin{cases} \dfrac{\sigma_{VK}^2}{(qh)^2} = \dfrac{\delta_\eta n_\eta S_{VK}(n)}{(qh)^2} \equiv \tilde{C}_\eta^2 \\ \dfrac{\sigma_{MK}^2}{(qh^2)^2} = \dfrac{\delta_\theta n_\theta S_{MK}(n)}{(qh^2)^2} \equiv \tilde{C}_\theta^2 \end{cases}, \tag{79}$$

where σ^2_{iK} ($i = V$ or M) is the variance of load acting per unit length and $S_{iK}(n)$ ($i = V$ or M) is the associated one-sided spectral density.

To inspect the soundness of the assumptions taken, the expressions for variance responses of the section model immersed in turbulent flow, are formulated. These responses can be shown to be

$$\begin{cases} \dfrac{\sigma_\eta^2}{h^2} = \displaystyle\int_{n_\eta\left(1-\frac{\delta_\eta}{2}\right)}^{n_\eta\left(1+\frac{\delta_\eta}{2}\right)} S_{VK}(n)\,|H_\eta(n)|^2\,dn \equiv \frac{1}{64\pi^4}\left(\frac{\rho h^2}{m}\right)^2\left(\frac{U}{hn_\eta}\right)^4 \frac{I_\eta(\delta_\eta)}{\delta_\eta}\,\tilde{C}_\eta^2 \\ \sigma_\theta^2 = \displaystyle\int_{n_\theta\left(1-\frac{\delta_\theta}{2}\right)}^{n_\theta\left(1+\frac{\delta_\theta}{2}\right)} S_{MK}(n)\,|H_\theta(n)|^2\,dn \equiv \frac{1}{64\pi^4}\left(\frac{\rho h^4}{J}\right)^2\left(\frac{U}{hn_\theta}\right)^4 \frac{I_\theta(\delta_\theta)}{\delta_\theta}\,\tilde{C}_\theta^2 \end{cases}, \tag{80}$$

where an abbreviation for the dimensionless integral function is introduced as

$$I_i(\delta_i) \equiv \int_{1-\frac{\delta_i}{2}}^{1+\frac{\delta_i}{2}} \frac{d\delta}{(\delta_i^2 - 1)^2 + (2\zeta_i\delta_i)^2}, \qquad (i = \eta \text{ or } \theta). \tag{81}$$

Here, the integral of Eq. (81) can be solved in closed form [97] to yield

$$I_i(\delta_i) = \frac{1}{8\sqrt{1-\zeta_i^2}} \Big/_{1-\frac{\delta_i}{2}}^{1+\frac{\delta_i}{2}} I_1(\delta) + \frac{1}{4\zeta_i}\left[\Big/_{1+}^{1+\frac{\delta_i}{2}} I_2(\delta) + \Big/_{1-\frac{\delta_i}{2}}^{1-} I_2(\delta)\right], \quad (i = \eta \text{ or } \theta), \tag{82}$$

where

$$\begin{cases} I_1(\delta) \equiv \ln\dfrac{\delta^2 + 2\delta\sqrt{1-\zeta_i^2} + 1}{\delta^2 - 2\delta\sqrt{1-\zeta_i^2} + 1} \\ I_2(\delta) \equiv \arctan\dfrac{2\delta\zeta_i}{1 - \delta^2}. \end{cases} \tag{83}$$

The response reduction effects together with the aeroelastic effects implied by the present model are illustrated in *Fig. 10*. Shown in the figure are the hypothetical section model responses for the perfectly correlated load excitation. It can be observed that the response decreases with the increasing *u*-component of the turbulence intensity and with the increasing excitation bandwidth assumed for the body at rest. Furthermore, with the increasing amplitude, the reduction effects of these two decrease. In this format KAWATANI *et al*. [43], among others, have shown empirical data for turbulence effects on section models representing bridge decks. From their study, it can be verified that the reduction characteristics of the present model are on a reasonable level. On the other hand, the data for bridge decks of KAWATANI *et al*. [43] and MATSUMOTO *et al*. [56] indicates that, for some cross-sectional shapes, the turbulence reduction effects are more pronounced than others. As far as the present formulation is concerned, this suggests that the smooth-flow bandwidth can be significantly dependent upon the cross-section's shape. The ultimate observations of MATSUMOTO *et al*. [56], that turbulence can increase the vortex-induced response of some bridge decks, are not compatible with the present model. The present turbulence reduction model is not directly dependent upon the turbulence scale. It can be postulated, however, that the proportionality constant k_{iu} in Eq. (76) can exhibit some dependence, if examined through wind tunnel experiments.

The normalized excitation bandwidth can be applied to characterise the implications of dissimilar damping ratios. The zero-bandwidth excitation model of Eqs (67) implies that the prototype bridge response is proportional to such ratios as ζ_i/ζ_j, in which ζ_i and ζ_j are the damping ratios of the scale model and the prototype bridge, respectively. Through the present excitation model, the proportionality can be shown to approach $(\zeta_i/\zeta_j)^{1/2}$ with the increasing values of excitation bandwidth. Obviously, the vortex-shedding response cannot be predicted accurately by means of the measured response of an aeroelastic section model that has a dissimilar damping ratio, unless the details of the load spectrum are known or assumed (as in the present model).

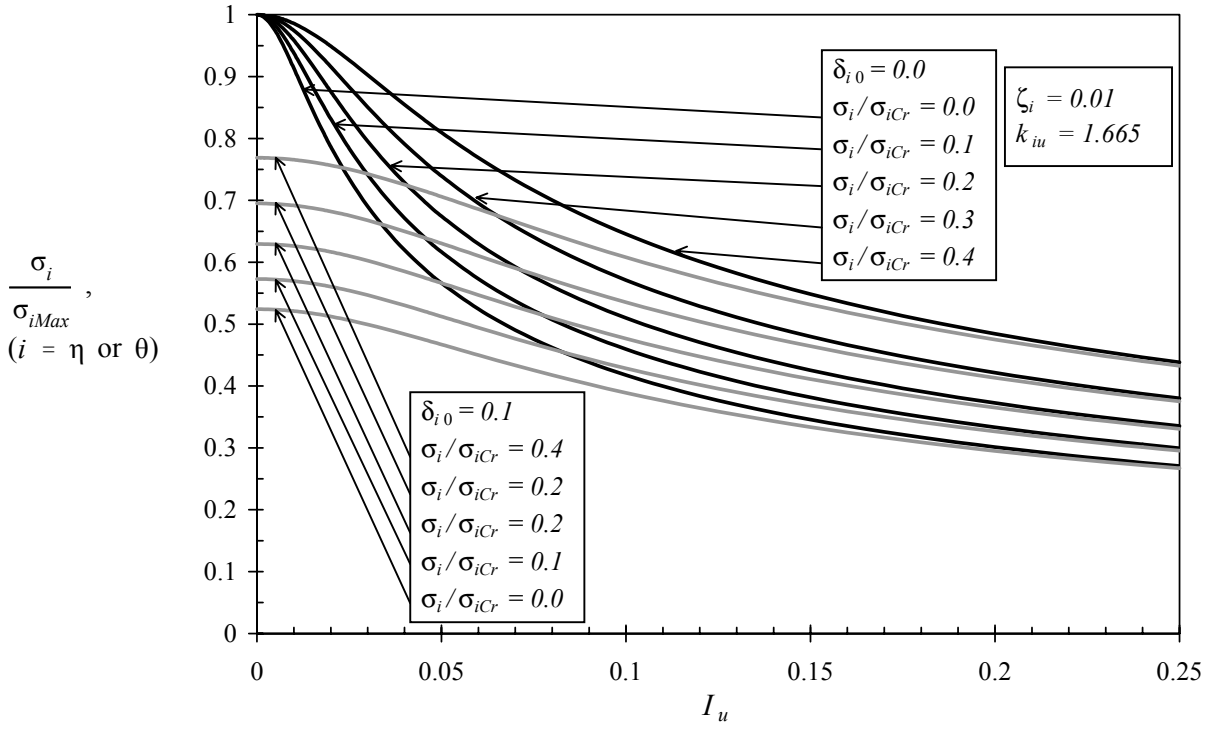

Fig. 10 Illustration of turbulence and amplitude effects on the vortex-induced response of a section model as a consequence of the assumptions made. Normalization is with respect to the maximum value of standard deviation response σ_{iMax} occurring in smooth flow with the zero excitation bandwidth.

With the changing excitation bandwidth, response level and turbulence intensity, the peak factors associated with the response are expected to alter. As far as the peak factor's dependence on bandwidth is concerned, analytical results might be reachable through theoretical considerations. Simple approximations, however, are devoted to the present development. Namely, for the pure harmonic motion the zero-bandwidth model is adequate with the peak factor $\sqrt{2}$ .With increasing bandwidth, a rapid transition up to values of order 4 is expected. It is assumed that the peak factor changes in the same way as the response standard deviation of single-degree-of-freedom linear oscillator is dependent upon the excitation bandwidth. The resulting approximation is given by the formula

$$\begin{cases} g_i(\delta_i) \approx \sqrt{2} + \sqrt{\dfrac{A_1}{A_2}}\,(g_{iMax} - \sqrt{2}) , \quad (i = \eta \text{ or } \theta) \\ \dfrac{A_1}{A_2} = \dfrac{I_i(\delta_i)}{\dfrac{\pi}{4\zeta_i}} , \end{cases} \tag{84}$$

in which g_{iMax} is the peak factor at infinite band excitation. Here, the value of the parameter g_{iMax} can be accessed through the buffeting theory using Eq. (63), with zero up-crossing frequency equal to a natural frequency. The relation imbedded in Eqs (84) is depicted in *Fig. 11* to illustrate the desired rapid transition of magnitude of the peak factor when the bandwidth of the excitation spectrum exceeds the bandwidth of the frequency response function (= $2\zeta_i$). Here, the trend agrees with the experimental data of VICKERY and BASU [103] obtained with the circular cylinders. Their

results are, however, expressed by means of the damping coefficients.

It can be noted that, if a relation like Eqs (84) could be verified, a typical wind tunnel experiment fixes the excitation bandwidth with the observed peak factor and the amplitude, to be used for evaluating the free parameters of Eq. (78).

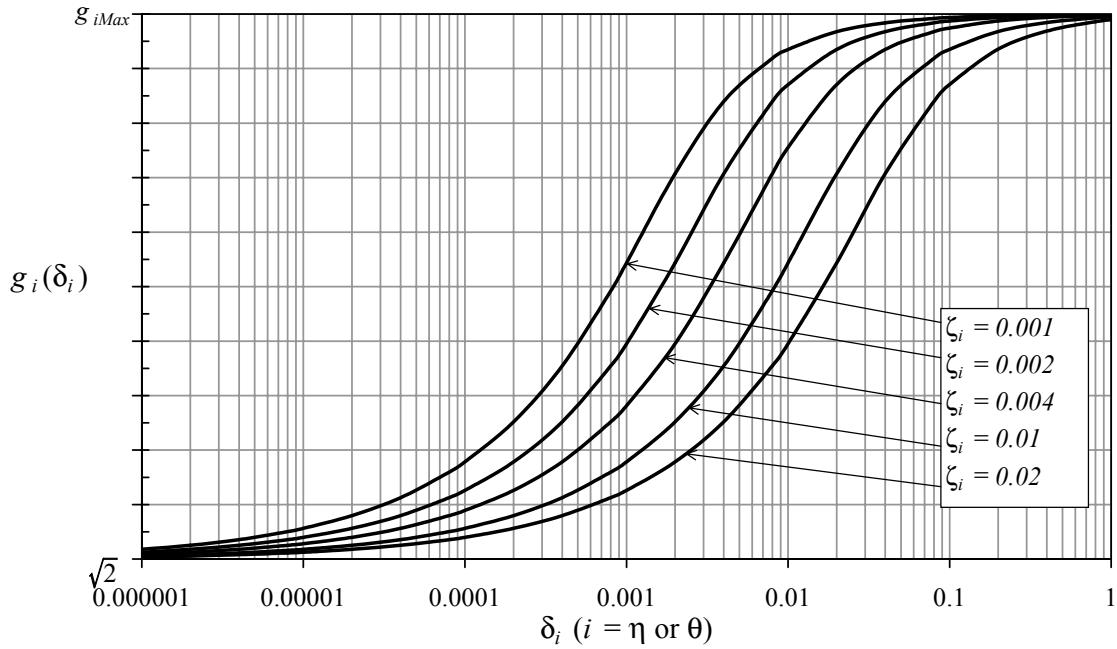

Fig. 11 The assumed dependence of peak factor on normalized excitation bandwidth.

3.1.3 Effects of spanwise load correlation

For cylindrical bodies undergoing small amplitude motion in resonant condition, the loss of correlation of vortex-excitation is known to have marked reduction effect on the response. The degree of correlation, conveniently measured by a covariance function, is found to be dependent on the amplitude of motion. Experiments of EHSAN and BOSCH [20], among others, show that the same tendency of response reduction holds for section models representing bridge girders.

As discussed by various authors [21,77], the presence of turbulence can reduce the spanwise correlation of aerodynamic forces in comparison to that in smooth flow. In the present model, the effect of turbulence is conservatively neglected. This is mainly because of the loss of design data and experimental results available. It can be emphasized that the effect of turbulence could be easily included in the expressions of covariance functions, if experimental data became available. Following the earlier correlation models developed, the frequency and wind speed dependence of the correlation is omitted. This can be considered reasonable as the excitation is modelled by a narrow-band random process occurring in a narrow range of reduced wind velocities.

In general, there seems to be very little public data for the correlation properties of bridge decks. EHSAN and BOSCH [20], based on the smooth flow wind tunnel tests of H-shaped section, have presented the normalized covariance in the form

$$\begin{cases} \tilde{R}_i(\Delta_s) = e^{-c_i}, \qquad (i = \eta \text{ or } \theta) \\ c_\eta = \dfrac{a_1}{a_2 + \dfrac{|\eta_p|}{h}} \sqrt{\dfrac{|\Delta_s|}{h}} \\ c_\theta = \dfrac{a_3}{a_4 + \dfrac{|\theta_p| B}{2h}} \sqrt{\dfrac{|\Delta_s|}{h}}, \end{cases} \tag{85}$$

in which a_j (j = 1, 2, 3 or 4) is the empirical constant, Δ_s is the spanwise separation and $\tilde{R}_i(\Delta_s)$ is the normalized covariance function. The empirical coefficients extracted were: a_1 = 0.01578, a_2 = 0.02694, a_3 = 0.01102 and a_4 = 0.02116.

The behaviour of the correlation model of EHSAN and BOSCH [20] is illustrated in *Fig. 12*. Also shown in the figure is the model of BLEVINS and BURTON [5] for the circular cylinder. Clearly, the former model predicts slower correlation decay resulting higher response estimates. A verification of the correctness of this model can be obtained from the experimental data of WILKINSON [106] for the square section cylinder; from that reference the trend of slower decay characteristics in comparison to the behaviour of circular cylinders can also be observed. It can be suggested that different correlation models might be required for the analysis of pylons and bridge decks.

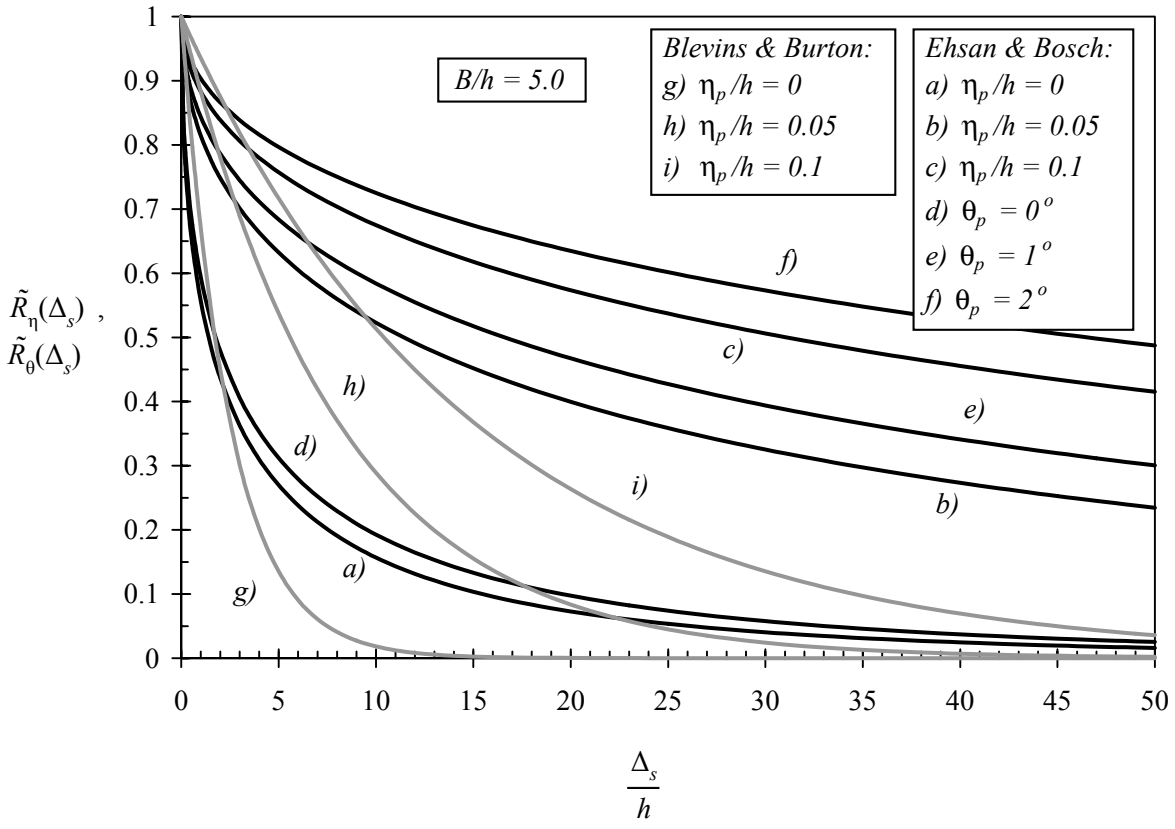

Fig. 12 Comparison of normalized covariance functions established for the H-shaped bridge decks (Ehsan & Bosch) and for the circular cylinders (Blevins & Burton).

To make provision for the present model for systematic calculus of the load spectral densities, the relations of Eqs (85) are generalized into the form

$$\begin{cases} \tilde{R}_i(\Delta_s) = e^{-\tilde{c}_i}, & (i = \eta \text{ or } \theta) \\ \tilde{c}_\eta = \dfrac{\tilde{a}_1}{\tilde{a}_2 + \dfrac{\sigma_{\eta m}}{h}} \sqrt{\dfrac{|\Delta_s|}{h}} \\ \tilde{c}_\theta = \dfrac{\tilde{a}_3}{\tilde{a}_4 + \dfrac{\sigma_{\theta m} B}{2h}} \sqrt{\dfrac{|\Delta_s|}{h}}, \end{cases} \tag{86}$$

in which the average of the values occurring at two spanwise coordinates are employed. Denoting the spanwise coordinates by s_i and s_j the average values are given by

$$\begin{cases} \tilde{a}_l = \dfrac{a_l}{\sqrt{2}}, & (l = 1, 2, 3 \text{ or } 4) \\ h_m = \dfrac{h(s_i) + h(s_j)}{2} \\ B_m = \dfrac{B(s_i) + B(s_j)}{2} \\ \sigma_{km} = \dfrac{\sigma_k(s_i) + \sigma_k(s_j)}{2}, & (k = \eta \text{ or } \theta), \end{cases} \tag{87}$$

where arguments s_i and s_j are added to the symbols to denote the possible spanwise dependence. The undesired implications of the generalization are assumed to be insignificant.

3.2 Response calculation for vortex-induced vibrations

The response calculation of a prototype bridge follows the principles of spectral analysis outlined in Chapter 2. The complexities due to the amplitude dependence of the correlation model, however, make the mathematical simplifications devoted. Namely, it is assumed that the modal responses are uncorrelated. It is possible that this assumption can be accepted even for weakly separated mode shapes as the phenomenon of vortex lock-in tends to select a particular mode shape for resonance [82]. Taking into account the mutual frequency independence of load spectrum, the variance of the normal coordinate associated with mode shape i is expressed by

$$\sigma^2_{(0)qi} = {}^1S_{Qi}(n_i) \int_{n_i\left(1-\frac{\delta_\eta}{2}\right)}^{n_i\left(1+\frac{\delta_\eta}{2}\right)} |H_i(n)|^2 \, dn + {}^2S_{Qi}(n_i) \int_{n_i\left(1-\frac{\delta_\theta}{2}\right)}^{n_i\left(1+\frac{\delta_\theta}{2}\right)} |H_i(n)|^2 \, dn, \tag{88}$$

where

$$\begin{cases} {}^{1}S_{Qi}(n_i) = \int_0^{l_b}\int_0^{l_b} \sqrt{S_{VK}(n_i,s_1)S_{VK}(n_i,s_2)}\ |\varphi_{\eta i}(s_1)||\varphi_{\eta i}(s_2)|\ \tilde{R}_{\eta}(\Delta_s)\, ds_1 ds_2 \\ {}^{2}S_{Qi}(n_i) = \int_0^{l_b}\int_0^{l_b} \sqrt{S_{MK}(n_i,s_1)S_{MK}(n_i,s_2)}\ |\varphi_{\theta i}(s_1)||\varphi_{\theta i}(s_2)|\ \tilde{R}_{\theta}(\Delta_s)\, ds_1 ds_2 \ . \end{cases} \quad \textbf{(89)}$$

Here, l_b is the length of the structural member studied (a stiffening girder or a pylon) and the spanwise position is distinguished by arguments s_1 and s_2 added to the symbols. The load spectral densities are calculated by means of Eqs (79) and may, in a general case, be dependent upon spanwise coordinate s. Absolute values are taken for mode shape values as it is assumed that the excitation force can reverse sign with the mode shape [35]. By taking Eq. (81) into account, the integrals involved in Eq. (88) take the form

$$\int_{n_i\left(1-\frac{\delta_j}{2}\right)}^{n_i\left(1+\frac{\delta_j}{2}\right)} |H_i(n)|^2\, dn = \frac{n_i I_i(\delta_j)}{\tilde{K}_i^2}\ , \qquad (j = \eta \text{ or } \theta). \quad \textbf{(90)}$$

The variance responses in the nodal coordinate system are given by

$$\sigma_{(\gamma)}^2 = \sum_{i=1}^{N} \varphi_i^2 \left[(2\pi n_i)^{\gamma}\ \sigma_{(0)qi}\right]^2 , \qquad (\gamma = 0,\ 1 \text{ or } 2), \quad \textbf{(91)}$$

where the relation is an approximate for the velocity and acceleration responses (i.e. for $\gamma = 1$ or 2). The implications of this proximity are considered insignificant because of the narrowness of the bandwidth of the modal frequency response function.

The response calculation is to be carried out by fixed-point iteration since the value of the covariance functions is dependent upon the standard deviation response. The numerical model given by Eqs (83)...(91) is programmed as a part of the BWIND-3 code described in Chapter 2.4. The double integrals in Eqs (89) are approximated by the double summation expressions. Furthermore, the nodal-load correlation correction (Chapter 2, Appendix A) can be applied to reduce the error due to lumping the loads to finite number of nodes. The aerodynamic input parameters employed contain the RMS exciting coefficients to be extracted through wind tunnel experiments. Also employed are the decay parameters of correlation model and the free parameters defining the excitation bandwidth characteristics via Eq. (78). For simplicity, the actual direction of the centre-lines of structural members are not inputted but there is a choice enabled between the horizontal members (a bridge girder) and the vertical members (pylons).

The present vortex-induced vibration model suffers from the same inconsistency as the buffeting models do. Namely, the correlation (or coherence) model has a considerable effect on response and should be reasonably chosen. On the other hand, correction factors analog to aerodynamic admittances are not required but there are uncertainties related to excitation spectrum details. From these point of views, uncertainties being at least of the same order as in the buffeting analysis can be expected to exist.

3.3 Calculation model for signature turbulence

Owing to the present distinction between the vortex and signature turbulence induced excitation, the bandwidth of load spectrum in the latter case is several times wider than the bandwidth of the frequency response function of vibration system. It is assumed that the spectrums of the signature turbulence do not contain significant low-frequency components. Under these assumptions, the approximative formula given for the resonant response in Eq. (14) is known to yield accurate results. The basic quantity determining the response, according to the approximation, is the magnitude of load spectral density at the natural frequency. The resonant response of an aeroelastic section model can be written in the form

$$\begin{cases} \dfrac{\sigma_\eta^2}{h^2} = \dfrac{1}{256\pi^3\zeta_\eta}\left(\dfrac{\rho h^2}{m}\right)^2\left(\dfrac{U}{hn_\eta}\right)^4 \tilde{S}_{VS}(n_\eta)\, J_\eta(n_\eta) \\ \sigma_\theta^2 = \dfrac{1}{256\pi^3\zeta_\theta}\left(\dfrac{\rho h^4}{J}\right)^2\left(\dfrac{U}{hn_\theta}\right)^4 \tilde{S}_{MS}(n_\theta)\, J_\theta(n_\theta)\ , \end{cases} \tag{92}$$

in which $J_i(n_i)$ (i = η or θ) is the coherence reduction factor. This factor is dependent upon the length-to-height ratio of the section model. Furthermore, the symbols for the normalized spectral densities are

$$\begin{cases} \tilde{S}_{VS}(n_\eta) \equiv \dfrac{n_\eta S_{VS}(n_\eta)}{(\bar{q}h)^2} \\ \tilde{S}_{MS}(n_\theta) = \dfrac{n_\theta S_{MS}(n_\theta)}{(\bar{q}h^2)^2}\ . \end{cases} \tag{93}$$

Here, $S_{VS}(n_\eta)$ and $S_{MS}(n_\theta)$ are, respectively, the one-sided spectral densities of the signature turbulence induced across-wind force and twisting moment acting on the unit length. These spectral densities are the primary quantities to be extracted through the section model experiments. It can be noted that, by considering Eqs (68), the relations

$$\begin{cases} \tilde{S}_{VS}(n_\eta)\, J_\eta(n_\eta) = \dfrac{\pi}{\zeta_\eta}\tilde{C}_\eta^2 \\ \tilde{S}_{MS}(n_\theta)\, J_\theta(n_\theta) = \dfrac{\pi}{\zeta_\theta}\tilde{C}_\theta^2\ , \end{cases} \tag{94}$$

hold. Thus, in the present model, the wind tunnel data extracted for the signature turbulence is essentially the same as that used for the vortex-induced vibrations.

According to the dimensional analysis, there is some freedom to form the dimensionless products [48] employing an excitation spectrum. For example, the natural frequencies of the section model in Eqs (93) could be replaced by term U/h that has a dimension of 1/s like desired. This form might illustrate the physical phenomenon better. The normalization of Eqs (93) is, however, favoured in the present study, as it serves some convenience for curve-fitting procedures.

The coherence reduction factors are included in Eqs (92) to account for the possible imperfect coherence of spectrums due to the length-to-height ratio of the section model, i.e. the theory is formulated for two-dimensional objects while the section model has always a finite length. In the

approximations for the coherence reduction factor, the relations given in Appendix A can be utilized by letting $J_i(n_i) = J_{AA}$.

To be completed, the signature-turbulence model requires expressions for the spanwise coherence. As in the case of natural wind turbulence, it seems reasonable to assume that the coherence fall-of characteristics are dependent upon the spanwise separation and the apparent wavelength (U/n) of the turbulent velocity fluctuations. The conventional exponential decay law of Eq. (44) is chosen for the present study for its mathematical simplicity. The possible amplitude and approach-flow turbulence dependence of the coherence is to be taken into account through the decay coefficient. In general, it can be believed that the coherence of signature turbulence induced loads is more strictly controlled by the vibration amplitude than what the natural wind turbulence induced buffeting loads are.

In order to estimate the response of the full structure, the approximation is made that the modal responses are statistically uncorrelated. This proximity is invoked mainly for the mathematical convenience. The rigorous coupled-mode signature turbulence analysis could be formulated as well by applying, e.g., the methods outlined in Chapter 2. The variance of response component x due to the signature turbulence is obtained by summation of the modal resonant responses as

$$\sigma^2_{(\gamma)x} = \sum_{i=1}^{N_m} (2\pi n_i)^{2\gamma} \varphi^2_{xi} \frac{\pi n_i}{4\zeta_i \tilde{K}_i^2} S_{Qi}(n_i) , \qquad (\gamma = 0,\ 1 \text{ or } 2), \tag{95}$$

where the spectral densities of the modal loads at natural frequency are given by

$$\begin{aligned} S_Q(n_i) = \int_0^{l_b}\int_0^{l_b} & \sqrt{S_{VS}(n_i,s_1)S_{VS}(n_i,s_2)}\ \varphi_{\eta i}(s_1)\varphi_{\eta i}(s_2)\ \chi_{VS}(n_i) + \\ & + \sqrt{S_{MS}(n_i,s_1)S_{MS}(n_i,s_2)}\ \varphi_{\theta i}(y_1)\varphi_{\theta i}(s_2)\ \chi_{MS}(n_i)\ ds_1 ds_2 . \end{aligned} \tag{96}$$

Here, $\chi_{VS}(n_i)$ and $\chi_{MS}(n_i)$ are the root-coherence functions for the signature turbulence induced across-wind force and the twisting moment, respectively. Furthermore, the excitation spectrums are to be calculated via Eqs (93).

For the BWIND-3 code, the signature turbulence analysis model is implemented by the means of Eqs (95) and (96). The double integral of Eq. (96) is approximated by the double summation expression. Analogous to the buffeting and vortex-induced vibration analysis, the nodal-load correlation correction (Chapter 2, Appendix A) can be applied. The aerodynamic input parameters employed contain the non-dimensional excitation spectrums, coherence decay parameter and direction (vertical or horizontal) flag for structural members.

Decisive conclusions cannot be reached through the comparison of the present calculation model with others, as the design data and developed models for the signature turbulence seem to be absent almost completely. In some tentative models, the signature turbulence spectrum is considered to be additive to the approach-flow buffeting spectrum. Furthermore, in some recent models, the effects of signature turbulence are superimposed to the experimental aerodynamic admittance functions [40]. Obviously, in the present approach the most significant uncertainty is related to the coherence model. As a first approximation, the signature-turbulence coherence is assumed to possess the same characteristics as the coherence of natural wind turbulence. It can be emphasized that relatively simple wind tunnel experiments can be conducted to inspect the signature-turbulence coherence; experiments with taut-strip or section models with altering length-to-height ratios in smooth flow would relate the coherence decay parameter by means of Eqs (92).

For the case of a constant cross-section, two dimensional mode shapes and constant spanwise mass distribution, the present model yields simplified equations for the responses as

$$\begin{cases} \dfrac{\sigma^2_{(\gamma)\eta}}{h^2} = \displaystyle\sum_{i=1}^{N_m} \frac{(2\pi n_i)^{2\gamma}\ \varphi^2_{\eta i}}{256\pi^3\zeta_i} \left(\frac{\rho h^2}{m}\right)^2 \left(\frac{U}{h n_\eta}\right)^4 \tilde{S}_{VS}(n_i)\, J_i(n_i)\ , \qquad (\gamma = 0,\ 1 \text{ or } 2) \\ \sigma^2_{(\gamma)\theta} = \displaystyle\sum_{i=1}^{N_m} \frac{(2\pi n_i)^{2\gamma}\ \varphi^2_{\theta i}}{256\pi^3\zeta_i} \left(\frac{\rho h^4}{J}\right)^2 \left(\frac{U}{h n_i}\right)^4 \tilde{S}_{MS}(n_i)\, J_i(n_i)\ , \end{cases} \tag{97}$$

where the non-dimensional joint acceptance function can be approximated by the formula [82,85]

$$J_i(n_i) \approx \frac{l_b}{\displaystyle\int_0^{l_b} \varphi_i^2 dy} \frac{2\left(\dfrac{c_s n_i l_b}{\bar{U}} - 1\right)}{\left(\dfrac{c_s n_i l_b}{\bar{U}}\right)^2}\ . \tag{98}$$

Here, c_s is the spanwise coherence decay coefficient for the signature turbulence. Eqs (97) and (98) are valid for non-dimensional mode shapes regardless the normalization employed. These equations can be applied for the verification purposes and are given in analog form with typical natural wind buffeting approximations for the resonant response. This analogue can be utilized for combining the excitation mechanisms. Furthermore, as the excitation spectrums of signature turbulence and aerodynamic admittances are assumed to be dependent primary upon the reduced velocity, it can be concluded that the present model is consistent with respect to the other two approaches mentioned.

4 EXPERIMENTAL STUDY WITH AN AEROELASTIC SECTION MODEL

In order to study the applicability of the calculation models deduced in Chapters 2 and 3, wind tunnel tests employing an aeroelastic section model were conducted by the author. The section model (*Fig. 13*) was a replica in the geometric scale of 1:25 of the suspended structure of the Kärkinen Bridge in Finland. The primary objective of the experiments was to determine aerodynamic input parameters for the present analysis models to be used for the verification study. The parameters comprise the deck flutter derivatives, RMS exciting coefficients, steady-state response peak factors and normalized spectral densities for the signature turbulence. The steady aerodynamic coefficients of the Kärkinen Bridge deck have been reported elsewhere [109]. The secondary objective of the tests was to obtain experience on extracting the flutter derivatives by means of the modern system identification techniques.

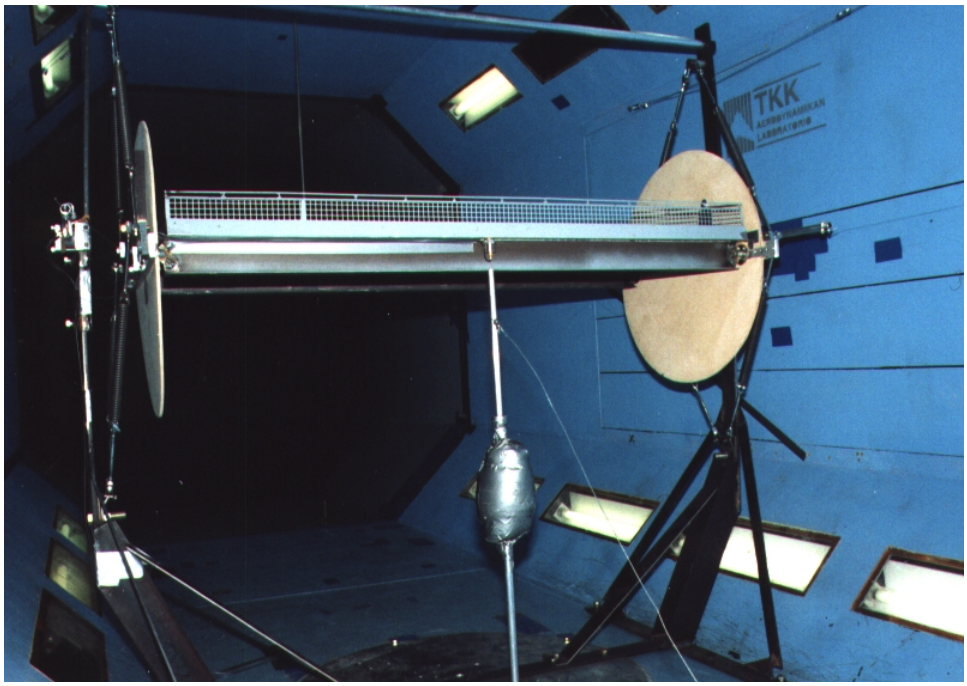

Fig. 13 Aeroelastic section model of the Kärkinen Bridge. Photo by the author.

The scale model was tested in a smooth flow in the wind tunnel of the Laboratory of Aerodynamics at Helsinki University of Technology during four days in November 1997. The cross-section of the wind tunnel's working section is octagonal with the horizontal and vertical clearance, both 2 m. The flow speeds used in the tests ranged from 4.5 m/s to 40 m/s.

4.1 Test setup and analysis procedures

4.1.1 Aeroelastic section model

The aeroelastic section model was prepared to be as stiff as possible to allow a rigid body motion due to the elastic spring constraints only. It was designed by taking into account the model scaling laws for the geometry and the mass density. The damping ratio of the model was intended to be lower than that expected for the prototype bridge. The ratio between the natural frequencies of the fundamental vertical bending mode and the fundamental torsional mode were chosen to be similar with respect to the prototype bridge. This was not a necessity according to the theory but it was applied to ensure that the vortex-induced lock-in vibrations of the modes were separated. The spring support was relatively stiff to push the fundamental vortex-induced resonance beyond the lower flow speed limit of the wind tunnel.

The cross-sectional dimensions of the Kärkinen Bridge and the section model are given in *Fig. 14*. The cable anchorages located outside the I-girders were not included in the model. The length and height of the section model were 1.4 m and 0.094 m, respectively. The model height results the blockage ratio of 3.6 %. No corrections due to the blockage or the end plate effects were accounted for.

The model was fabricated from a plywood deck, wooden strips and steel sheets. A steel sheet was fastened by screws and glue under the plywood deck in order to increase the stiffness of the model. I-beams and wind bracings were connected to this sheet by point-welds. The deck geometry and edge beams were finalized by strips connected by screws and glue. The railings of the model were made of a steel net and threads. The solidity ratio of the net was 36 %. Circular end plates made of plywood were attached on the model to guide the flow to retain its two-dimensional character. The centre of gravity of the prototype bridge was calculated by the nominal dimensions and masses of the deck section. The target mass and mass moment of inertia and the position of the centre of gravity were adjusted by attaching auxiliary weights ($2 \cdot 1.4$ kg) to the end plates. Simplified modal analysis was applied to ensure that the heaving and torsional modes remained uncoupled for an excitation in the centre of gravity and that the local vibrations of the rig and the vibrations of model did not interact.

The model was supported from its ends by eight helical springs mounted at inclined alignment (*Figs 13* and *14*). Owing to this arrangement there was a theoretical nonlinearity effect in the twisting angle vs. twisting moment relation. The effect was precalculated and found negligible for the applied range of amplitudes. The mounting positions of springs were adjusted so that the elastic centre and the centre of gravity of the cross-section coincided. Also controllable by the mounting position of springs was the ratio between the natural frequencies of the heaving and torsional modes. The other ends of springs were attached to the vertical posts of the test rig. The along-wind vibration of the model was restrained by guys fixed to the horizontal cantilever bars of the test rig. Ball bearings were installed to the joints between the guys and the section model to allow an undisturbed torsional motion.

The test rig was mounted on a plywood floor of the working section of the wind tunnel. In order to suppress unintentional vibrations, the rig was guyed to the wind tunnel walls. The tests rig was relatively light-weighted in comparison to the section model.

For the flutter derivative tests there was a simple triggering device attached to the rig. The device (*Fig. 13*) comprised a vertical bar that could be pushed under the leeward I-beam of the model. A wire was fixed to the upper end of the bar allowing a triggering operation by pulling. By lifting the leeward I-beam, simultaneous initial deflection and rotation were induced to the model. The lifting distances applied were about 2...4 mm depending on the flow speed of the test run.

In order to extract the dynamic properties of the section model, a series of free-vibration tests was carried out in actual test conditions. To produce consistent reference data for the flutter derivative tests, the triggering device was applied to excite the structure. Furthermore, the natural frequencies and damping were evaluated by the same time-domain system identification technique as used for the flutter derivatives (Chapter 4.1.3).

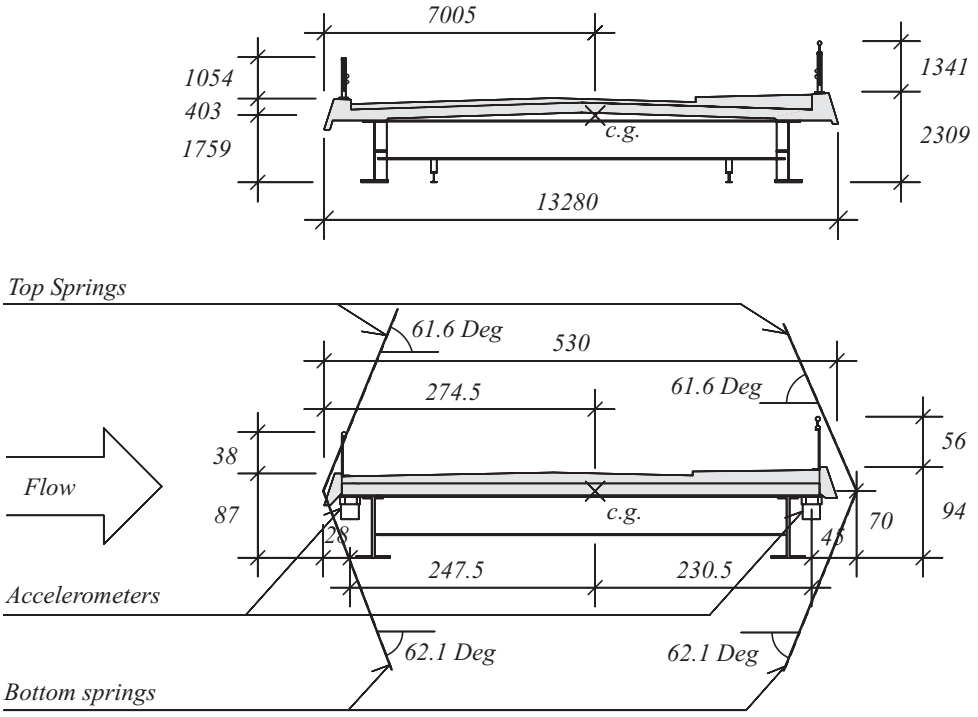

Fig. 14 Cross-sectional dimensions (in millimetres) of the Kärkinen Bridge and the section model. The dimensions of the section model are based on measurements from the finalized model.

The dynamic characteristics together with the conventional model data are given in *Table 1*. Also given is the estimated data for the prototype bridge and the target scaling. A typical approximation of including 1/3 of the spring masses to scale model inertia terms is accounted for [33].

Table 1 Technical data of the section model and the prototype bridge.

Property	*Section model*		*Per cent error due to model disparity*	*Prototype bridge* [3)]	*Target scale (λ = 1:25)*
	measured	*target*			
Width, B	0.530 m	0.530 m	± 0 %	13.280 m	λ
Height, h	0.094 m	0.092 m	2.20 %	2.309 m	λ
Mass per unit length, m	27.0 kg/m	27.5 kg/m	-1.80 %	17193 kg/m	λ^2
Mass moment of inertia per unit length, J	0.799 kgm	0.784 kgm	+1.9%	306218 kgm	λ^4
Natural frequency, heaving, n_η	8.2199 Hz[2)]	-	-	0.4646 Hz	-
Natural frequency, torsion, n_θ	12.948 Hz[2)]	-	-	0.7012 Hz	-
Damping ratio, heaving, ζ_η	0.0014[2)]	< 0.0064[1)]	-	-	-
Damping ratio, torsion, ζ_θ	0.0018[2)]	< 0.0064[1)]	-	-	-

Notes:

1) Estimate for the prototype bridge.

2) Mean value based on six experiments carried out in different occasions during the test days.

3) Data based on designs and the finite element models of the references [45,109].

4.1.2 Measuring instrumentation

The vertical accelerations were the primary quantities to be measured in the experiments. Two piezoelectric accelerometers (Brüel&Kjær, type 4338) were mounted by screws to the bottom of the deck slab. The accelerometers were located near the edge beams at the model mid-span (*Fig. 14*). The signals of the accelerometers were amplified by two charge amplifiers (Brüel&Kjær, type 2624) and preconditioned by the passive first-order bandpass filtering with 3 dB attenuation points at 0.1 Hz and 2.1 kHz. The sampling was conducted by the analog-to-digital converter (Io-Tech DaqBook200) with the resolution of 16 bits allowing 65536 different signal levels to be recorded theoretically. The sampling frequency of 300 Hz was used for the signals of both channels (accelerometers). Prior to sampling, averaging of 100 adjacent readings per channel taken with the maximum of 100 kHz acquisition rate was conducted by the analog-to-digital converter. The sampled signals were logged to the computer by saving data from each test run in a separate file. The flow speed was recorded manually from the permanent equipments of the wind tunnel.

The vertical and torsional accelerations at the reference point (centre of gravity) were calculated from the data of the two channels by assuming the geometry given in *Fig. 14*. The postprocessing of data was carried out mainly by the tailor-made computer code developed by the author. In addition, a common spread sheet program was applied in the extraction of flutter derivatives.

4.1.3 Instrumental variable method for extracting flutter derivatives

The modern system identification methods allow, in principle, the extraction of all 18 flutter derivatives from the sampled coupled-motion time histories. The perceived advantages obtained through coupled-motion tests are that the number of test runs needed in a wind tunnel is reduced and the test setup is simplified. Ideally, in usual case in which the aeroelastic drag component is not included in a test program, the coupled-motion approach requires 1/3 of the test runs of the conventional method described by SCANLAN and TOMKO [78]. The fundamental problem in the successful application of exclusive coupled-motion tests is to find out a system identification method that produces consistent and correct results.

In the present study, the Instrumental variable method and coupled-motion tests were applied to evaluate the eight flutter derivatives associated with the heaving and torsional modes of the section model. The principle of the Instrumental variable method is to suppress the effect of signal noise from the least squares estimate through an iterative process. The formulation of the Instrumental variable method can be done by several ways. The method described by SHINOZUKA *et al*. [93], however, is closely followed in the present development. The required modifications are due to the application of acceleration signal input and are subjected primary to the treatment of initial conditions. The modified method is described subsequently.

The equations of motion of the section model at free-vibrations conditions can be converted to the first-order linear differential equation system with the state-space expansion by

$$\dot{\mathbf{Y}} = \mathbf{A}\mathbf{Y} \ , \qquad \textbf{(99)}$$

where, respectively, system matrix **A** and state vector **Y** are

$$\begin{cases} \mathbf{A} \equiv \begin{bmatrix} 0 & \mathbf{I} \\ -\mathbf{M}^{-1}(\mathbf{C} - \mathbf{C}_{Ae}) & -\mathbf{M}^{-1}(\mathbf{K} - \mathbf{K}_{Ae}) \end{bmatrix} = \\ \quad = \begin{bmatrix} 0 & 0 & 1 & 0 \\ 0 & 0 & 0 & 1 \\ \dfrac{\rho B^2 \tilde{\omega}_\eta H_1^*}{2m} - 2\zeta_\eta \omega_\eta & \dfrac{\rho B^3 \tilde{\omega}_\theta H_2^*}{2m} & \dfrac{\rho B^2 \tilde{\omega}_\eta^2 H_4^*}{2m} - \omega_\eta^2 & \dfrac{\rho B^3 \tilde{\omega}_\theta^2 H_3^*}{2m} \\ \dfrac{\rho B^3 \tilde{\omega}_\eta A_1^*}{2J} & \dfrac{\rho B^4 \tilde{\omega}_\theta A_2^*}{2J} - 2\zeta_\theta \omega_\theta & \dfrac{\rho B^3 \tilde{\omega}_\eta^2 A_4^*}{2J} & \dfrac{\rho B^4 \tilde{\omega}_\theta^2 A_3^*}{2J} - \omega_\theta^2 \end{bmatrix} \\ \mathbf{Y} \equiv \begin{Bmatrix} \mathbf{X} \\ \dot{\mathbf{X}} \end{Bmatrix} = \begin{Bmatrix} \eta \\ \theta \\ \dot{\eta} \\ \dot{\theta} \end{Bmatrix} . \end{cases} \quad \textbf{(100)}$$

Here, symbols $\tilde{\omega}_\eta$ and $\tilde{\omega}_\theta$ denote the measured circular frequencies of the heaving and the torsional modes, respectively. These two frequencies are dependent upon the aeroelastic action of flow. The system matrix is square and has the size of 4 x 4 in the present problem. By considering a constant time increment Δ_t, the solution of Eq. (99) can be written as [93]

$$\mathbf{Y}_{i+1} = \mathbf{B}\mathbf{Y}_i , \quad \textbf{(101)}$$

where the subscript $i + 1$ stands for the time instant $t + \Delta_t$ and the exact value of state transition matrix **B** is obtained through the exponent matrix series

$$\mathbf{B} = e^{\Delta_t \mathbf{A}} \equiv \mathbf{I} + \Delta_t \mathbf{A} + \frac{\Delta_t^2}{2!}\mathbf{A}^2 + \frac{\Delta_t^3}{3!}\mathbf{A}^3 + \ldots . \quad \textbf{(102)}$$

In this solution no special requirements are imposed for the properties of the system matrix. Provided that state transition matrix **B** is known after the system identification, system matrix **A** can be constructed so that it satisfies Eq. (102). In consequence of Eqs (100), the unknown flutter derivatives can be evaluated. In the present context, only the acceleration data is expected to be observed in the experiments making a direct application of Eq. (101) unworkable, as this equation comprises the defection and velocity data. By differentiating twice with respect to time Eq. (101) yields

$$\ddot{\mathbf{Y}}_{i+1} = \mathbf{B}\ddot{\mathbf{Y}}_i \equiv \begin{bmatrix} \mathbf{b}_{11} & \mathbf{b}_{21} \\ \mathbf{b}_{21} & \mathbf{b}_{22} \end{bmatrix} \ddot{\mathbf{Y}}_i , \quad \textbf{(103)}$$

where submatrix $\mathbf{b}_{ij}$ (i, j = 1 or 2) of the size 2 x 2 is introduced to denote the structure of the state transition matrix. The third time derivatives of coordinates, inherent in this equation, should be eliminated for the present development. The elimination can be carried out by extending the equation to contain one additional time increment. It results the autoregressive moving average model [93]

for the acceleration responses by

$$\ddot{\mathbf{X}}_{i+1} = \mathbf{F}_1\ddot{\mathbf{X}}_i + \mathbf{F}_2\ddot{\mathbf{X}}_{i-1} + \mathbf{W}_{i+1} , \tag{104}$$

where $\mathbf{W}_{i+1}$ is the observation error vector corresponding the time instant denoted by the subscript and

$$\begin{cases} \mathbf{F}_1 = \mathbf{b}_{11} + \mathbf{b}_{12}\mathbf{b}_{22}\mathbf{b}_{12}^{-1} \\ \mathbf{F}_2 = \mathbf{b}_{12}\mathbf{b}_{21} - \mathbf{b}_{12}\mathbf{b}_{22}\mathbf{b}_{12}^{-1}\mathbf{b}_{11} . \end{cases} \tag{105}$$

In Eq. (104), the observation error vector is added to take into account the possible random type disturbances in measured signals. Eq. (104) implies the linear dependence between the accelerations for three successive instants of time and allows identification of matrices $\mathbf{F}_1$ and $\mathbf{F}_2$ from the sampled acceleration data. To show the dependence between matrices $\mathbf{F}_1$ and $\mathbf{F}_2$ and system matrix $\mathbf{A}$, vector $\tilde{\mathrm{Y}}$ of size 4 x 1, containing acceleration data at time i and i + 1, is defined as

$$\tilde{\mathbf{Y}}_i \equiv \begin{Bmatrix} \ddot{\mathbf{X}}_i \\ \ddot{\mathbf{X}}_{i+1} \end{Bmatrix} . \tag{106}$$

It follows from Eq. (104) that

$$\tilde{\mathbf{Y}}_{i+1} = \begin{bmatrix} 0 & \mathbf{I} \\ \mathbf{F}_2 & \mathbf{F}_1 \end{bmatrix} \tilde{\mathbf{Y}}_i \equiv \tilde{\mathbf{B}}\tilde{\mathbf{Y}}_i , \tag{107}$$

where symbol $\tilde{\mathbf{B}}$ is used to denote the given square matrix. This equation, consistent with Eqs (99) and (101), represents the solution for the first-order differential equation

$$\dot{\tilde{\mathbf{Y}}} = \tilde{\mathbf{A}}\tilde{\mathbf{Y}} \equiv \begin{bmatrix} \tilde{\mathbf{a}}_{11} & \tilde{\mathbf{a}}_{12} \\ \tilde{\mathbf{a}}_{21} & \tilde{\mathbf{a}}_{22} \end{bmatrix} \tilde{\mathbf{Y}} , \tag{108}$$

in which the usage of square submatrices $\tilde{\mathbf{a}}_{ij}$ (i, j = 1 or 2) is the same as in Eq. (103). With the known matrix $\tilde{\mathbf{B}}$, matrix $\tilde{\mathbf{A}}$ can be constructed by means of the relation $\tilde{\mathbf{B}} = e^{\Delta t\tilde{\mathbf{A}}}$. The second time derivative of the state vector $\mathbf{Y}$ is related to vector $\tilde{\mathbf{Y}}$ by

$$\ddot{\mathbf{Y}} = \begin{bmatrix} \mathbf{I} & 0 \\ \tilde{\mathbf{a}}_{11} & \tilde{\mathbf{a}}_{12} \end{bmatrix} \tilde{\mathbf{Y}} \equiv \tilde{\mathbf{R}}\tilde{\mathbf{Y}} , \tag{109}$$

where symbol $\tilde{\mathbf{R}}$ is used to denote the given transformation matrix. By differentiating Eq. (99) twice with respect to time and by considering Eq. (109), it follows that the original system matrix $\mathbf{A}$ can be reconstructed by the formula

$$\mathbf{A} = \tilde{\mathbf{R}}\tilde{\mathbf{A}}\tilde{\mathbf{R}}^{-1} . \tag{110}$$

This formula provides the solution of the problem as far as matrices $\mathbf{F}_1$ and $\mathbf{F}_2$ are identified. The

ordinary least squares estimate of these matrices, denoted here by symbols $\tilde{\mathbf{F}}_1$ and $\tilde{\mathbf{F}}_2$, respectively, can be expressed in the form [93]

$$\left[\tilde{\mathbf{F}}_1 \;\; \tilde{\mathbf{F}}_2\right] = \boldsymbol{\Psi}_2 \boldsymbol{\Psi}_1^T \left[\boldsymbol{\Psi}_1 \, \boldsymbol{\Psi}_1^T\right]^{-1} , \tag{111}$$

where matrices $\boldsymbol{\Psi}_1$ and $\boldsymbol{\Psi}_2$ contain the measured acceleration data as

$$\begin{cases} \boldsymbol{\Psi}_1 \equiv \begin{bmatrix} \ddot{\mathbf{X}}_0 + \mathbf{W}_0 & \ddot{\mathbf{X}}_1 + \mathbf{W}_1 & \ddot{\mathbf{X}}_2 + \mathbf{W}_2 & \cdots & \ddot{\mathbf{X}}_{N_d-1} + \mathbf{W}_{N_d-1} \\ \ddot{\mathbf{X}}_{-1} + \mathbf{W}_{-1} & \ddot{\mathbf{X}}_0 + \mathbf{W}_0 & \ddot{\mathbf{X}}_1 + \mathbf{W}_1 & \cdots & \ddot{\mathbf{X}}_{N_d-2} + \mathbf{W}_{N_d-2} \end{bmatrix}^T \\ \boldsymbol{\Psi}_2 \equiv \begin{bmatrix} \ddot{\mathbf{X}}_1 + \mathbf{W}_1 & \ddot{\mathbf{X}}_2 + \mathbf{W}_2 & \ddot{\mathbf{X}}_3 + \mathbf{W}_3 & \cdots & \ddot{\mathbf{X}}_{N_d} + \mathbf{W}_{N_d} \end{bmatrix} . \end{cases} \tag{112}$$

Here, the integer N_d denotes the highest data index considered in the analysis. Vectors $\ddot{\mathbf{X}}_{-1}$ and $\ddot{\mathbf{X}}_0$ have special purposes in the analysis as they determine the initial conditions of the problem. Error matrix $\mathbf{W}_F$, representing the error in estimates, can be defined as [93]

$$\mathbf{W}_F \equiv \left[\tilde{\mathbf{F}}_1 \;\; \tilde{\mathbf{F}}_2\right] - \left[\mathbf{F}_1 \;\; \mathbf{F}_2\right] = \boldsymbol{\Psi}_3 \boldsymbol{\Psi}_1^T \left[\boldsymbol{\Psi}_1 \, \boldsymbol{\Psi}_1^T\right]^{-1} , \tag{113}$$

where

$$\boldsymbol{\Psi}_3 \equiv \begin{bmatrix} \mathbf{W}_1 & \mathbf{W}_2 & \mathbf{W}_3 & \mathbf{W}_4 & \cdots & \mathbf{W}_{N_d} \end{bmatrix} . \tag{114}$$

In order to improve the estimates Eq. (111) provides for the noisy data, the Instrumental variable method can be utilized. In the method, the instrumental variable matrix $\boldsymbol{\Psi}_4$ is used to replace matrix $\boldsymbol{\Psi}_1{}^T$ in order to adjust the term $\boldsymbol{\Psi}_3 \boldsymbol{\Psi}_1^T$ in Eq. (113) to become zero. The instrumental variable matrix can be obtained through the iterative process as follows [93]:

a) Applying estimates for matrices $\mathbf{F}_1$ and $\mathbf{F}_2$, calculate the theoretical response. Initially, a least square estimate of Eq. (111) can be applied.
b) Applying the theoretical response thus obtained, construct instrumental variable matrix $\boldsymbol{\Psi}_4$ in the same way as matrix $\boldsymbol{\Psi}_1$ is constructed in Eqs (112).
c) Calculate the revised estimate through the equation

$$\left[\tilde{\mathbf{F}}_1 \;\; \tilde{\mathbf{F}}_2\right] = \boldsymbol{\Psi}_2 \boldsymbol{\Psi}_4^T \left[\boldsymbol{\Psi}_1 \, \boldsymbol{\Psi}_4^T\right]^{-1} . \tag{115}$$

d) Repeat the steps above, applying the revised estimate, until the sufficient convergence for the estimates of matrices $\mathbf{F}_1$ and $\mathbf{F}_2$ is achieved.

In general, the number of iterations required is proportional to the data noise level, i.e. for the noise-free data that obeys the mathematical model exactly, no iterations are needed as the least square estimate returns the correct result directly.

For the present development, the initial conditions for acceleration are to be related to the initial displacement and rotation of the scale model's centre of gravity. As long as the vibration frequencies

of the scale model are not identified by the method above, the relation is known only approximately, even though the values of initial displacement and rotation are known exactly. Therefore, an additional iteration process for finding the real initial conditions is required. Furthermore, the measured accelerations typically contain excessive noise just after the triggering operation. The noise is, e.g., on account of the higher modes of vibration, mechanical waves, flow transient effects or imperfections of the measuring instrumentation. To ensure consistent results in the system identification, it might be necessary to shift the time origin above the triggering instant. To overcome the aforementioned difficulties, the following iterative process can be followed:

a) Applying the estimate of system matrix **A**, and the known initial state vector $\mathbf{Y}_b$ associated with the instant of triggering operation, calculate the initial acceleration through Eq. (99).
b) Calculate the consistent value of initial accelerations at one time increment prior to the triggering operation through the formula

$$\dot{\mathbf{Y}}_{b-1} = \mathbf{A}\mathbf{B}^{-1}\mathbf{Y}_b \ . \qquad \textbf{(116)}$$

   The consistent initial accelerations thus obtained deviate from the physical zero values of accelerations occurring prior to the triggering.
c) Applying the time origin shift desired and Eq. (107), calculate the initial values (vectors $\ddot{\mathbf{X}}_{-1}$ and $\ddot{\mathbf{X}}_0$) required for the instrumental variable procedure. The associated observation error vectors are taken zero; $\mathbf{W}_{-1} = \mathbf{W}_0 = 0$.
d) Perform the system identification applying the Instrumental variable method.
e) Repeat the steps above applying the revised values for the estimated parameters until the sufficient convergence of initial conditions is achieved.

The most remarkable uncertainties in the initial conditions are most likely caused by flow speed effects on the zero level of the scale model, calibration of accelerometers and gain of amplifiers. The vibration frequencies of the section model, unknown initially, typically change only a few percent due to the aeroelastic action.

In any phase of the iteration process it might be advantageous to visually compare the theoretical and measured curves to ensure convergence towards the correct solution.

4.2 Results and details of the tests with discussion

4.2.1 Flutter derivative tests

The extracted flutter derivatives, to be applied in consistent with Eqs (6) or (17), are given in *Fig. 15*. Shown in the figure are the results for the individual tests (small circles), the average results (big circles) and the polynomial trend lines of varying order ranged from one to four. Nominally, there were five separate tests for each value of flow speed. The exception was the highest flow speed employed (40 m/s) to which only two tests were completed successfully due to a collapse of the test rig. The damping ratios due to the aerodynamic damping of heaving and torsional modes are shown in *Fig. 16*.

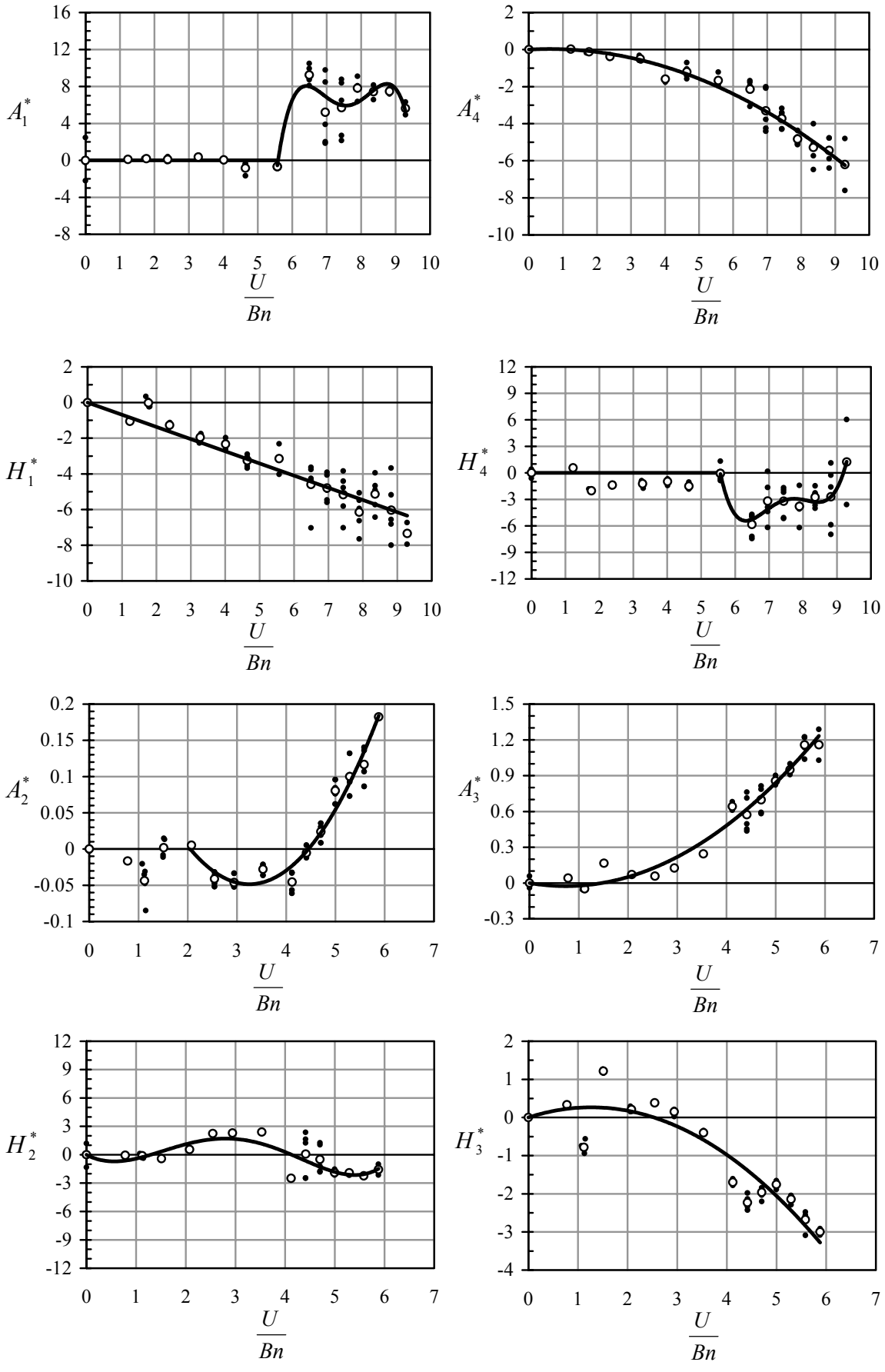

Fig. 15 Extracted flutter derivatives of the Kärkinen Bridge.

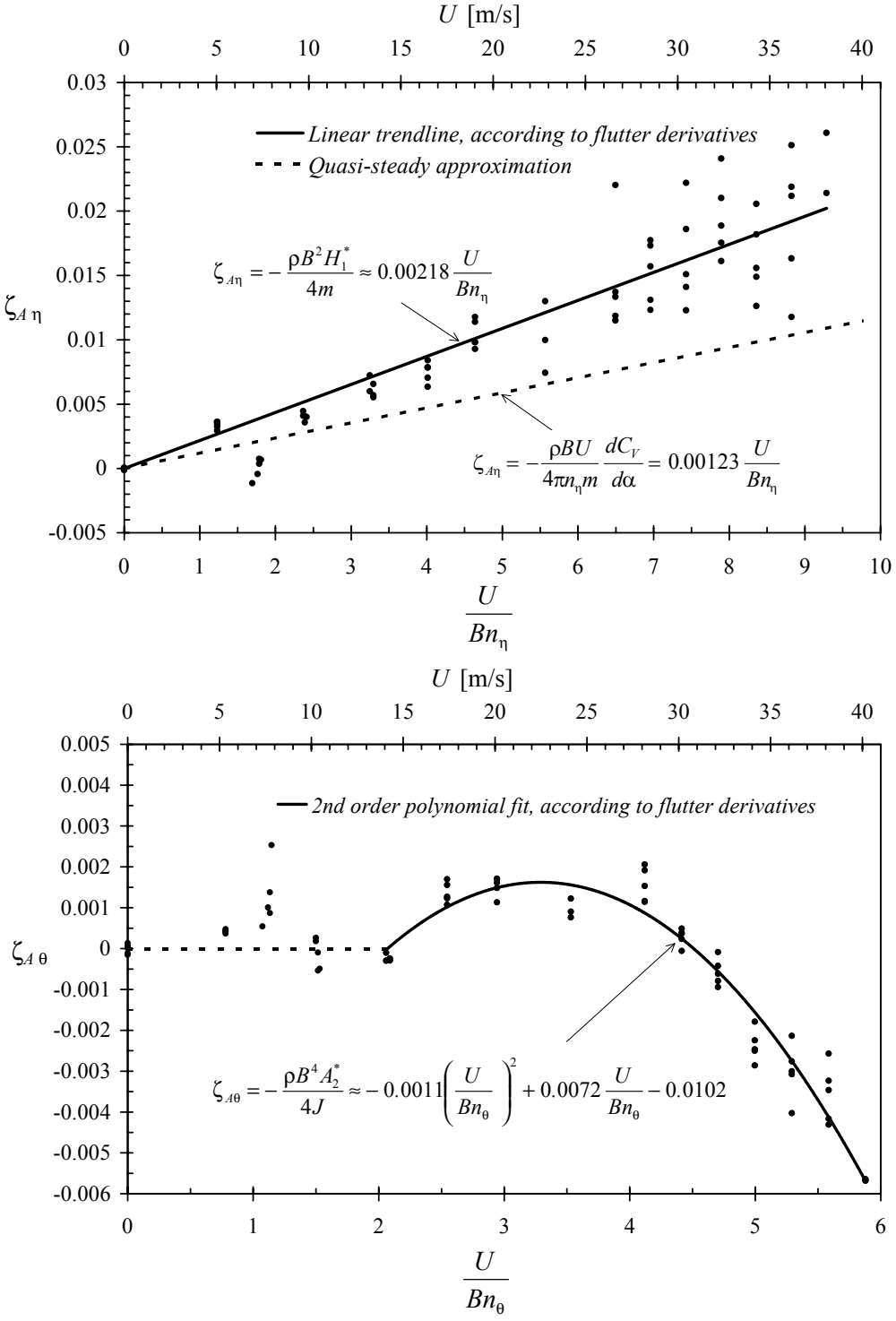

Fig. 16 Damping ratios associated with the aerodynamic damping. The dimensional wind velocity U refers to the flow speed in the wind tunnel.

It was found necessary to reduce the length of data sequences applied in the system identification with increasing flow speed. This was on account of the divergent torsional response beyond the flutter velocity and the rapid decay of the heaving mode. Also applied in the system identification, especially at the highest flow speeds, was the shifting of time origin past the triggering instant. This was because of spikes in signals observed in some tests during the first fractions of second of the recorded data. The length of data sequences, together with the time origin shifts applied,

are given in *Table 2*. Also given are the initial deflection and rotation of the model centre of gravity. Since their still-air values were relatively small, it was found necessary to perform additional iterations to calculate their values with respect to the steady-state value in flow, as suggested in Chapter 4.1.3. The initial deflections and twisting angles given in *Table 2* are approximative as their values were associated with the sensitivity of accelerometers and the gain of amplifiers.

Table 2 Data postprocessing details applied in flutter derivative tests.

Flow speed in wind tunnel [m/s]	*Numbers used for system indenfication per channel*	*Time origin shift [s]*	*Initial deflection [mm]*	*Initial twisting angle [Deg]*
5...30	6000	0…0.1	-1.2…-2.4	-0.2…-0.4
32	3000	0.1	-2.4	-0.4
34	1000	0.1	-2.4	-0.4
36…40	500	0.1…0.2	-2.4	-0.4

The ideal digital bandpass filtering involving the Fast Fourier Transform (FFT) techniques with the cutoff frequencies at 1 Hz and 100 Hz were applied to the sampled signals. The filtering was carried out mainly for convenience, as it accelerates the convergence of the Instrumental variable method. It also removed the erroneous low-frequency trends in the data caused by the electrical properties of equipments used.

With the aforementioned countermeasures, the flutter derivatives were successfully evaluated. The sample curve fits of the theoretical and observed responses are given in *Fig. 17*. The scatter of extracted flutter derivatives (*Fig. 15*) seems to increase with the increasing flow speed. This follows mainly from the randomness of the physical phenomenon studied rather than the defects of the identification technique. The technique used produces precise curve fits for the data sequences applied. However, general inconsistency exists because of the limited size of these sequences at flow speeds beyond the flutter velocity. As the truncated sequences should be applied, it is possible that an erroneous combination of the flutter derivatives produces better curve fits than the correct combination. It means here that the coupling flutter derivatives, associated with aerodynamic damping H_2^* and A_1^*, tend to produce alike exponential growth characteristics in the beginning motion as the uncoupled derivatives H_1^* and A_2^* do. Obviously, this kind of uncertainty cannot be avoided in the exclusive coupled-motion tests, as the presumed linear model is valid for a small amplitude motion only. It can be emphasized that the conventional extraction methods [78], involving the single-degree-of-freedom motion to extract H_1^* and A_2^*, do not suffer from this kind of uncertainty.

Another general problem of the system identification of some bridge deck models, like the present one, is the rapid decay of heaving oscillations at high flow speeds due to the aerodynamic damping. If the data sequence contains data for few vibration cycles only, it is complicate to obtain consistent results for the frequency and damping. Obviously, the number of samples (tests runs) should be increased in this case.

The evaluated flutter derivatives of the Kärkinen Bridge possess similar characteristics as those reported by SABSEVARI *et al.* [74], SCANLAN *et al.* [78] or given for the Raippaluoto Bridge in Ref. [108]. The flutter derivative A_2^* changes sign towards the higher values of reduced velocity indicating the negative aerodynamic damping in torsion and the deck susceptibility to the torsional flutter. The flutter derivative H_1^*, associated with the aerodynamic damping of the heaving mode, increases almost linearly with the reduced velocity imposing that the quasi-steady aerodynamic theory could give reasonable estimates. In the present case, however, the quasi-steady theory seems to underestimate the aerodynamic damping of the heaving mode (*Fig. 16*).

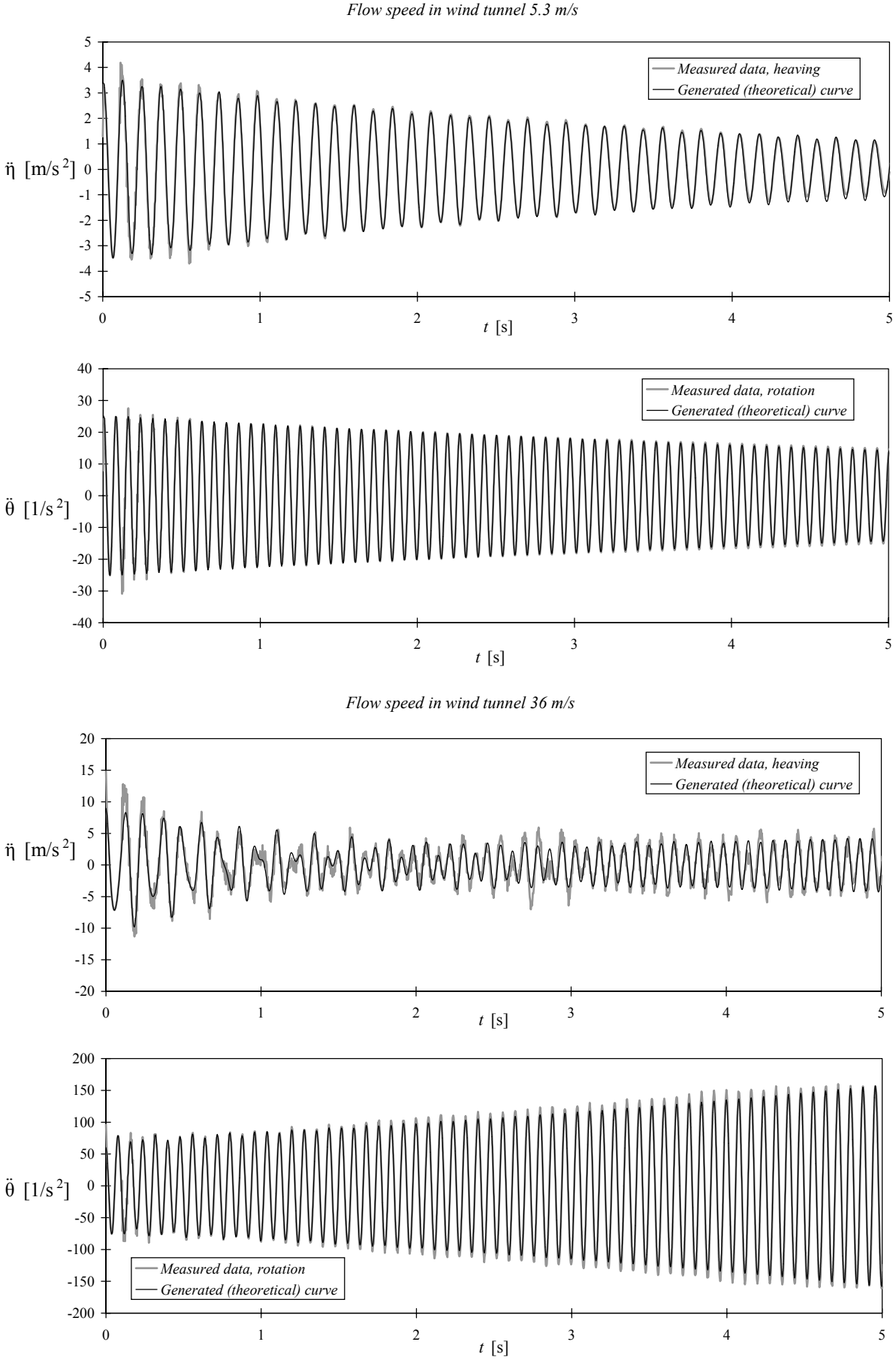

Fig. 17 Sample curve fits for acceleration responses obtained in the flutter derivatives extraction.

There seems to be discontinuities and rapid changes at damping characteristics around the vortex-shedding lock-in regimes (*Figs 15* and *16*). The damping ratio for the aerodynamic damping in torsion possesses maximum positive value near the upper end of the lock-in regime of the heaving mode. It might be related to the scale model's lock-in rotation mode around axes parallel to the flow direction.

4.2.2 Vortex and signature turbulence induced vibration tests

The standard deviation displacement and rotation responses of the scale model are shown in *Fig. 18*. The responses are determined from the acceleration data through division by the associated circular natural frequency squared. Although this simple approach is valid for the harmonic motion only, the implied error can be assumed to be negligible, as the motion was found almost harmonic at lock-in.

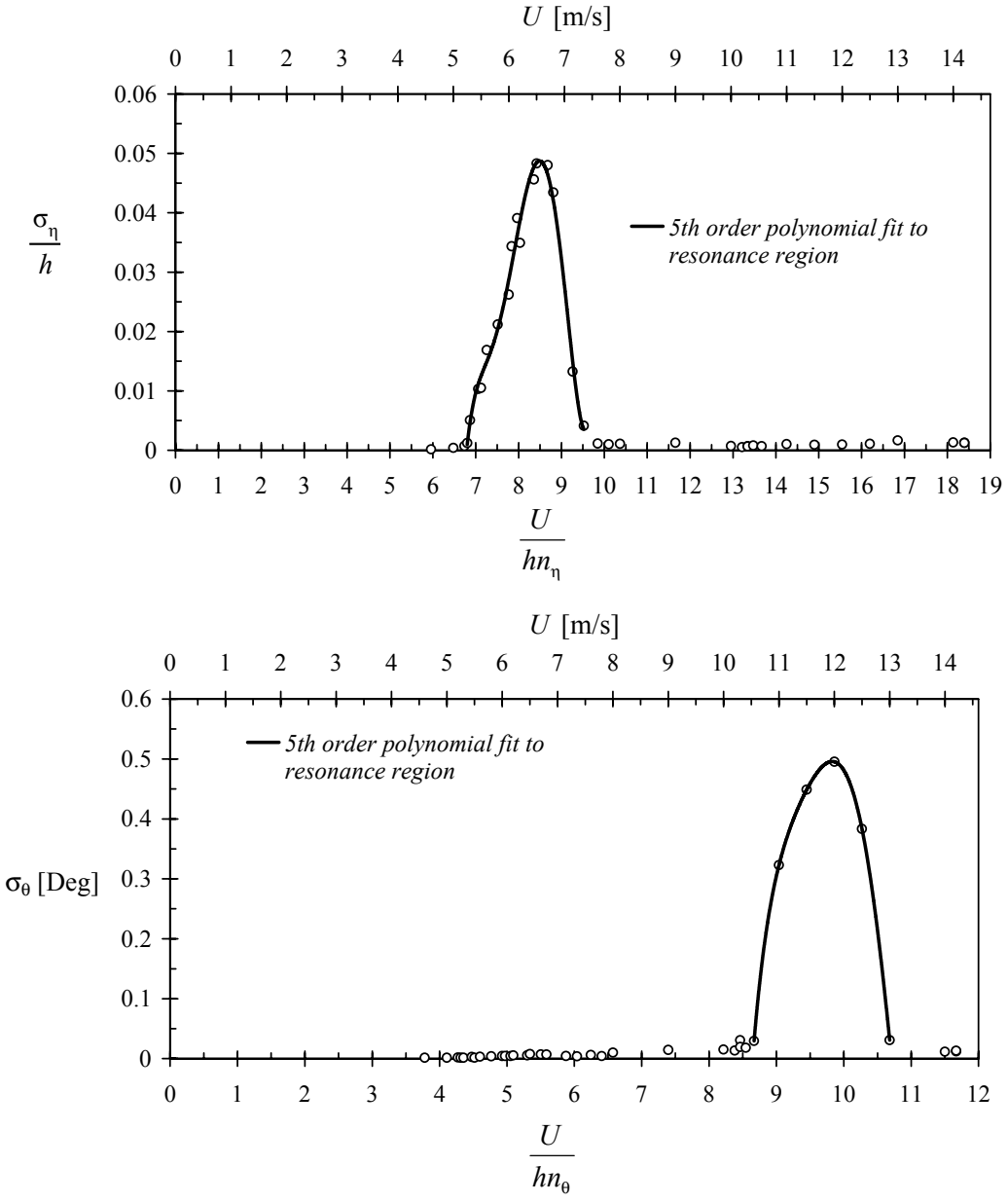

Fig. 18 Standard deviation responses of the heaving and torsional modes of the section model. The dimensional wind velocity U refers to the flow speed in the wind tunnel.

According to the response observed, there is one distinct lock-in regime for both the heaving and the torsional modes. The shapes of peak response curves can be concluded to be usual, as far as the sections models representing bridge decks are concerned.

The Strouhal numbers for the heaving and torsional excitations, when determined according to the lowest flow speed of lock-in, are 0.147 and 0.116, respectively. The resonant Strouhal numbers, defined according to the peak response, are 0.117 and 0.101, respectively. The resonant Strouhal number for the heaving mode is equal to the one reported elsewhere [109] for the 1:100 full model of the bridge stiffening girder, while the torsional mode has not been examined in detail.

The RMS exciting coefficients, to be applied in the vortex-shedding model of Chapter 3, are given in *Fig. 19*. The aerodynamic exciting coefficients, frequently dealt in literature, can be obtained by multiplying the present values by a factor $\sqrt{2}$. The polynomial curve fits shown are given by the formulae

$$\begin{cases} \tilde{C}_\eta \approx -0.0562\left(\dfrac{U}{hn_\eta}\right)^3 + 1.2044\left(\dfrac{U}{hn_\eta}\right)^2 + \\ \qquad -8.3335\dfrac{U}{hn_\eta} + 18.704\ , \qquad (6.8 \le \dfrac{U}{hn_\eta} \le 9.5) \\ \tilde{C}_\theta \approx 0.0117\left(\dfrac{U}{hn_\theta}\right)^3 - 0.5289\left(\dfrac{U}{hn_\theta}\right)^2 + \\ \qquad +6.9356\dfrac{U}{hn_\theta} - 27.961\ , \qquad (8.6 \le \dfrac{U}{hn_\theta} \le 10.7). \end{cases} \tag{117}$$

Here, the RMS exciting coefficients can be taken as zeros outside the range given for the reduced velocities.

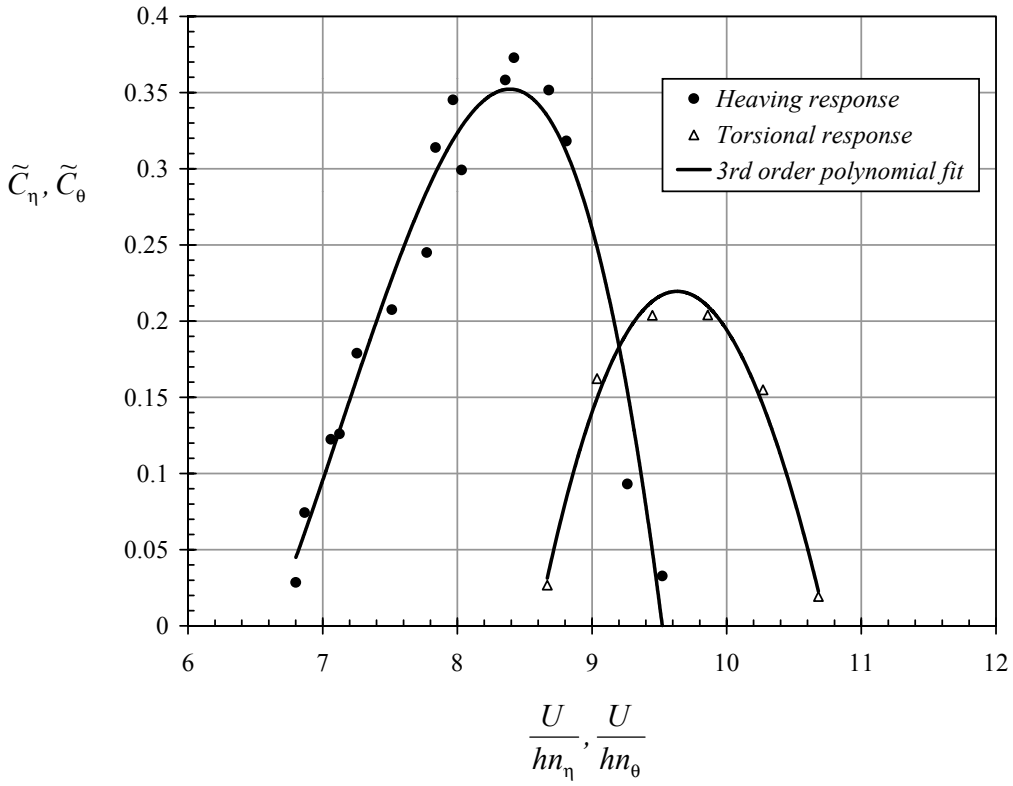

Fig. 19 RMS exciting coefficients for the heaving and the torsional modes.

The peak factors for the acceleration responses of the section model are shown in *Fig. 20*. The data is based on the recording time of $T = 33$ s that should be scaled to obtain equivalent values for the prototype bridge. The proper scaling can be obtained through the similarity of the dimensionless product $n_i T$ ($i = \eta$ or θ). The full-scale recording time of approximately 10 min can be deduced for the fundamental modes. In the lock-in regimes, peak factors lie close to the theoretical value of $\sqrt{2}$ of the harmonic motion. Outside these regimes, the scatter of results is considerable, but the trend is the same as expected for a typical bridge buffeting.

The normalized spectral densities of Eqs (93) for the signature turbulence are calculated according to the variance response of the section model via Eqs (92). The data employed is essentially the same as shown in *Fig. 18*, except that the flow speeds outside the lock-in regimes are concerned. The normalized spectral densities, shown in *Fig. 21*, are presented in a coordinate system supporting the evaluation of the relationship assumed. Furthermore, they are given with respect to unity coherence reduction factor, i.e. to the perfect spanwise correlation of loads. For other assumptions for the coherence, the values can be corrected through Eqs (92). A scatter of data indicates that a clear functional relationship, between the normalized spectral densities and the reduced velocities, cannot be deduced. Therefore, only the linear trendlines are illustrated. Owing to these lines, the formulae for normalized spectral densities are given as

$$\begin{cases} \tilde{S}_{VS} \approx \left(\dfrac{0.5638}{\dfrac{U}{hn_\eta}} \right)^2, & \left(\dfrac{U}{hn_\eta} \le 6.8 \text{ or } 9.5 < \dfrac{U}{hn_\eta} < 19 \right) \\ \tilde{S}_{MS} \approx \left(\dfrac{0.5579}{\dfrac{U}{hn_\theta}} \right)^2, & \left(\dfrac{U}{hn_\theta} \le 8.6 \text{ or } 10.7 < \dfrac{U}{hn_\eta} < 12 \right). \end{cases} \tag{118}$$

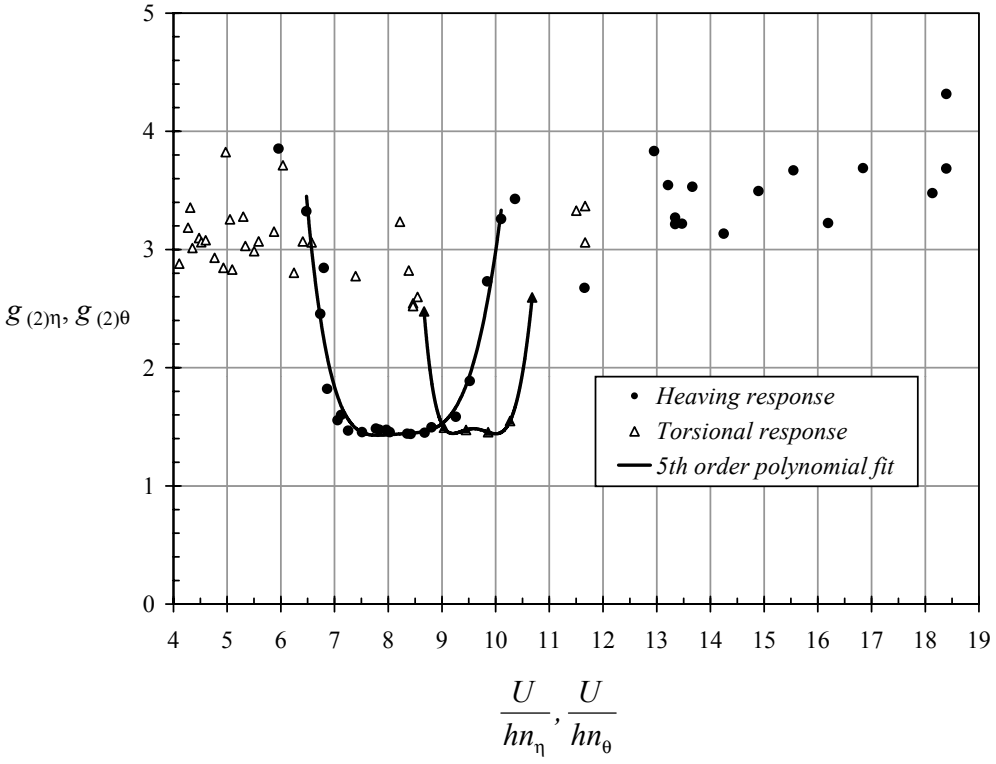

Fig. 20 Peak factors of the acceleration responses of the section model.

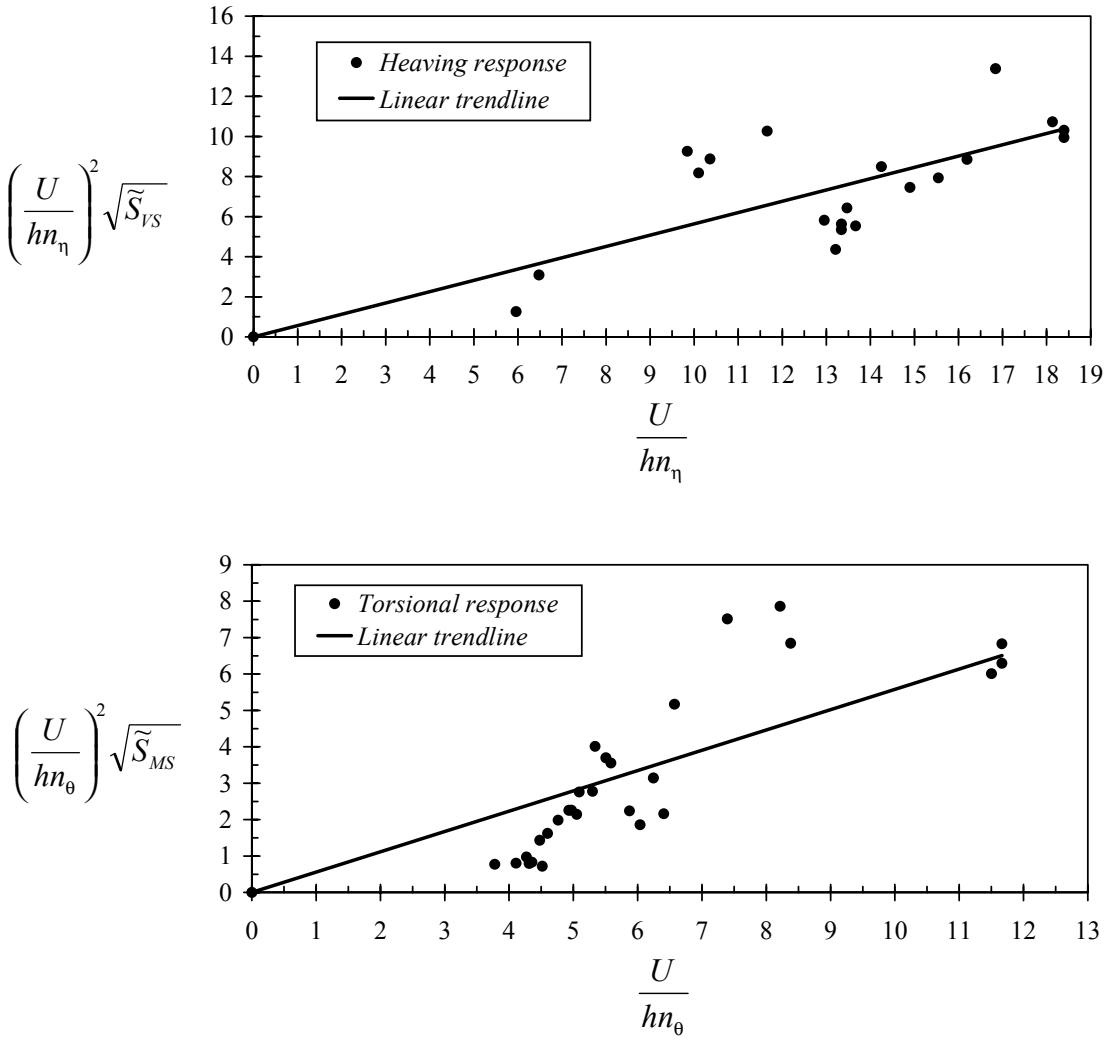

Fig. 21 Normalized spectral densities due to the signature turbulence. The reduced ordinate axis is invoked for the curve-fitting purposes.

4.2.3 Performance of the measuring instrumentation

The electrical properties of the instrumentation chain were found to be adequate for the purpose used. Evidence was obtained, however, that the performance of the instrumentation can be improved in future applications. The accelerometers used were 26 years old, while the factory calibration is guaranteed for one year typically. The sensitivity of one anemometer was tested to be still close to the original calibration value (98.6 pC/g), while for another it was about 60 % of the reference. Furthermore, the latter accelerometer mentioned ceased to operate after the collapse of the model. The signal-to-noise ratio of this accelerometer was not in optimum during the tests.

The frequency and phase responses of the data acquisition chain can be expected to be constants over the frequency range of interest. This is because of the technical specifications of electrical devices and the theoretical response of the bandpass filter. For the shock performance of the electrical circuits, no theoretical assessments were made. This observation, together with the fact that unshielded cables were used, indicate that the aforementioned initial signal spikes may be caused by the properties of electrical circuits.

There was no detrimental skewness (“asynchronous”) observed between the signals of two

channels. The applications of the Instrumental variable method suggested that, for some data sequences, the error of curve fits decreased when the artificial delay of order 0.001 s was added between the channels. As this was not the general trend, and had little effect on flutter derivatives identified, this manipulation was not pursued.

The contact of the test rig with the plywood-floor of wind tunnel's working section was unintentional and was because of the disparity of the prefabricated mounting system. The connection increased slightly mechanical damping in comparison with the laboratory-floor attachment. This observation, together with the visual inspection during the tests, indicated that the floor vibrated under the influence of the heaving oscillations of the model. The implications of this deficiency were tried to be minimized by employing the still-air damping and frequency measurements in the actual tests condition, in which the test rig was mounted on the working section's floor.

5 VERIFICATION STUDY

Two cable-stayed bridges (*Fig. 22*), opened to traffic in 1997, are analysed for the present study by the author applying the calculation models presented. The results are compared with the on-site measurements. The bridges concerned are the Raippaluoto Bridge and the Kärkinen Bridge having the longest spans in Finland of 250 m and 240 m, respectively. The former bridge is located in the coastal area and the latter in the rural area in the inland conditions.

Fig. 22 The Raippaluoto Bridge (top) and the Kärkinen Bridge (bottom) as photographed by the author during the test days.

The Raippaluoto Bridge has the same type of cross-section as it is illustrated for the Kärkinen Bridge in *Fig. 14*. An expectation is that the former bridge contains horizontal buffet plates at the bottom level of the stiffening girder to improve the aerodynamic performance. Furthermore, the I-girders are closer to the edge beams than what they are in the Kärkinen Bridge. The stay-cables of both bridges have their lowest natural frequencies above 1 Hz. It can be expected that no coupling exists between the lowest bending modes of the stiffening girder and the cable modes.

The Raippaluoto Bridge is located in the East-West direction the eastern end being on the continent side. The Kärkinen Bridge is sited about 15 Deg counter-clockwise from the South-North line when looking from South to North.

5.1 Input parameters for calculation models

The summary of the input parameters assumed is shown in *Table 3*. The wind tunnel data applied for the analysis of the Kärkinen Bridge comprises the results described in the present study and the data of Ref. [109]. For the Raippaluoto Bridge, the aerodynamic parameters are deduced from the wind-tunnel tests conducted by the Danish Maritime Institute (DMI) [108]. The vortex shedding and signature turbulence data is absent. In the context of buffet plate design, however, the relative reduction effect is shown for the vortex-induced vibration of the aeroelastic section model. The RMS exciting coefficients are roughly approximated to coalesce with the Kärkinen Bridge but taken 50% of the original values to account for the suggested improvement in the aerodynamic performance. Here, the reported reduction is not fully applied as it contains also the load correlation amplitude effects. The signature turbulence data is assumed to be identical to both bridges and is based on the present study.

Aerodynamic admittances given in *Table 3* are applied only for the vertical load and twisting moment; for the horizontal force component they are taken as unity. The drag forces of cables are subjected to interference lengths calculated from the bridge geometry. The associated loads are lumped to the nodes at cable ends. An expectation is the Raippaluoto Bridge girder to which the cable-induced drag force is superimposed to the deck drag to decrease the number of loaded nodes.

The FE-models applied for the modal analysis were prepared by the author and are described elsewhere [45]. The models were detailed three dimensional and were analysed using the sub-space iteration technique. The stress stiffening analysis option (the effect of normal forces) was invoked for the Raippaluoto Bridge model, but its effects were found insignificant.

Table 3 Input parameters assumed for the analysis (no correction made due to measurements).

Parameter	*Raippaluoto Bridge*	*Reference*	*Kärkinen Bridge*	*Reference*
Modes:		[45]		[45,109]
total number extracted	20		8	
number applied in wind analysis, N_m	14		8	
stress stiffening effects considered	yes		no	
1st vertical, n_1	0.4215 Hz[1)]		0.4646 Hz	
2nd vertical	0.4526 Hz[1)]		0.4894 Hz[1)]	
3rd vertical	0.5868 Hz		0.6787 Hz	
4th vertical	0.8330 Hz		0.9606 Hz	
1 st horizontal	0.5625 Hz		0.5805 Hz	
1 st torsion	1.062 Hz		0.7012 Hz	
Modal damping ratios (mechanical damping):				
to each mode, ζ_i	0.0064	[45]	0.0064	[45,109]
Physical dimensions:				[109]
deck width and height, B, h	15.1 m, 2.2 m		12.8 m, 2.3 m	
average height of deck c.g. above the ground level	27.5 m		20.0 m	
Turbulence model:				
surface roughness length, z_0	0.003 m	[22]	0.05 m	[22]
spectral densities $S_{uu}(n)$, $S_{ww}(n)$	ESDU 85020	[22]	ESDU 85020	[22]
coherence model	ESDU 86010	[23]	ESDU 86010	[23]
cross-spectrum $S_{uw}(n)$	Kaimal	Eq. (39)	Kaimal	Eq. (39)
deduced parameters:				
turbulence intensity, I_u, I_w *at deck level*	11.2%, 6.1 %		18.0%, 9.9 %	
${}^xL_u$, ${}^xL_w$ *(for mean wind 15 m/s at deck level)*	133 m, 11 m		146 m, 12 m	
$S_{uu}(n_1)$ *(for mean wind 15 m/s at deck level)*	0.4 m^2/s		0.8 m^2/s	
$S_{ww}(n_1)$ *(for mean wind 15 m/s at deck level)*	0.4 m^2/s		0.9 m^2/s	
Staedy aerodynamic coefficients:				
deck; C_H, C_V, C_M	0.24[2)], 0.16, 0.005[3)]	[108]	0.23, 0.22, 0.11	[109]
deck; $dC_H/d\alpha$, $dC_V/d\alpha$, $dC_M/d\alpha$	-0.20, -6.02, 0.43	[108]	-0.48, -2.38, 0.17	[109]
windward and leeward pylon leg; C_H	1.2, 1.2		1.2, 2.3	[109]
cable (reference width = 0.1 m); C_H	1.2		1.2	[109]
Aerodynamic admittances:				
for u, w components, Θ_u, Θ_w	Sears, Horlock	Eq. (24)	Sears, Horlock	Eq. (24)
Flutter derivatives:	DMI	[108]	the present study	Fig. 15
P_1^* *according to the quasi-steady theory*	$-2C_H/K$		$-2C_H/K$	
deduced sign reversal U/(Bn) for A_2^*	4.2		4.4	
Vortex and signature turbulence induced vibration:				
RMS exciting coefficients	the present study[4)]		the present study	Fig. 19
correlation model	Ehsan & Bosch	Eq. (84)	Ehsan & Bosch	Eq. (84)
excitation bandwidths for the body at rest, $\delta_{\eta 0}$, $\delta_{\theta 0}$	0.08, 0.08		0.08, 0.08	
critical standard deviation, $\sigma_{\eta Cr}$, $\sigma_{\theta Cr}$	0.05, 0.006 [5)]		0.05, 0.006 [6)]	
proport. constant for I_u *induced bandwidth,* $k_{\eta u}$, $k_{\theta u}$	1.665, 1.665		1.665, 1.665	
excitation spectrums for signature turbulence	the present study	Eq. (116)	the present study	Eq. (116)
span-wise coherence decay coefficient, c_s	4.0		4.0	
Specific wind analysis options:				
frequency range	0.0002 … 1.6 Hz		0.0002 … 1.1 Hz	
frequency separation at resonant regions	0.001 Hz		0.001 Hz	
average nodal load interference length for deck, l_i	5 m		14 m	
nodal load correlation correction applied	yes		yes	

Notes:

1) Combined to the bridge spanwise movement of the deck and the pylon bending.

2) Original value increased by 20 % to account for the drag of cables and the actual height of girder.

3) Taken reverse sign in comparison to the original value, as the present branch leads to dominant mean response.

4) Taken as 50 % of the values meant for the Kärkinen Bridge to account the effect of buffet plates.

5) Taken equal to the Kärkinen Bridge.

6) Taken equal to peak response observed in wind tunnel experiments as the response was found almost harmonic.

5.2 On-site measurements

The on-site measurements were carried out in 1999-2000. The measurements were designed and conducted by the author. The measuring instrumentation was designed to be portable and was transferred to the bridges on demand. There were three basic quantities recorded: instantaneous wind speed, vertical accelerations and displacements. During the scheduled measurement period in the beginning of 1999, the bridge sites were silent upon strong winds. It took about one year till the suitable conditions appeared at the sites.

Measurements were carried out in three separate 2-day occasions starting 30-Nov-1999 & 13-Dec-1999 (the Raippaluoto Bridge) and 13-Feb-2000 (the Kärkinen Bridge). During the first occasion, the sea was free of ice with wave heights about 1 m, while in the other cases the sea/lake was frozen and covered with snow. For brevity, these conditions are termed as "Autumn" and "Winter", respectively.

5.2.1 Instrumentation and postprocessing procedures

A general view of the instrumentation used is given in *Fig. 23*. The data acquisition was conducted within the car parked at the bridge pavement. The measurements did not disturb the traffic or cause any destructions to the structures.

The instantaneous wind velocity was measured by the cup anemometer (Vaisala WAA15A). It was fixed to the railing about 1.2 m above the deck (*Fig. 24*). The binary signal of the anemometer was converted to the velocities involving 1.0 s and 0.2 s averaging times. The usage of data was twofold: calculation of mean wind velocity and determination of longitudinal turbulence properties. The mean wind direction as well as the additional records of mean and 1 s gust wind velocity were obtained from the permanent road weather station sited on the Raippaluoto Bridge (*Fig. 24*) and hosted by the Finnish National Road Administration. For the Kärkinen Bridge this kind of information was not available and the wind direction was inspected visually observing the analog large wind vane mounted permanently on the bridge mid-span (*Fig. 24*).

Horizontal and vertical deflections were measured with a laser-optical device (NOPTEL PSM 90). The equipment (*Fig. 25*) contains a laser transmitter and a detector. The transmitter was mounted on the railing at the pylon, where deflections and rotations were assumed to be insignificant. The transmitter was considered to be at rest. The detector was installed on the railings at the target measurement point and vibrated together with the bridge deck. The detector uses the 0.5 kHz internal acquisition rate for the displacement readings of the horizontal and vertical components. The sampling frequency of approximately 50 Hz was applied to the data saved in the computer disk.

The accelerations were measured employing the equipments described in Chapter 4, but two new piezoelectric accelerometers (Brüel&Kjær, type 4338) having a calibration sensitivity about 99 pC/g, were used. The accelerometers were located on the pavement side of the deck and fixed by magnets to the basement plates of the railing posts. The acceleration data was sampled with 1 kHz frequency. Each sample lasted 10 min.

The measuring devices were powered by the car battery and external batteries. There were no mechanical vibrations or electrical noise caused by generators, car motors or alike devices disturbing the measurements.

The signals were filtered internally by the instruments and by the software. The details of the filtering procedures are given in Appendix B. The spectral densities shown in the present study are calculated by means of the FFT-technique. For acceleration data, the FFT array lengths applied were long containing 2^{20} numbers per channel.

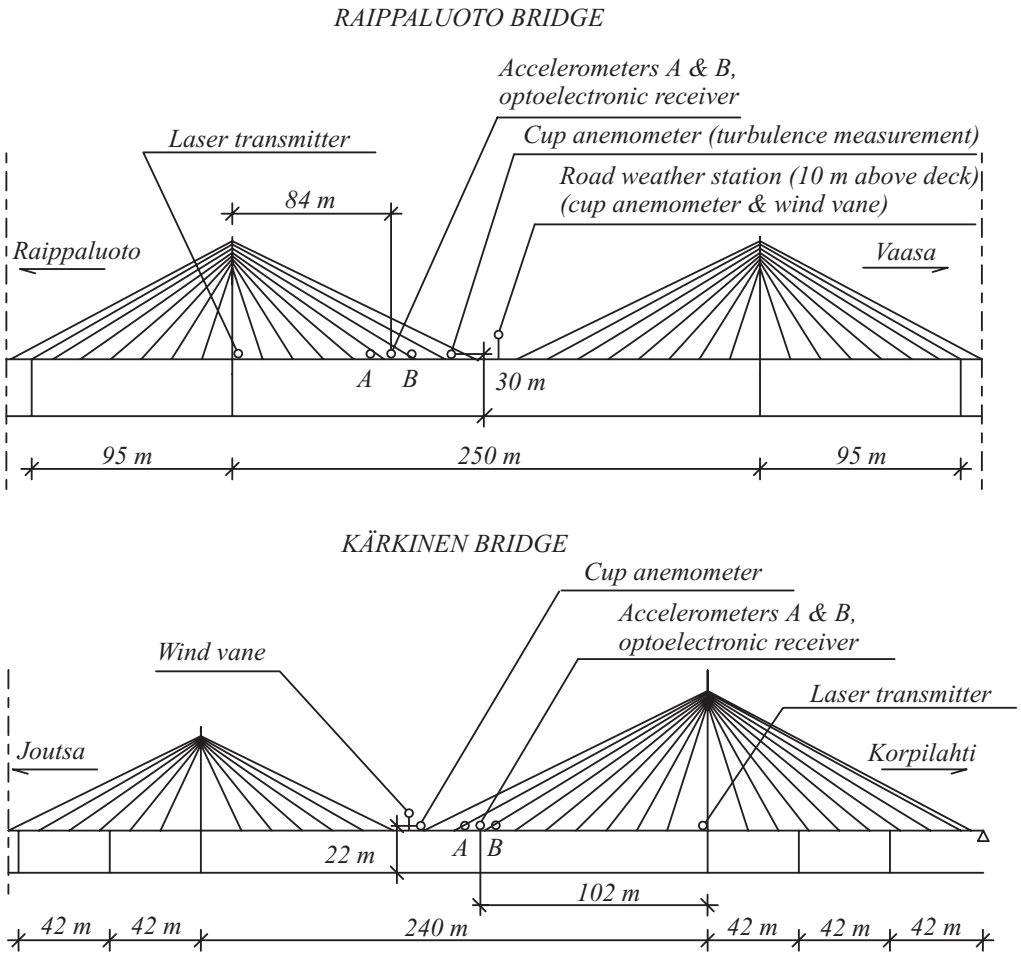

Fig. 23 Instrumentation layout.

Fig. 24 Left: the road weather station of the Raippaluoto Bridge with wind velocity and direction measurement capabilities. Right: the analog wind vane of the Kärkinen Bridge and the cup anemometer's positioning to the railing. Photos by the author.

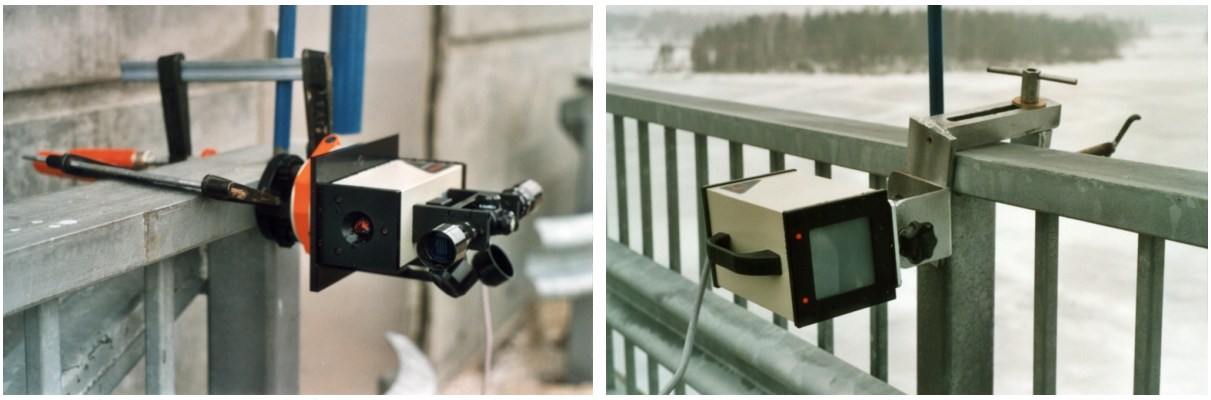

Fig. 25 The laser transmitter (left) and the optoelectronic receiver (right) installed on the Kärkinen Bridge. Photos by the author.

5.2.2 Measured turbulence properties

The characteristics of mean and gust wind velocities are shown in *Fig. 26*. As far as the present aims are concerned, both measurement occasions for the Raippaluoto Bridge were successful in the sense that the wind was directed almost perpendicular to the bridge and was strong enough ($U_{10} \geq 10$ m/s) for the presumed turbulence model to be valid. An opposite experience was gained from the measurements at the Kärkinen Bridge where the mean wind velocity was found to be unsteady and not reaching the target level except in short duration gusts. Furthermore, the wind was inclined away from the optimum direction.

The extracted longitudinal components of turbulence intensities are given in *Table 4*. The dimensional forms of the longitudinal turbulence spectrums are depicted in *Fig. 27*.

Table 4 Measured turbulence intensities.

	I_u	*Samples* [1)]	σ [2)]	*Omitted samples* [3)]	*Condition*
Raippaluoto Bridge					
North wind	8.8 %	9	1.1 %	2	Winter
South wind	15.0 %	7	0.8 %	-	Autumn
West wind	19.2 %	4	1.9 %	-	Autumn
South-West wind [4)]	10.8 %	1	-	-	Autumn
Kärkinen Bridge				-	
South-East wind	35.1 %[5)]	6	4.2 %	-	Winter
South wind	26.7%[5)]	9	1.7 %	-	Winter

Notes:

1) Number of samples contributing to the result. One sample = 10 min measuring period.

2) σ = sample standard deviation.

3) Number of samples omitted due to mean wind nonstationarities during the observation periods.

4) Assumed to blow directly from the open sea.

5) High values are associted to the wind gustiness and the low mean velocity of order 5 m/s.

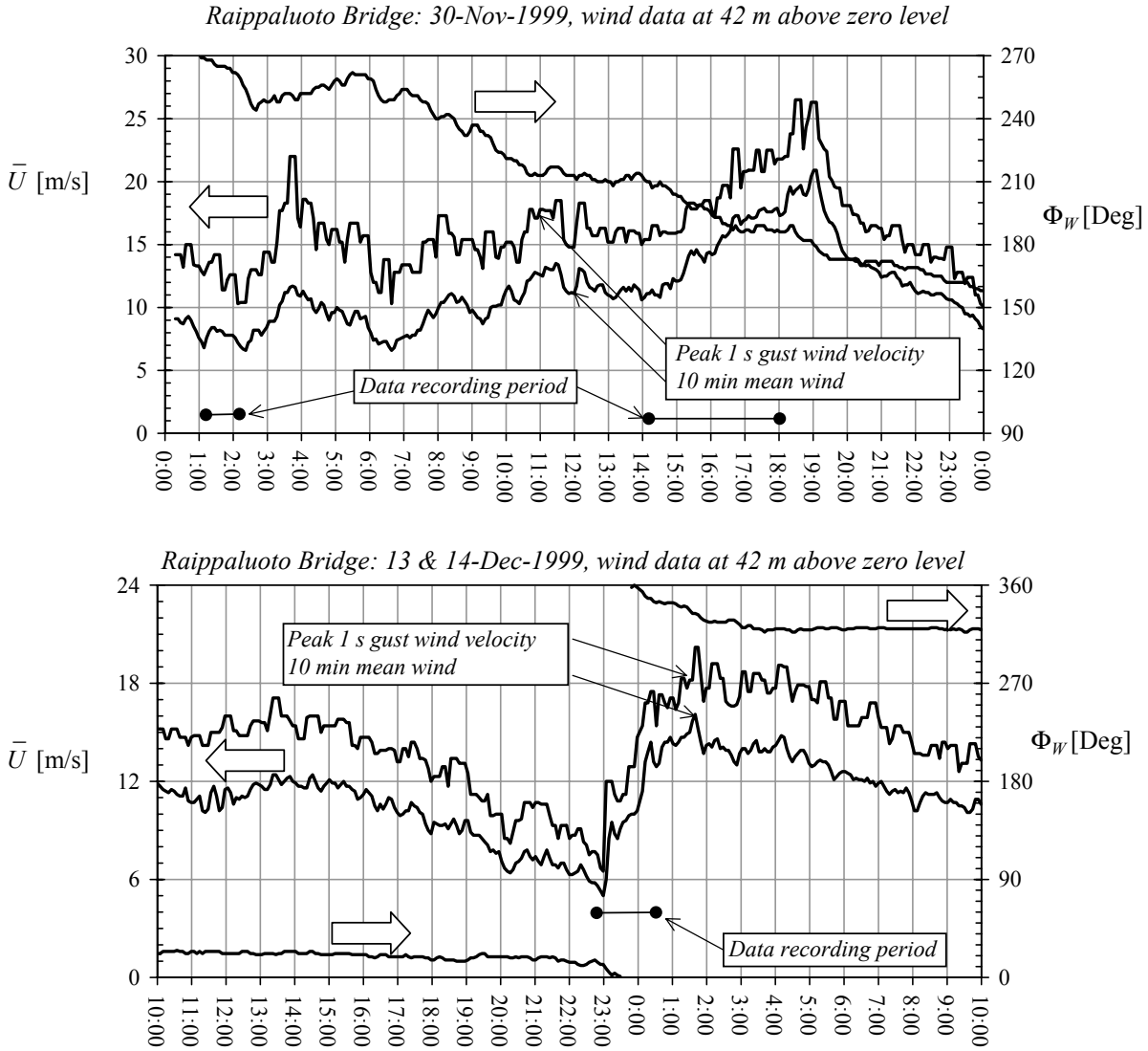

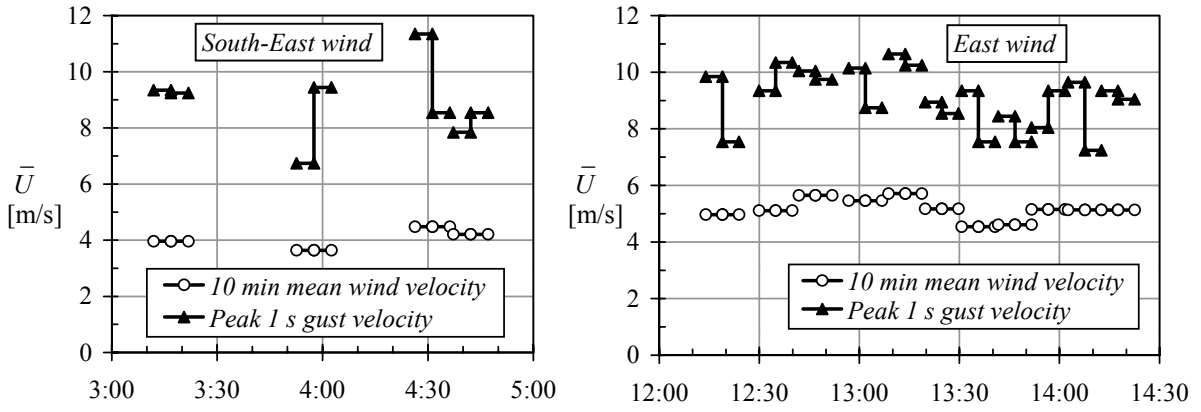

Fig. 26 Wind velocity and direction during the measurements. The wind direction angle zero (Φ_W = 0) is in the North and 90 Deg refers to the East wind that is also parallel to the Raippaluoto Bridge span.

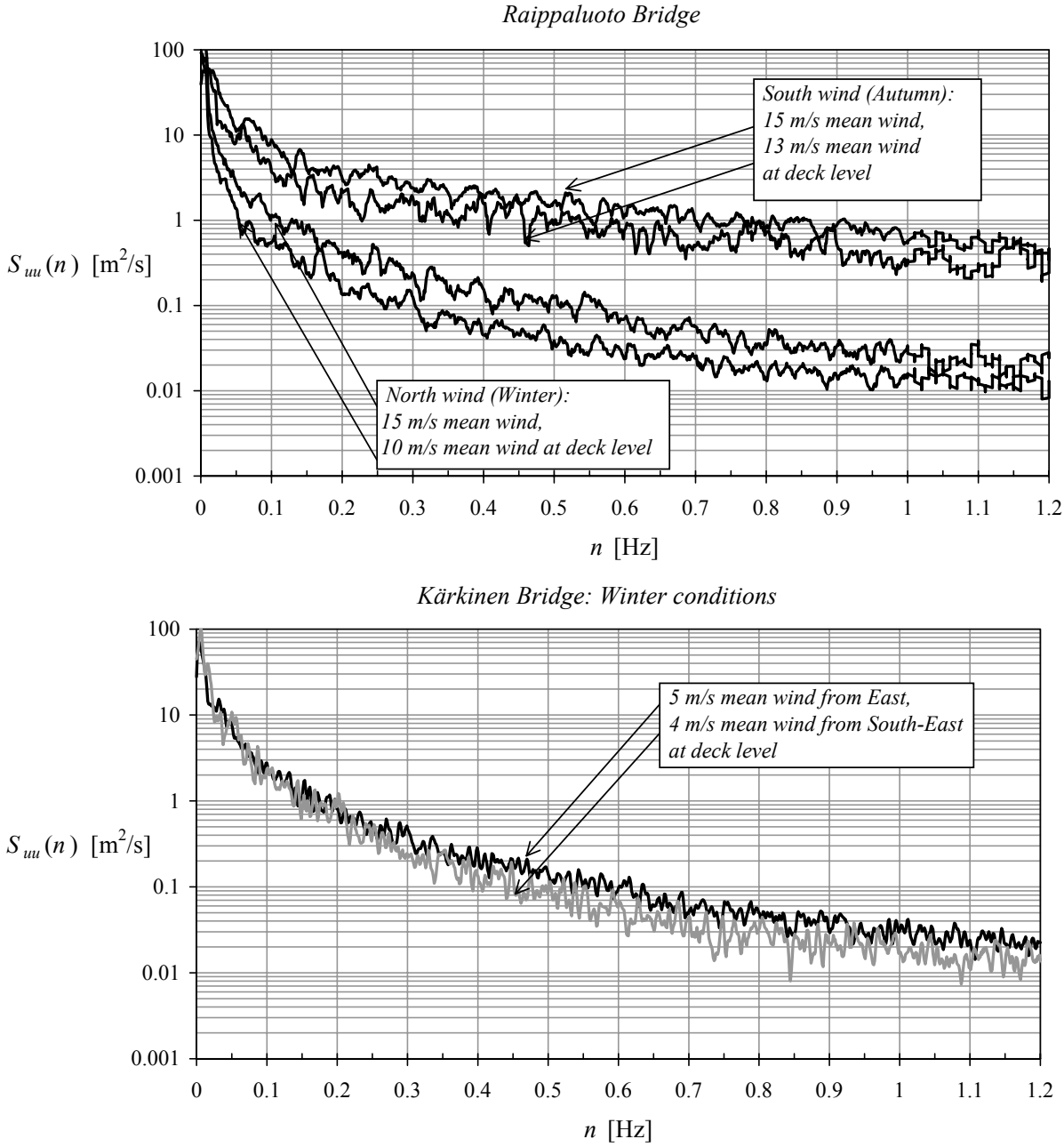

Fig. 27 Extracted dimensional forms of the turbulence spectrums: the Raippaluoto Bridge (top) and the Kärkinen Bridge (bottom).

5.2.3 Measured modal parameters

The ambient vibration technique was applied to detect the lowest natural frequencies of the bridges from the recorded vibration data. The main source of excitation was the wind, but as the traffic was not closed during the tests, it contributed to the response. The traffic was rare (couple of vehicles per hour if any) and its effect was verified to be negligible, except in the case of the Kärkinen Bridge, in which a loaded timber truck passing the bridge caused the third mode to become identifiable. The averaged unity normalized spectrums deduced are shown in *Fig. 28*. The spectrums are due to acceleration and displacement data for the Raippaluoto Bridge and the Kärkinen Bridge, respectively.

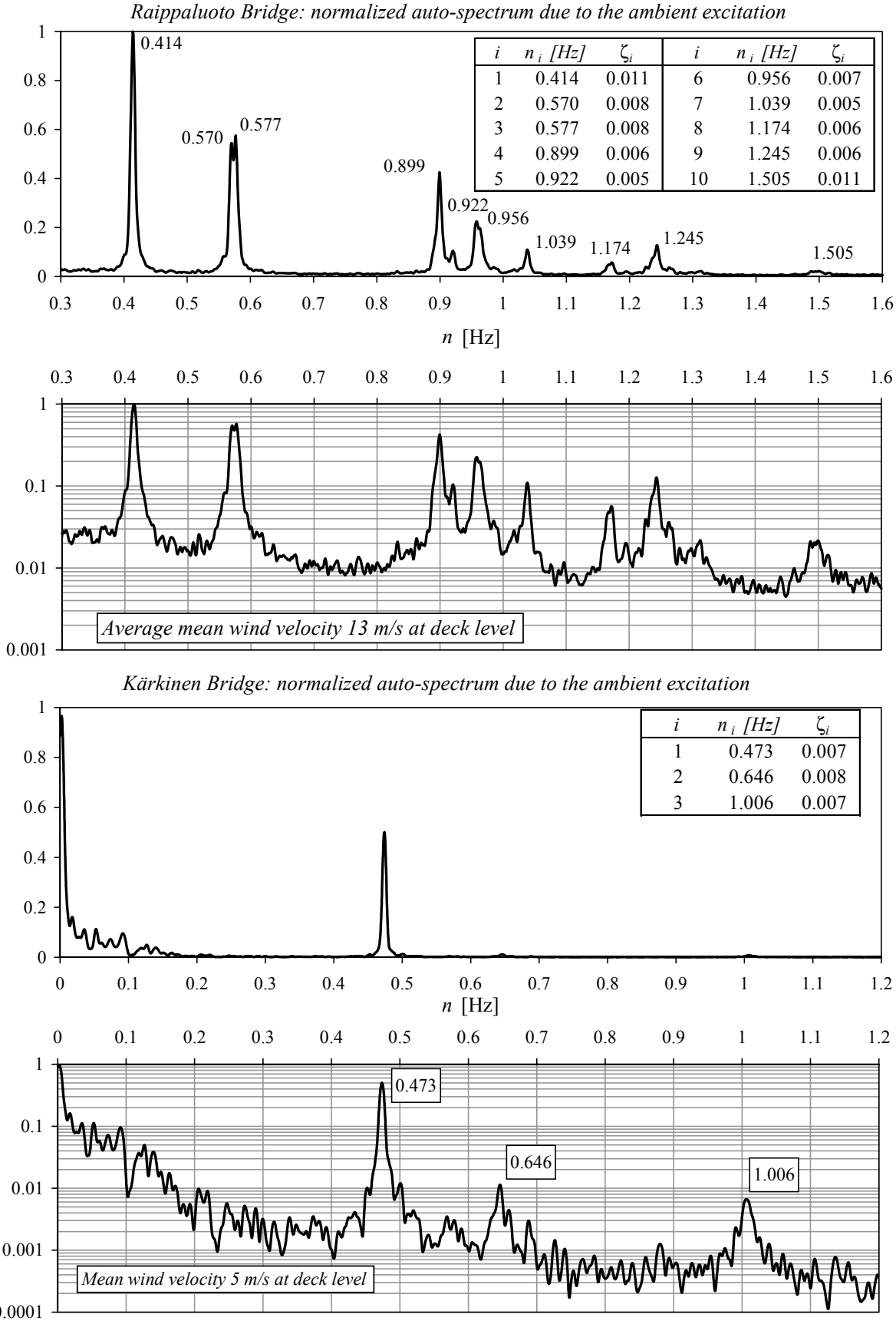

Fig. 28 Unity normalized auto-spectrums after the ambient vibration study involving the wind excitation and the rear traffic passing the bridge. Also shown are the estimates for the modal damping ratios (mechanical plus aerodynamic) calculated by the half-power bandwidth method.

5.2.4 Performance of the measuring instrumentation

In measurements of the longitudinal component of turbulence by the cup anemometer, two theoretical errors are implied. First, the distance constant of 1.5 m of the anemometer indicates that the smallest eddies of turbulence will be hidden, and second, the effect of turbulence across-wind lateral component (v-component) in not isolated from the readings. The effect of distance constant is that the wind speed is averaged over that distance. As discussed by LAWSON [49], the reduction factor to spectrum equals to the term $[\sin(\pi nT)/(\pi nT)]^2$, in which T is the averaging time. Thus, it can be deduced that 3 dB attenuation point for the spectral density at the mean wind of 15 m/s is about 4 Hz. In comparison to the structural natural frequency range of interest, the frequency response of the anemometer is adequate. Discussion with the expert of the anemometer's manufacturer confirmed, that no provision should be made to the second error source. It is believed that the error is insignificant and appears probably in most cup-anemometer-based data published.

The main reason for imperfection in the wind measurement setup was the anemometer's positioning relatively close to the deck. It is evident that the flow separation on the deck windward edge and the associated wake have added energy to the spectrums of *Fig. 27* in the high-frequency range. This is assumed to occur at frequencies where the apparent wavelength (U/n) is comparable to the dimensions of the cross-section. This assumption, and the comparison of spectrums of the South and North winds of the Raippaluoto Bridge, suggest that the frequency range beyond about 0.2 Hz might be disturbed. Here, the disturbance was not expected to occur in the North winds as the anemometer was located on the deck windward edge. The effect of the assumed imperfection is inspected to be small for the reported turbulence intensities as their magnitudes mainly reflect the slow variations in the wind velocity.

In the displacement measurements of the Raippaluoto Bridge, there occurred a phenomenon against which no precautions were taken: turbulence induced significant rapid random movement to the laser beam, mainly in the vertical direction. The vertical movement at the position of the detector was of order of the available measurement range (80 mm), while along the horizontal direction it was about half of it. The frequency content of beam's vertical movement in comparison to the sampling frequency was on a level where the aliasing error was likely to occur. It is possible that some high-frequency vibration component of railing at the mounting position of the transmitter contributed to the response. Discussion with the instrument manufacturer's expert validated, however, that the turbulence problems in strong winds can be expected. Furthermore, their effects cannot be isolated by filtering the high-frequency components only. One solution for the problem is to locate a laser beam in a wind-shield, if possible.

It has been assumed by the author that the Raippaluoto Bridge displacement data has useful signal content as the first fundamental resonance is identifiable; the deflection responses are given in Ref. [46]. The re-analysis of the data (*Fig. 29*) for the present study indicates, however, that evidently some serious noise disturbance has occurred in the whole frequency range. This suspicion is supported by the fact that the estimated static deflection (n = 0 Hz) due to the maximum gust wind speed observed is around the value of 3 mm, while the low-frequency trends in the data indicate deflection of about 5 times this value. It can be noted that the aerodynamic admittance does not considerably act to responses around zero frequency while the coherence model does (*Figs 6* and *29*). For the present study, only the vertical standard deviation response deduced through *Fig. 29* is retained for comparison purposes, while other data is omitted.

The noise problems were likely to occur in the horizontal displacement measurements, too. In general, these measurements impose that only the background response of the Raippaluoto Bridge was waked. The horizontal displacement responses are retained for the present study, as no indicator was found to judge, whether the data is corrupted or not. Owing to the deficiencies in the displacement measurement setup, the acceleration data was found superior for deducing the modal characteristics in the ambient vibration study of the Raippaluoto Bridge.

In the Kärkinen Bridge experiments, where wind velocity was lower than in the case of the Raippaluoto Bridge, the laser-optical device performed correctly. Furthermore, the spectrums deduced from its data for ambient vibration study were found as informative as those deduced via acceleration measurements. As also the low-frequency band was identifiable, the displacement spectrums were chosen to be presented in *Fig. 28.*

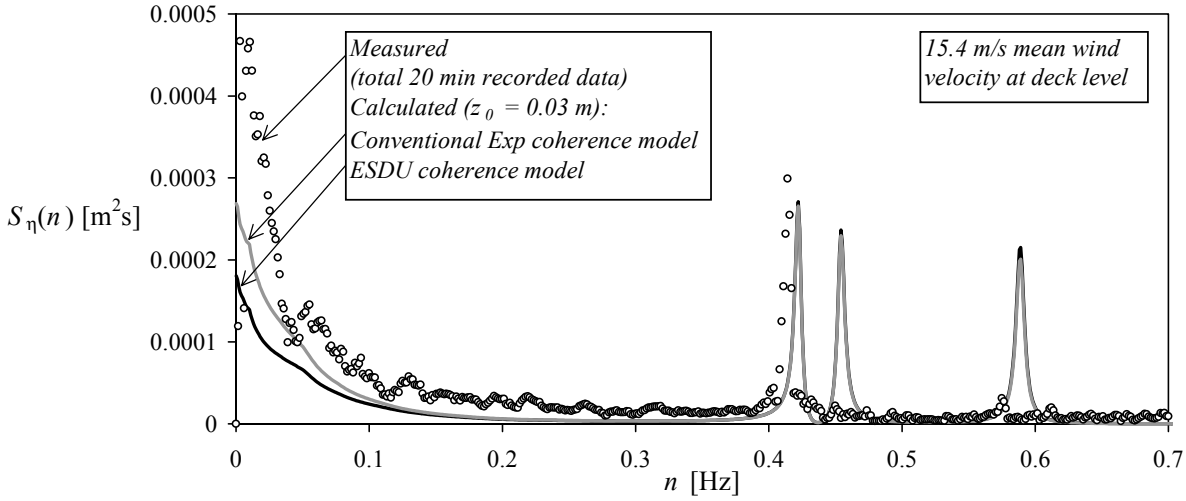

Fig. 29 Study of the turbulence-induced noise in measured vertical deflection response of the Raippaluoto Bridge; comparison of the calculated (Chapter 5.3.2) and the measured spectral densities, where the measured data is for two samples considered to have smaller disturbance than others.

The acceleration measurements were not free of noise problems either. The accelerometer cable's movements, caused by the wind, are believed to be the main source of the low-frequency noise observed in spectrums. In particular, an attempt was made to locate an accelerometer on the opposite edge of the deck vs. the present measuring point in order to identify the torsional modes of the Raippaluoto Bridge. To this end, the accelerometer's cable was installed below the bridge deck to avoid the traffic disturbance. In the present experiment there was no possibility to fix the cable to the structure and that is why the cable vibrated loosely in wind making the noise problems detrimental. Another source of disturbance in the low-frequency range was the temperature variations of the accelerometers and the electronic properties of instrumentation chain in general. There were overflow problems for the charge amplifiers detected on some occasions. They caused some data losses. The overflows were probably caused by the wetting of cables and contacts on account of the melted snow and water, as the replacement of dry cables removed the problems. Moreover, it is possible that some grounding problems were evidenced.

The noise is not affecting significantly the acceleration responses presented, as the low-frequency range is filtered out. It is possible that also the low-frequency range could be measured by replacing the piezoelectric accelerometers with some other type. The main parameter causing the uncertainty in results, is probably the calibration of accelerometers to which ±10% error should be accepted according to the manufacturer's specifications.

5.3 Computational results and comparison with the measurements

5.3.1 Adequacy of the input parameters

In general, the calculated modal parameters and estimated damping ratios are in agreement

with the measurements and need no additional treatment. The calculated second vertical bending mode (0.452 Hz) of the Raippaluoto Bridge, however, was not waked during the measurements making the comparison impossible.

According to the measurements carried out, the most significant errors detected in the presumed input parameters were in the surface roughness parameter and the associated turbulence intensities for the Raippaluoto Bridge. The observed South wind was blowing over the continent rather than directly from the open sea as assumed. The surface roughness parameter, that is in close agreement with the measured turbulence intensity, is $z_0 = 0.03$ m described as "open country" [22]. In the present case, a roughness change exists as the South wind, blowing over the continent, reaches the site over the sea.

The measured North wind at the Raippaluoto Bridge blowed directly from the ice and snow covered open sea. The wind was very smooth. The surface roughness parameter, that matches the measured turbulence intensity, is given by $z_0 = 0.0003$ m.

The turbulence intensities deduced through the Kärkinen Bridge measurements are high. Probably, this is related to the unsteadiness and the low magnitude of the measured mean wind velocity rather than severe inadequateness of the surface roughness parameter in target winds.

In general, the effects of ice, snow and low mean wind velocity on the turbulence characteristics are reflected to the vortex-induced vibrations of bridges.

It can be admitted that the wind observation periods used in the present study are not long enough to evaluate the longitudinal integral length scale of turbulence with a great confidence. Tentative assessment is, however, carried out via Eq. (39) for the Raippaluoto Bridge. For the mean velocity of 15 m/s at the deck level it suggests values of ${}^{x}L_u \approx 60$ m and ${}^{x}L_u \approx 180$ m for the South (Autumn) and the North (Winter) winds, respectively. As these parameters fall roughly to the range expected, limited usefulness for Eq. (39) for extracting ${}^{x}L_u$ can be argued.

For the South wind of the Raippaluoto Bridge, the dimensional values of the spectral densities (*Fig. 27*) at the first fundamental resonance are not in agreement with the turbulence model (*Table 3*). This holds also for the corrected model ($z_0 = 0.03$ m) and reinforces the suspicion that the wake, caused by the leading edge of the bridge deck, has added energy to the high-frequency range.

5.3.2 Computational results with comparison

Spectrums deduced through the simultaneous buffeting and flutter analysis model of the present study are illustrated in *Fig. 30*. Symbol $\bar{U}_{\perp}$ in the figure refers to the mean wind velocity component perpendicular to the bridge span at the deck level. Also shown are the combined responses up to the flutter velocities. These responses are calculated by assuming the various excitation mechanisms to be statistically independent, i.e. by assuming that the variances of the response components are additive. The peak values are approximated through the simple standard deviation weighted average. The combined responses are given by

$$\begin{cases} \sigma_{(\gamma)} \approx \sqrt{\sigma^2_{(\gamma)b} + \sigma^2_{(\gamma)S} + \sigma^2_{(\gamma)K}}, & (\gamma = 0,\ 1 \text{ or } 2) \\ g_{(\gamma)} \approx \sqrt{\dfrac{g^2_{(\gamma)b}\sigma^2_{(\gamma)b} + g^2_{(\gamma)S}\sigma^2_{(\gamma)S} + g^2_{(\gamma)K}\sigma^2_{(\gamma)K}}{\sigma^2_{(\gamma)}}}, \end{cases} \tag{119}$$

where subscripts *b*, *S* and *K* refer to the response components due to the buffeting, the signature turbulence and the vortex shedding, respectively.

Spectral densities for the vertical deflection amplitude at the span mid-point, deck leeward edge:

Raippaluoto Bridge *Kärkinen Bridge*

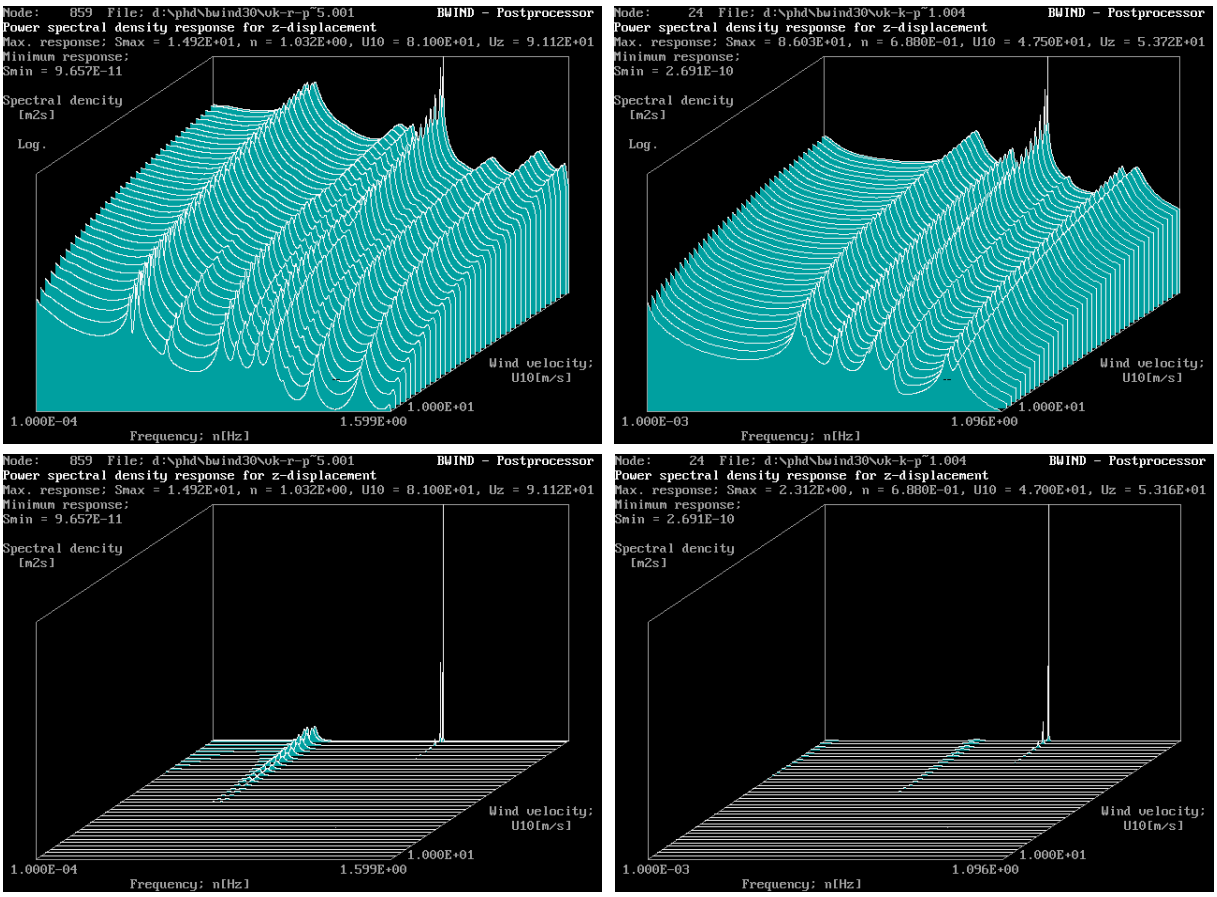

Calculated responses for twisting angles at span mid-points

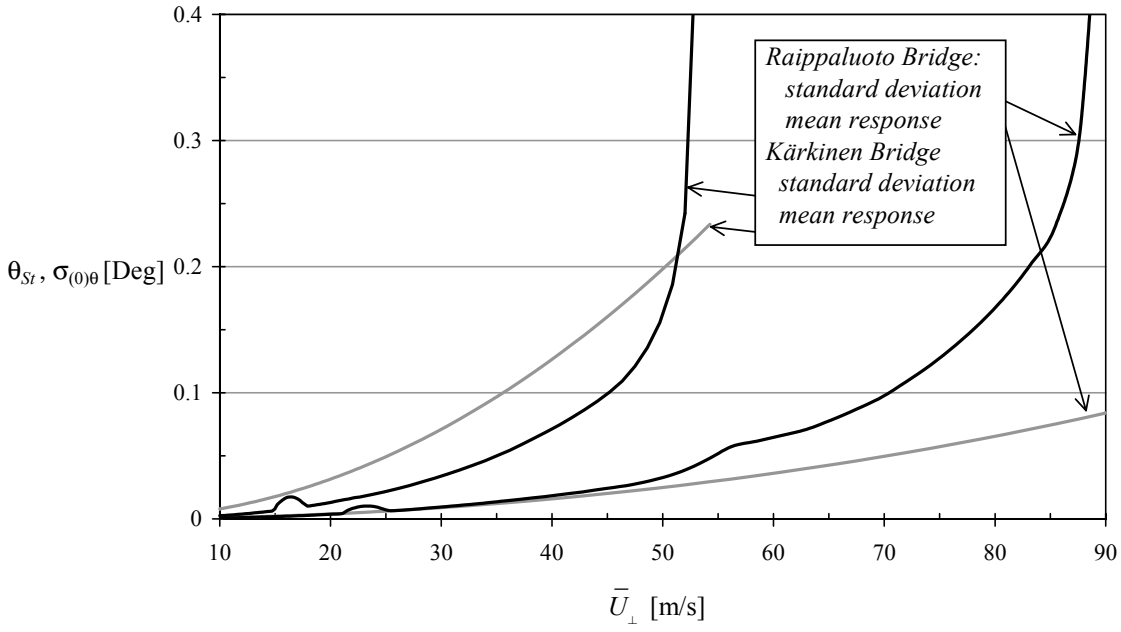

Fig. 30 The spectral chart displays applied on detection of flutter velocities in the simultaneous buffeting and flutter analysis and the torsional responses at the deck mid-point. For the spectral displays the spectrums are given in both logarithmic and linear scales.

The flutter characteristics of the two bridges are summarized in *Table 5*. The calculated buffeting responses are in agreement with the earlier results gained by the author [45]. The flutter derivatives of the Kärkinen Bridge became available, as the first time, due to the experiments conducted for the present study. By using these derivatives, the estimate for flutter velocity at the deck level [45] reduces from 58 m/s to 55 m/s. The vibration amplitudes remain small enough for the linear flutter theory to be valid. Furthermore, the static twisting angles due to the mean wind action remain small causing the zero-angle-of-attack flutter derivatives to be appropriate in the analysis.

Table 5 Calculated flutter characteristics.

	Raippaluoto Bridge	*Kärkinen Bridge*
Flutter velocity at the deck level	91.0 m/s	54.0 m/s
Flutter velocity at 10 m height	81.0 m/s	47.5 m/s
Flutter mode	torsion	torsion
Flutter frequency	1.032 Hz	0.688 Hz
Downward shift from the torsional natural frequency	2.8 %	1.9 %
Critical reduced velocity at the deck level	5.8	5.9

Considering the present calculation model it can be noted that the flutter velocity and frequency can be detected from spectral charts without difficulties, as presumed. Here, if only the flutter velocity is of interest, it can be found from the response standard deviation vs. wind velocity graphs as well.

Significant statistical dependence, i.e. coupling due to buffeting loads, is found between responses of some mode shapes. This reflects in the fact that the covariance matrices of normal coordinates have significant non-diagonal elements and associated modal correlation coefficients. It is found that the modal correlation coefficients between separate mode shapes are in maximum about 0.5 for some pairs of modes. Furthermore, they show significant dependence upon the wind velocity and thus upon the aeroelastic actions. The calculated modal correlation coefficients for the first four almost pure vertical bending modes are shown in *Table 6*. These results, concerning the modal correlation coefficients, demonstrate the necessity of coupled-mode approach in rigorous buffeting response calculations of cable-stayed bridges.

Table 6 Calculated modal correlation coefficients between the selected vertical bending modes.

Raippaluoto Bridge									
$\bar{U}$ = 15 m/s at the deck level					$\bar{U}$ = 91 m/s at the deck level				
Mode	*1st*	*2nd*	*3rd*	*4th*	*Mode*	*1st*	*2nd*	*3rd*	*4th*
1st	1	0.30	0.06	-0.01	*1st*	1	0.22	0.03	0.02
2nd	0.30	1	-0.03	0.06	*2nd*	0.22	1	-0.01	0.04
3rd	0.06	-0.03	1	0.00	*3rd*	0.03	-0.01	1	0.00
4th	-0.01	0.06	0.00	1	*4th*	0.02	0.04	0.00	1
Kärkinen Bridge									
$\bar{U}$ = 15 m/s at the deck level					$\bar{U}$ = 54 m/s at the deck level				
Mode	*1st*	*2nd*	*3rd*	*4th*	*Mode*	*1st*	*2nd*	*3rd*	*4th*
1st	1	0.12	-0.04	0.09	*1st*	1	0.13	-0.02	0.07
2nd	0.12	1	0.07	0.20	*2nd*	0.13	1	0.03	0.12
3rd	-0.04	0.07	1	0.02	*3rd*	-0.02	0.03	1	0.01
4th	0.09	0.20	0.02	1	*4th*	0.07	0.12	0.01	1

Comparison of the calculated results with the measured ones is shown in *Figs 31...34*. The

calculated results are for the original estimates to which the input parameters of *Table 3* are applied. Also shown for the Raippaluoto Bridge are the revised estimates obtained by changing the surface roughness parameter (Chapter 5.3.1) and the associated turbulence spectrums. The relation of vortex and signature turbulence induced vibration on the overall response is illustrated in *Fig. 33* for the Kärkinen Bridge. The effects of signature turbulence tend to be hidden under the approach-flow turbulence buffeting. An exception is the acceleration response. To this response, the contribution of higher modes is predicted to be marked. In maximum, the acceleration response for the signature turbulence alone is about 1/3 of the buffeting response. The predicted importance of the signature turbulence on the acceleration response is in agreement with the preliminary observations of BOSCH [7].

In addition to the responses shown in *Fig. 33*, an estimate for the vortex-induced vibration amplitude at the span mid-point of the Kärkinen Bridge was calculated by omitting the turbulence reduction effect. The result is comparable with the wind tunnel measurements of Ref. [109], in which the full model of the bridge stiffening girder has been tested in a smooth flow. The wind tunnel model estimate and the present smooth flow estimate were 11.3 mm and 8.8 mm, respectively. The agreement suggests that the presumed smooth-flow bandwidth and the correlation model's parameters are on a reasonable level.

The calculated results indicate that the response, at the low wind speed range, is the combination of buffeting, vortex shedding and signature turbulence induced vibration. It follows that rather than being smooth exponential type curves when plotted against the wind velocity, the response curves contain spikes related to the vortex-induced vibrations at a wide velocity range. In this context, the measured acceleration responses of the Raippaluoto Bridge for the South and North winds can be inspected. Theoretically, for the North wind the turbulence action should be of order lower than for the South wind. The measured accelerations are almost the same suggesting increased vortex-shedding activity as predicted by the present model. The peak factors are not estimated or found to alter significantly owing to the vortex-induced vibration components.

Unfortunately, the measured data for the Kärkinen Bridge does not range to the wind speed regime of primary interest. In the measurements, however, the critical wind speed for vortex-induced fundamental resonance was met in short duration gusts. This might contribute to the shown underestimation of response in the very low wind velocity range.

When extending the discussion concerning the present results, it can be noted:

- The measured data is based on relatively short recording periods. For example, the second fundamental bending mode of the Raippaluoto Bridge was not waked during the measurements but it contributes to the calculated response.
- The comparison study is based on the mean wind velocities about 15 m/s while the design wind speeds of bridges are higher.
- The observed vibration amplitudes of the two bridges are small. Aeroelastic actions associated with the vortex-induced vibrations have widely remained unexplored.
- Considerable uncertainties should be considered for measurement results because of the noise problems and/or to the unfavourable positioning of devices.
- The number of required input parameters is high and the errors in them can cancel the effects of each other.

The results achieved are, however, promising. It can be observed that calculated amplitudes are obtained through reductions for a) the imperfect load correlation and turbulence effects on the vortex-induced vibrations and b) the aerodynamic admittance and turbulence coherence effects on the buffeting. If these reduction parameters are conservatively approximated or omitted in the analysis, as it is sometimes done in bridge design, it is not unusual to obtain response overestimates of some 2...5 times.

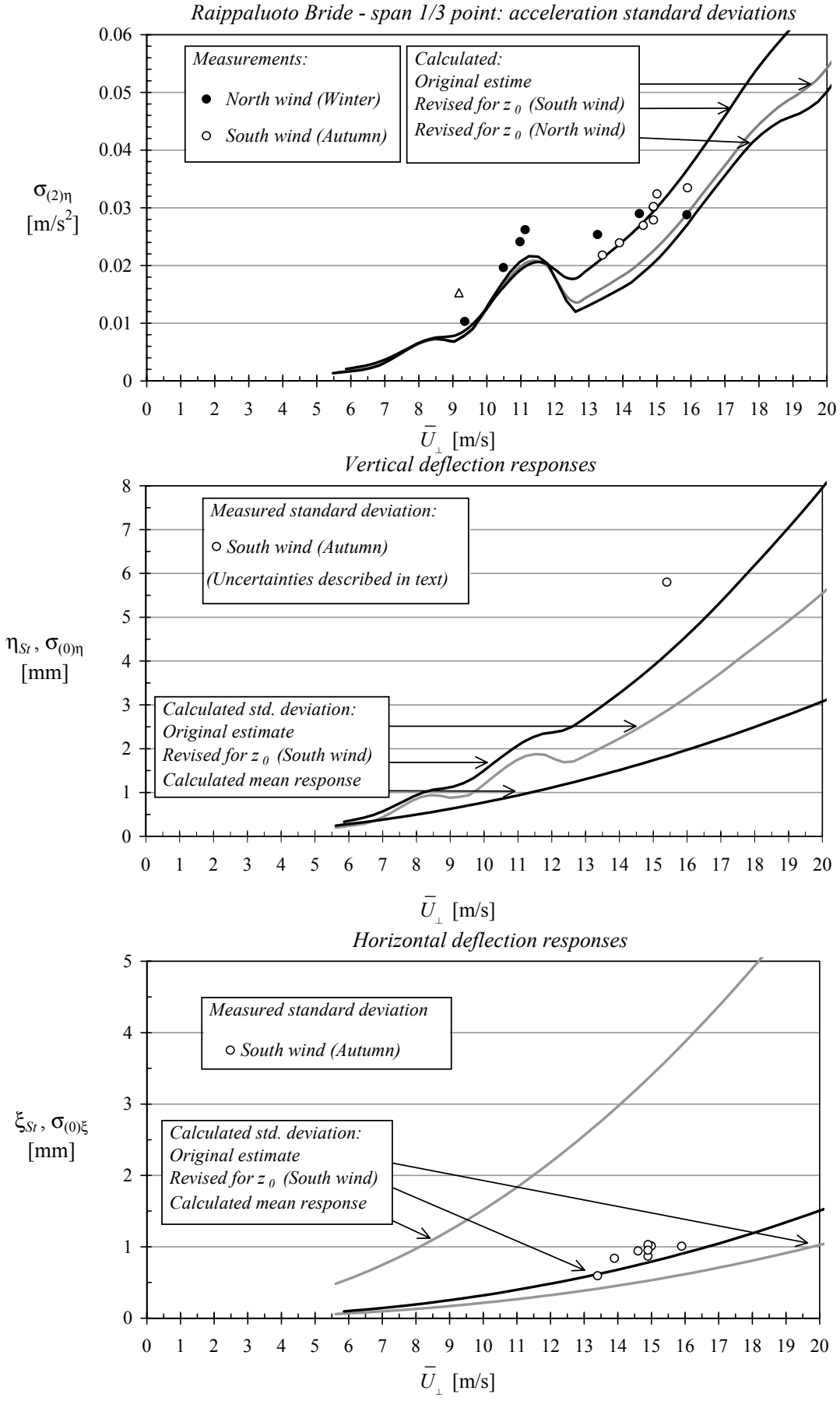

Fig. 31 Comparison of responses at the span 1/3 point of the Raippaluoto Bridge.

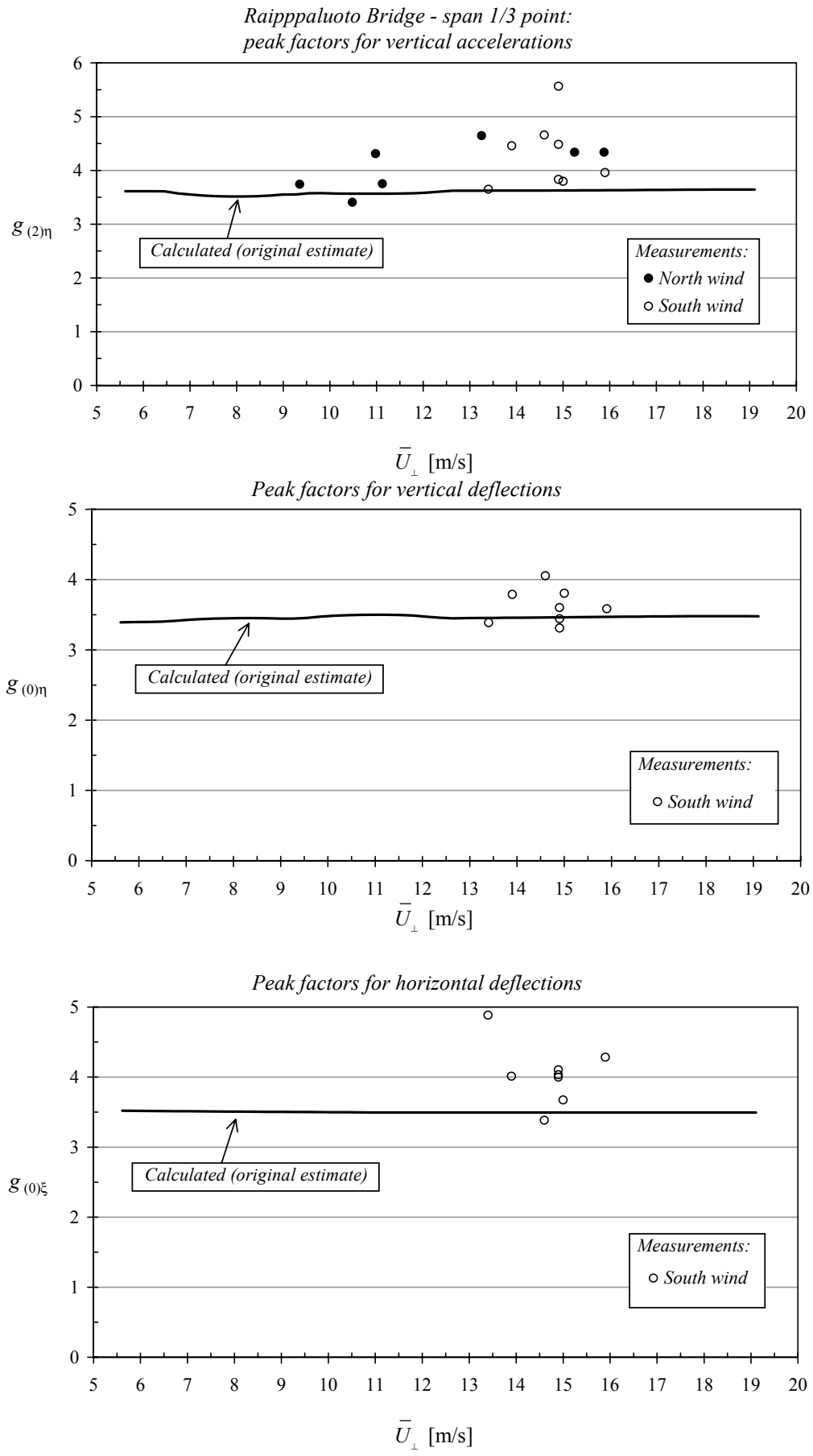

Fig. 32 Comparison of the peak factors at the span 1/3 point of the Raippaluoto Bridge.

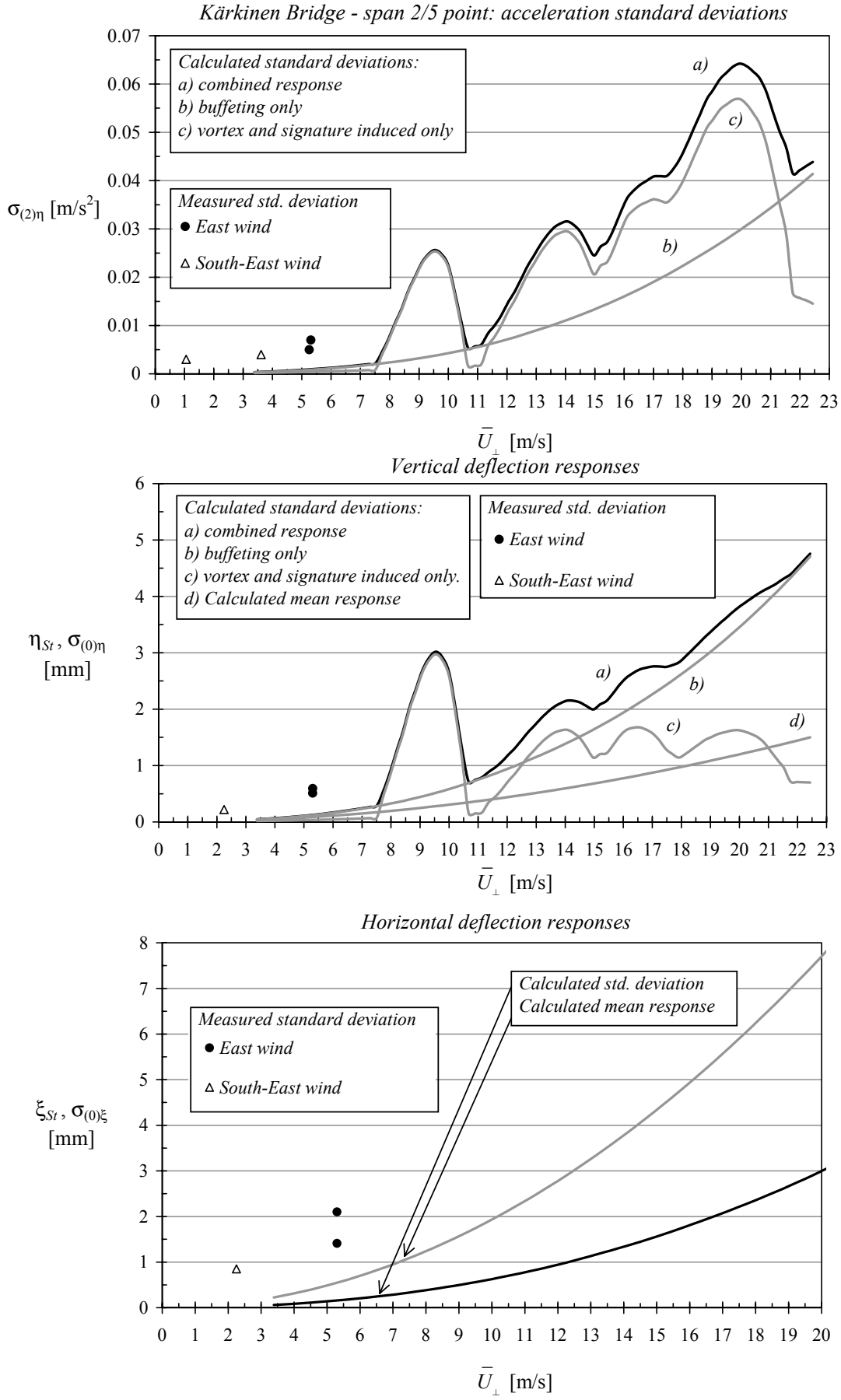

Fig. 33 Comparison of responses of the Kärkinen Bridge: the span 2/5 point, at distance of 102 m from the tall pylon.

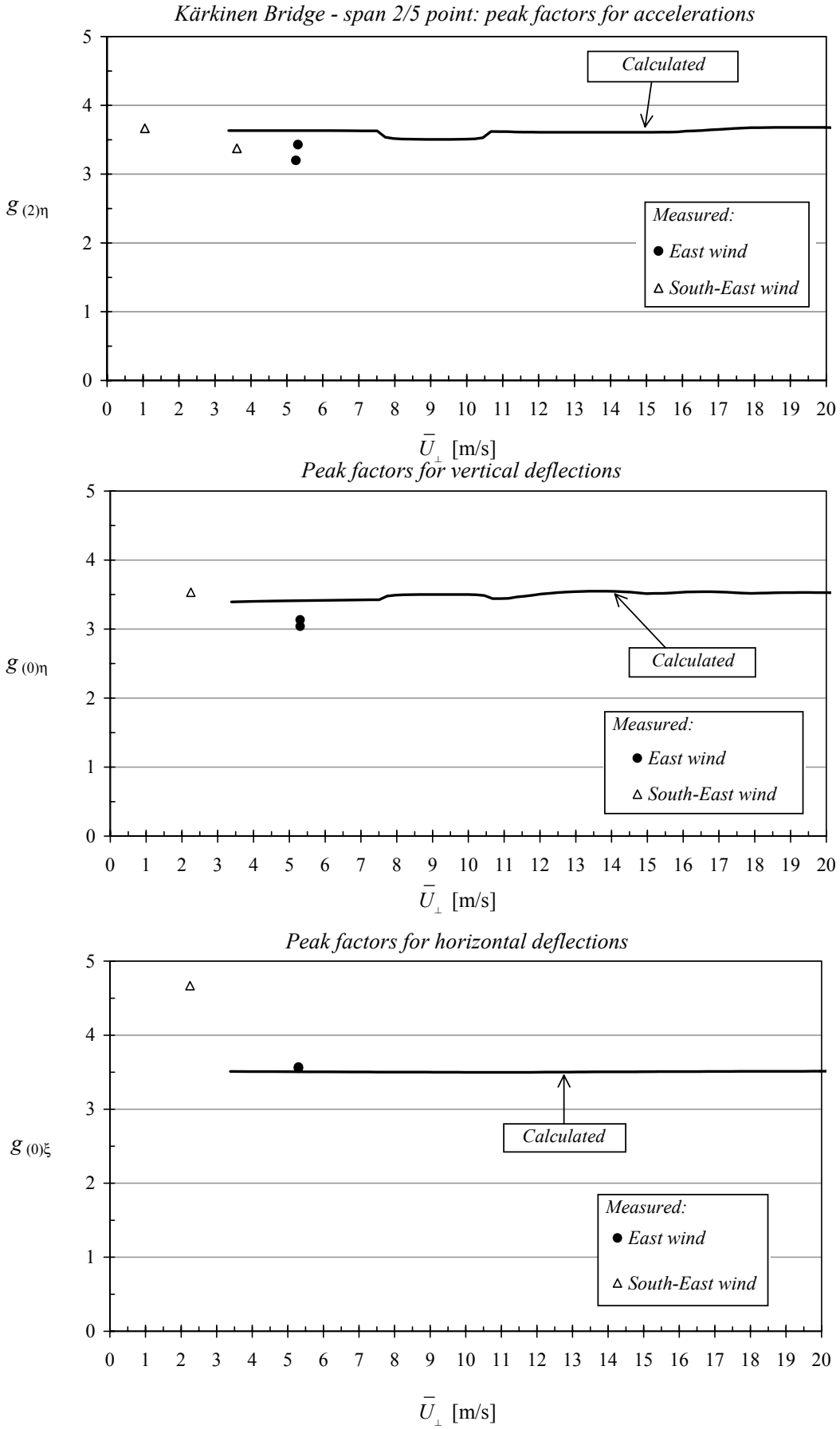

Fig. 34 Comparison of peak factors of the Kärkinen Bridge: the span 2/5 point, at distance of 102 m from the tall pylon.

6 CONCLUSIONS

In the present study, the frequency-domain calculation models are deduced for the simultaneous buffeting and flutter analysis and for the vortex and signature turbulence induced response assessments of long-span bridges. The wind tunnel experiments with the aeroelastic section model and the verification study involving the on-site measurements are included. Outside the main body of the present publication, the calculation models are implemented to the computer code BWIND-3 by the author. The results calculated with this code are referred in the verification study.

6.1 Buffeting and flutter analysis

The theories behind flutter and buffeting of long-span bridges are well established and numerous applications are available. As far as the linear mathematical models are concerned, the frequency-domain approach has several fundamental advantages over the time-domain approach. The spectral analysis has become a standard tool when modelling the buffeting response and interacting aeroelastic loads. The present calculation model involves the flutter derivative presentation of aeroelastic loads. It allows the detailed modelling of aerodynamic admittances and turbulence characteristics of bridge sites. The flutter velocity and frequency are detected by the inspection of calculated spectral densities associated with buffeting responses in gradually increased wind speeds. This considerably simplifies the flutter analysis in comparison with the approach involving the state-space expansion and the complex eigenvalue analysis of the resulting system matrix. By the fundamental theories these approaches are the same. The following conclusions are drawn:

- Cable-stayed bridges in comparison to suspension bridges generally comprise complicated 3-dimensional mode shapes, in which pylons interact and natural frequencies can lie close to each other. As far as the present technologies are concerned, the coupled-mode approach, like the present one, proves to be an indispensable tool for reliable wind-induced vibration analysis of cable-stayed bridges. Even for circumstances where the coupling due to the aeroealastic loads is weak, the modes having natural frequencies close to each other can remain coupled due to the buffeting loads.
- Flutter velocity and frequency can be observed, without difficulties, from buffeting response spectrums containing the reasonable frequency and wind speed resolutions.
- A considerable error can occur when the spectrums of buffeting loads are lumped to a finite number of nodes of a typical element model. This occurs when the coherence decay is rapid (usually when frequency is high and wind velocity is low) in comparison with the interference length of nodal-load. A practical correction deduced in the present study can be made for this error.
- The computational efforts required by the present model, although considerable, do not exceed the requirements of generally applied structural analysis codes in the engineering field. The

model presented is directly applicable to bridge design or to detailed parametric studies.

6.2 Vortex and signature turbulence induced vibration analysis

Reliable calculation models for vortex-induced vibrations of bridges are in progress and need applications, design data and verification studies. There are fundamental complexities in the detailed modelling of the phenomenon, causing models to contain many simplifying hypothesis and varying number of free parameters to be evaluated through wind tunnel experiments. Verification of them can require special wind tunnel instrumentation and other considerable efforts.

The calculation models and design data for the signature turbulence induced vibrations of bridges are absent almost completely. In some tentative models argued, the signature turbulence spectrum is treated to be additive to the buffeting spectrum. In some recent models, the effects of signature turbulence are superimposed to the experimental aerodynamic admittance functions.

In the vortex-shedding model deduced in the present study, excitation spectrums are assumed to be an equivalent band-limited white noise type at the lock-in. The effect of wind turbulence is modelled to widen spectrum's bandwidth while keeping the load variance invariant. The spanwise correlation effects of loading are considered by means of the empirical covariance functions proposed by other investigators. The correlation model involved is dependent on the amplitude of the motion, implying a nonlinear character to be treated by the simple fixed-point iteration. The fundamental aerodynamic input parameter for the vortex-shedding model is the RMS exciting coefficients whose flow speed dependence is determined through the response of an aeroaelastic section model.

The signature-turbulence model employs the simplified arithmetics borrowed from the bridge buffeting models. The aerodynamic input parameters include the non-dimensional excitation spectral densities and the coherence decay model. The former of the parameters is to be evaluated simultaneously with the vortex-induced vibration data through wind tunnel experiments.

The present two models overcome the detailed analysis of aerodynamic damping and aeroelastic stiffness by employing the same similarity requirements for the aeroelastic section model as required for the free-vibration flutter derivatives extraction. The conclusions include:

- The band-limited white noise excitation model is found versatile and promising on modelling the turbulence and load correlation effects for the vortex-induced vibrations of bridges. It has the advantage of containing the simple harmonic excitation model as a special case, allowing verification against public design data and calculation of the worst-case scenarios for bridge design.
- The model deduced for the signature turbulence induced vibrations is mathematically simple and easy to apply. The main source of uncertainty is due to the spanwise load coherence, which is not as well understood and widely investigated as what the natural wind coherence is. The present model, together with others based on the same theories, can be considered useful in the sense that they reveal the possibility to use simple wind tunnel setups to investigate the phenomenon further.
- The models deduced are directly applicable to bridge design and detailed parametric studies. Due to uncertainties in a source data, however, conservative values for input parameters should be accounted for when applied to the former purpose.

6.3 Experimental study with an aeroelastic section model

In the present experimental study, the aeroelastic section model was tested in the wind tunnel. The model, exposed to the smooth flow, was 1:25 replica of the deck segment of the Kärkinen Bridge. As a part of the study the flutter derivatives A_i^* and H_i^* (i = 1, 2, 3 or 4) were identified applying the Instrumental variable method, acceleration signals and exclusive coupled-motion test runs. The required provisions on the identification method are deduced. The method gives precise curve fits to the data sequences applied, yielding conclusions for the bluff deck section studied:

- The small amplitude free vibrations can be presented accurately by the linear equations of motion in the wind speed regime of interest.
- The flutter derivatives of the heaving and torsional modes can be successfully extracted from the acceleration data through the Instrumental variable method.

The flutter derivative A_2^*, related to the torsional flutter tendency, gave the major contribution to the aeroelastic action of the scale model. The plots of aerodynamic damping for the heaving and torsional modes are abrupt in the vicinity of vortex-shedding lock-in regimes. The flutter derivative test setup was simple and the wind tunnel part of the tests was conducted efficiently. A considerable time was spent, however, in the identification phase. The flutter derivative study suggests that:

- Only the uncoupled-mode flutter derivatives A_2^*, A_3^* and H_1^* are required to be evaluated and considered in the analysis of bridges having alike cross-sections with the studied one. These derivatives can be evaluated through single-degree-of-freedom tests as well and probably with better reliability than with coupled-motion tests.

There was one well-established lock-in regime for the vortex-induced heaving and torsional vibrations. At lock-in, the peak factor (= peak to standard deviation ratio) was close to that of the harmonic motion. Outside the lock-in regimes, the peak factors fall to values typical to the natural wind buffeting. These observations lead to the conclusion:

- The results of the present experiments are in agreement with the assumptions and hypothesis made for the development of the three calculation models of this study.

6.4 Verification study

In the verification study, the calculated wind responses of the Raippaluoto Bridge (250 m span) and the Kärkinen Bridge (240 m span) are compared with the on-site measurements. These two cable-stayed bridges have the double I-girder steel-concrete composite deck. The measurements were carried out during 3 separate occasions in suitable storm or strong wind conditions. Accelerations, displacements and wind properties were recorded. Through the verification study, the following conclusions are reached:

- The measurements of the Raippaluoto Bridge reveal the high number of mode shapes contributing the acceleration response of the deck. This observation, and the measured natural frequencies in general, are in agreement with the calculations. In the Raippaluoto Bridge case it was evidenced that at least one calculated low-frequency mode did not wake. Whether this

is caused by the inconsistency of the FE-model, short observation periods, influence of vortex shedding or some other reason, remains an open question.

- For bridges in cold-climate regions and coastal areas, two completely different turbulence conditions can occur: wind over continent and wind over snow-covered frozen sea.
- The along-wind component of turbulence intensity, relatively easy to be measured, may be a useful quantity to choose between terrain categories for alternating wind directions. In the direct application of tabulated turbulence models for bridges, one should typically consider surface roughness changes that might rise uncertainties in the analysis.
- The response of the Raippaluoto Bridge deck was predicted very satisfactorily by the calculation models presented. In the mean velocity regime about 15 m/s at the deck level, the calculated responses consist significant components due to the buffeting, vortex-induced vibrations and signature turbulence. The measured data for the Raippaluoto Bridge is in agreement with this result.
- The study of the Raippaluoto Bridge suggests that the ESDU coherence model and the theoretical aerodynamic admittance functions are useful when aiming for precise buffeting response estimation. From the designer's point of view, by applying this coherence model, one avoids subjective choice of decay coefficients of the conventional exponential decay law.
- For bridges in inland conditions in Finland, like the Kärkinen Bridge in the present study, wind speeds are not likely to meet the range of interest in the wind-induced vibration analysis. The gust wind velocity of order 10 m/s was found sufficient, however, to excite the bridge enough for making the lowest natural frequencies identifiable through the ambient vibration technique. The present smooth flow vortex-induced vibration estimate is in good agreement with the full model wind tunnel experiments conducted for the Kärkinen Bridge stiffening girder elsewhere. In the present study, the signature turbulence induced acceleration response is predicted to be in maximum about 1/3 of the buffeting response.
- Accurate measurements of bridge deflections in strong winds obtained via laser optical devices might be problematic as the turbulence distorts the steadiness of the laser beam. To avoid this phenomenon, it might be advantageous to locate the beam in a wind-shield. Generally, one should deal with considerable uncertainties, not only in the analysis models and their input parameters, but also in on-site measurement results.

6.5 New contributions of the present study and suggestions for further research

The major new contributions of the present study are summarised as follows:

- The multimode buffeting and flutter analysis is presented in a theoretically complete form, in which most of the unintentional simplifications involved in earlier models are removed. The principle of detecting flutter velocity and frequency by inspecting solely the buffeting response spectral charts is new in the present context.
- The model is presented for vortex-induced vibrations that can be considered to be a new candidate towards generally accepted method on calculating the response by means of the section model experiments. It has perceived advantages from reproducing the turbulence and load correlation reduction effects through the mutually simple mathematical formulation. An evidence is obtained of the versatility and usefulness of the frequency-domain approach on modelling the vortex-induced vibrations of bridge girders.
- Algorithms for calculation of major wind actions on long-span bridges are presented in a rational form and are successfully programmed for computers. The code's properties and

logical interface to general finite element programs via mode shape result files make the code applicable to the analysis of the most rigorous models. This can be done with efficiency that meets the requirements of extensive numerical simulation and bridge design.

- The instrumental variable method is formulated for acceleration signals to extract flutter derivatives related to the heaving and torsional modes of a section model. The study, despite it was found rather time-consuming in the postprocessing phase, gives evidence for the usefulness of modern system identification techniques in the flutter derivatives extraction.
- According to the verification study, the deduced calculation models show promising accuracy when applied to the double I-girder steel-concrete composite designs. The models can be used, e.g., when making the choice between a box and an open-section girder. In the case of a cable-stayed bridge, this choice has in most cases special economical importance.
- The evidence obtained through the two bridges studied imposes that, instead of finding smooth exponential type standard deviation response vs. wind velocity curves, one can find complicated patterns owing to the contributions of vortex and signature turbulence induced vibrations.

With the aforementioned conclusions and contributions, it is considered that the aims given for the present study are fulfilled and the models presented are suitable for detailed parametric studies to give additional contributions in the future. In order to improve the reliability of wind-induced vibration analysis of bridges in general, five topics call for refined and better verified models:

- Coherence models for the signature turbulence. The effect of approach-flow turbulence to this coherence.
- Correlation models for the vortex-induced vibrations of bridge decks and pylons.
- Reynolds number effects in the context of vortex-induced vibration analysis of bridge decks.
- The relation of approach-flow turbulence coherence to the coherence of buffeting loads of bridge girders.
- The aerodynamic admittances of bridge sections.

Investments to the continuous or remote-controlled measurements of wind-induced vibrations and turbulence can be recommended, especially in the cases where strong winds are rare and not lasting long. Along with the comparison studies, on-site measurements are needed for scientific aims as well as for the engineering work dealing with long-span bridges.

References

1. BEARMAN, P. W., An investigation of the forces on flat plates normal to a turbulent flow. *Journal of Fluid Mechanics*, **46**(1971)1, pp. 177...198.
2. BELIVEAU, J. G., VAICAITES, R. and SHINOZUKA, M., Motion of suspension bridge subject to wind load. *Journal of the Structural Division*, **103**(1977)6, ASCE, pp. 1189...1205.
3. BIETRY, J., DELANAY, D. and CONTI, E., Comparison of full-scale measurements and computation of wind effects on a cable-stayed bridge. Vol. 1, proc., Cable-stayed and suspension bridges, Dauville, France, October 1994, pp. 91...100.
4. BLEICH, F., Dynamic Instability of truss-stiffened suspension bridges under wind action. *Transactions of ASCE*, **114**(1949) Paper No. 2385, pp. 1177...1222; Discussion, pp. 1223...1232.
5. BLEVINS, R. D. and BURTON, T. E., Fluid forces induced by vortex shedding. *Journal of Fluids Engineering*, **98**(1976)1, Transactions of the ASME series I, pp. 19...24.
6. BLEVINS, R. D. Flow-induced vibration. Van Nostrand Reinhold, New York 1977, 363 p.
7. BOSCH, H. R., Monitoring the aerodynamic performance of a classic suspension bridge. Wind and seismic effects, NIST SP 796, Proc. of the 22nd joint meeting of the U.S.-Japan cooperative program in natural resources panel on wind and seismic effects, National Institute of Standards and Technology, Washington 1990, pp. 24...32.
8. BUCHER, C. G. and LIN, Y. K., Effects of spanwise correlation of turbulence field on the motion stability of long-span bridges. *Journal of Fluids and Structures*, **2**(1998)5, pp. 437...451.
9. BUCHER, C. G. and LIN, Y. K., Stochastic stability of bridges considering coupled modes. *Journal of Engineering Mechanics*, **114**(1988)12, ASCE, pp. 2055...2071.
10. BUCHER, C. G. and LIN, Y. K., Stochastic stability of bridges considering coupled modes II. *Journal of Engineering Mechanics*, **115**(1989)12, ASCE, pp. 384...400.
11. CHEN, Y. N., Fluctuating lift forces on the Karman vortex streets on single circular cylinders and in tube bundles; part 1 - the vortex street geometry of the single circular cylinder & part 2 - lift forces of single cylinders. *Journal of Engineering for Industry*, **94**(1972)2, Transactions of the ASME series B, pp. 603...612 & 613...622.
12. CHEN, X., MATSUMOTO, M. and KAREEM, A., Aerodynamic coupling effects on flutter and buffeting responses of bridges. *Journal of Engineering Mechanics*, **126**(2000)1, pp. 17...26.
13. CORLESS, R. M. and PARKINSON, G. V., A model of the combined effects of vortex-induced oscillation and galloping. *Journal of Fluids and Structures*, (1988)2. pp. 203...220.
14. DAVENPORT, A. G., The application of statistical concepts to the wind loading of structures. *Proceedings Instition of Civil Engineers*, **19**(1961), pp. 449...472.
15. DAVENPORT, A. G., The response of slender, line-like structures to gusty wind. *Proceedings Institution of Civil Engineers*, **23**(1962), pp. 389...408.
16. DAVENPORT, A. G., Buffeting of a suspension bridge by storm winds. *Journal of the Structural Division*, **88**(1962)3, ASCE, pp. 233...268.
17. DAVENPORT, A. G., ISYUMOV, N., ROTHMAN, H. and TANAKA, H. Wind induced response of suspension bridges - wind tunnel model and full scale observations. Wind engineering; proceedings of the fifth international conference, Fort Collins, Colorado, USA, July 1979, Volume 2. Cermak, J. E. (Ed.), Pergamon Press, Oxford, pp. 841...852.
18. DAVENPORT, A. G., Comparison of model anf full scale tests on bridges. Proc. of the international workshop on wind tunnel modelling criteria and techniques in civil engineering applications, Gaithersburg, Maryland, USA, April 1982. Reinhold, T. A. (Ed.),

Campridge University Press, London 1982, pp. 619....636.
19. DAVENPORT, A. G., KING, J. P. C. and LAROSE, G. L., Taut strip model tests. Proc. of the first international symposium on aerodynamics of large bridges, Copenhagen, Denmark, February 1992, Larsen. A. (Ed.), Balkema, Rotterdam 1992, pp. 113...114.
20. EHSAN, F. and BOSCH, H. R., Modelling of the effect of spanwise coherence of aerodynamic forces on full-bridge response. Wind and seismic effects, NIST SP 760, Proc. of the 20th joint meeting of the U.S.-Japan cooperative program in natural resources panel on wind and seismic effects, National Institute of Standards and Technology, Washington 1989, pp. 3...17.
21. EHSAN, F. and SCANLAN, R. H., Vortex-induced vibrations of flexible bridges. *Journal of Engineering Mechanics*, **116**(1990)6, ASCE, pp. 1392...1411.
22. ESDU data item 85020, Characteristics of atmospheric turbulence near the ground, part II: single point data for strong winds (neutral atmosphere). Engineering Science Data Unit, London 1990, 35 p.
23. ESDU data item 86010, Characteristics of atmospheric turbulence near the ground, part III: variations in space and time for strong winds (neutral atmosphere). Engineering Science Data Unit, London 1990, 33 p.
24. FARQUHARSON, F. B., Aerodynamic stability of suspension bridges with special reference to the Tacoma Narrows Bridge. University of Washington Engineering Experiment Station, Bulletin No. 116 Part 1 (1950), 108 p.
25. Failure of the Tacoma Narrows Bridge, report of the special committee of the board of direction. American Society of Civil Engineers, Proc. ASCE, **69**(1943), pp. 1555...1586.
26. FUNG, Y. C., An introduction to the theory of aeroelasticity. Dover, New York 1969, 498 p.
27. FUNG, Y. C., Fluctuating lift and drag acting on a cylinder in a flow at supercritical Reynolds number. *Journal of the Aerospace Sciences*, **27**(1960)11, pp. 801...814.
28. GARRICK, I. E. and REED III, W. H., Historical development of aircraft flutter. *Journal of Aircraft*, **19**(1981)11, AIAA, pp. 897...912.
29. HARTOG, DEN, Transmission line vibration due to sleet. *Transactions of the American Institute of Electrical Engineers*, 51(1932) October, AIEE, pp. 1074...1076.
30. HARTOG, DEN, Mechanical vibrations. 4th Edit. McGraw-Hill, New York 1956. 436 p.
31. HARTLEN, R. T. and CURRIE, I. G., Lift-oscillator model of vortex-induced vibration. *Journal of the Engineering Mechanics Division*, **96**(1970)5, ASCE, pp. 577...591.
32. HORLOCK, J. H., Fluctuating lift force on aerofoils moving through transverse and chordwise gusts. *Journal of Basic Engineering*, Transactions of ASME Series D, **90**(1968)4, pp. 494...500.
33. HJORTH-HANSEN, E., Sectional model tests. Aerodynamics of large bridges, Proc. of the first international symposium on aerodynamics of large bridges, Copenhagen, Denmark, February 1992, Larsen. A. (Ed.), Balkema, Rotterdam 1992, pp. 95...112.
34. IRWIN, H. P. A. H., Centre of rotation for torsional vibration of bridges. *Journal of Industrial Aerodynamics*, (1979)4, pp. 123...132.
35. IRWIN, P. A., The role of wind tunnel modelling in the prediction of wind effects of bridges. Bridge aerodynamics, Proc. of the international symposium on advances in bridge aerodynamics/Copenhagen/10-13 May 1998, Larsen, A. (Ed.) and Esdahl, S. (Ed). Balkema, Rotterdam 1998, pp. 99...117.
36. IWAN, W. D. and BLEVINS, R. D., A model for vortex induced oscillation of structures. *Journal of Applied Mechanics*, **41**(1974)3, Transactions of the ASME series E, pp. 581...586.
37. IWAN, W. D., The vortex induced oscillation of elastical structural elements. *Journal of Engineering for Industry*, November 1975, Transactions of the ASME series B, pp.

1378...1382.

38. JAIN, A., JONES, N. P. and SCANLAN, R. H., Coupled flutter and buffeting analysis of long-span bridges. *Journal of Structural Engineering*, **122**(1996)7, ASCE, pp. 716...725.
39. JANCAUSKAS, E. D. and SANKARAN, R., The coherence of cross-wind velocity and the pressure on two-dimensional rectangular cylinders in turbulent wind. *Journal of Wind Engineering and Industrial Aerodynamics*. **41-44**(1992)1-3, pp. 809...810.
40. JONES, N. P., SCANLAN, R. H., JAIN A. and KATSUCHI, H., Advances (and challenges) in the prediction of long-span bridge to wind. Bridge aerodynamics, Proc. of the international symposium on advances in bridge aerodynamics/Copenhagen/10-13 May 1998, Larsen, A. (Ed.) and Esdahl, S. (Ed). Balkema, Rotterdam 1998, pp. 59...85.
41. KATSUCHI, H., JONES, N. P. and SCANLAN, R. H., Multimode coupled flutter and buffeting analysis of the Akashi-Kaikyo Bridge. *Journal of Structural Engineering*, **125**(1999)1, pp. 60...70.
42. KÁRMÁN, T., VON and RUBACH, H., Über den Mechanismus des Flüssigkeits- und Luftwiderstandes. *Physikalische Zeitschrift*, **15**(1912)2, pp. 49...59.
43. KAWATANI, M., KIM, H., UEJIMA, H. and KOBAYASHI, H., Effects of turbulent flows on vortex-induced oscillation of bridge girders with basic sections. *Journal of Wind Engineering and Industrial Aerodynamics*. **41-44**(1992)1-3, pp. 477...486.
44. KIVILUOMA, R., Pitkän jännevälin sillan aeroelastinen stabiilius [Aeroelastic stability of long-span bridges]. Lic.Tech. thesis, Helsinki University of Technology, Otaniemi 1996, 120 p. (in Finnish).
45. KIVILUOMA, R., Coupled-mode buffeting and flutter analysis of bridges. *Computers and Structures*, **70**(1998)2, pp. 219-228.
46. KIVILUOMA, R., Raippaluodon sillan tuuli- ja värähtelymittaukset [Wind and vibration measurements of the Raippaluoto Bridge]. Research report for the Vaasa District. Finnish National Road Administration, Helsinki 1999, 51 p (in Finnish, unpublished).
47. KWOK, K. C. S. and MELBOURNE, W. H., Freestream turbulence effects on galloping. *Journal of the Engineering Mechanics Division*, **106**(1980)2, ASCE, pp. 273...288.
48. LANGHAARD, H. L., Dimensional analysis and theory of models. Robert E. Krieger Publishing Company, Florida 1983, Printed orig. 1951, John Wiley & Sons, 166 p.
49. LAWSON, T. V., Wind effects on buildings, volume 2, statistics and meteorology. Applied Science Publishers Ltd, London 1980, 155 p.
50. LI, Q. C. and LIN, Y. K., New stochastic theory for bridge stability in turbulent flow II. *Journal of Engineering Mechanics*, **121**(1995)1, ASCE, pp. 102...116.
51. LIEPMANN, H. W., On the application of statistical concepts to the buffeting problem. *Journal of the Aeronautical Sciences*, **19**(1952)12, pp. 793...800.
52. LIN, Y. K., Motion of suspension bridges in turbulence winds. *Journal of the Engineering Mechanics Division*, **105**(1979)6, pp. 1...15.
53. LIN, Y. K. and YANG, J. N., Multimode bridge resonse to wind excitations. *Journal of Engineering Mechanics*, **109**(1983)2, ASCE, pp. 586...603.
54. LIN, Y. K. and LI, Q. C., New stochastic theory for bridge stability in turbulent flow. *Journal of Engineering Mechanics*, **119**(1992)7, pp. 113...127.
55. MANN, J., KRISTENSEN, L. and JENSEN, N. O., Uncertainties of extreme winds, spectra, and coherences. Proc. of the international symposium on advances in bridge aerodynamics/Copenhagen/10-13 May 1998, Larsen, A. (Ed.) and Esdahl, S. (Ed). Balkema, Rotterdam 1998, pp. 49...56.
56. MATSUMOTO, M., SHIRAISHI, N., SHIRATO, H., STOYANOFF, S. and YAGI, T., Mechanism of, and turbulence effect on vortex-induced oscillations for bridge box girders. *Journal of Wind Engineering and Industrial Aerodynamics*. **49**(1993)1-3, pp. 467...476.
57. NAKAMURA, Y. and MIZOTA, T., Unsteady lifts and wakes of oscillating rectangular prisms.

Journal of the Engineering Mechanics Division, **101**(1975)6, ASCE, pp. 855...871.
58. NAKAMURA, Y. and OHYA, Y., The effects of turbulence on the mean flow past two-dimensional rectangular cylinders. *Journal of Fluid Mechanics*, **149**(1984) December, pp. 255...283.
59. NAKAMURA, Y. and NAKASHIMA, M., Vortex excitation of prism with elongated rectangular, H and ⊦ cross-sections. *Journal of Fluid Mechanics*, **163**(1986), pp. 149...169.
60. NAKAMURA, Y., Bluff body aerodynamics and turbulence. *Journal of Wind Engineering and Industrial Aerodynamics*, **49**(1993)1-3, pp. 65...78.
61. NAMINI, A., ALBRECHT, P. and BOSCH, H., Finite element-based flutter analysis of cable-suspended bridges. *Journal of Structural Engineering*, **118**(1992)6, ASCE, pp. 1509...1525.
62. NOVAK, M., Aeroelastic galloping of prismatic bodies. *Journal of the Engineering Mechanics Division*, **95**(1969)1, ASCE, pp. 115...142.
63. NOVAK, M. and DAVENPORT, A. G., Aeroelastic instability of prism in turbulent flow. *Journal of the Engineering Mechanics Division*, **96**(1970)1, ASCE, pp. 17...39.
64. NOVAK, M., Galloping oscillations of prismatic bodies. *Journal of the Mechanics Division*, **98**(1972)1, ASCE, pp. 27...46.
65. NOVAK, M. and TANAKA, H., Effect of turbulence on galloping instability. *Journal of the Engineering Mechanics Division*, **100**(1974)1, ASCE, pp. 27...47.
66. OKAUCHI, I., TAJIMA, J. and AKIYAMA, H., Response of the large scale bridge model to natural wind. Wind engineering; proceedings of the fifth international conference, Fort Collins, Colorado, USA, July 1979, Volume 2. Cermak, J. E. (Ed.), Pergamon Press, Oxford, pp. 841...852.
67. PARKINSON, G. V. and BROOKS, N. P. H., On the aeroelastic instability of bluff cylinders. *Journal of Applied Mechanics*, **28**(1961), Transactions of the ASME series E, pp. 252...258.
68. PARKINSON, G. V. and SMITH, J. D., The square prism as an aeroelastic non-linear oscillator. *Quarterly Journal of Mechanics and Applied Mathematics*, Vol. XVII, Pt. 2. (1964), pp. 225...239.
69. PFEIL, M. G. and BATISTA, R. L., Aerodynamic stability analysis of cable-stayed bridges. *Journal of Structural Engineering*, **121**(1995)12, ASCE, pp. 1784...1788.
70. RAMBERG, S. E. and GRIFFIN, O. M., Velocity correlation and vortex spacing in the wake of a vibrating cable. *Journal of Fluids Engineering*, March 1976, Transactions of the ASME Series I, pp. 10...17.
71. REINDOLD, T. A., BRINCH, M. and DAMSGAARD, A., Wind tunnel tests of the Great Belt Bridge. Aerodynamics of large bridges, Proc. of the first international symposium on aerodynamics of large bridges, Copenhagen, Denmark, February 1992, Larsen. A. (Ed.), Balkema, Rotterdam 1992, pp. 225...267.
72. ROSHKO, A., On the wake and drag of bluff bodies. *Journal of the Aeronautical Science*, **22**(1955)2, pp. 124...132.
73. SABZEVARI, A. and SCANLAN, R. H., Aerodynamic instability of suspension bridges. *Journal of the American Society of Civil Engineers*, **94**(1968)2, ASCE, pp. 489...519.
74. SABZEVARI, A. and SCANLAN, R. H., Aerodynamic investigations of the box-girder bridges. *Journal of the Structural Division*, **95**(1969)7, ASCE, pp. 1517...1532.
75. SALLET, D. W., The lift and drag due to von Kármán vortex wake. *Journal of Hydronautics*, **7**(1973)4, pp. 161...165.
76. SARKAR, P. P., JONES, N. P. and SCANLAN, R. H., Identification of aeroelastic parameters of flexible bridges. *Journal of Engineering Mechanics*, **120**(1994)8, ASCE, pp. 1718...1742.
77. SARPKAYA, T., Vortex-induced oscillations; a selective review. *Journal of Applied Mechanics*, **46**(1979)2, ASME, pp. 241...258.

78. SCANLAN, R. H. and TOMKO, J. J., Airfoil and bridge flutter derivatives. *Journal of Engineering mechanics Division*, **97**(1971)6, ASCE, pp. 1717...1737.
79. SCANLAN, R. H., BÉLIVEAU, J. G. and BUDLONG, K. S., Indicial aerodynamic functions for bridge decks. *Journal of the Engineering Mechanics Division*, **100**(1974)4, ASCE, pp. 657...672.
80. SCANLAN, R. H. and LIN, W. H., Effects on turbulence in bridge futter derivatives. *Journal of the Engineering Mechanics Division*, **104**(1978)4, ASCE, pp. 719...733.
81. SCANLAN, R. H., The action of flexible bridges under wind, I: flutter theory & II: buffeting theory. *Journal of Sound and Vibration*, **60**(1978)2, pp. 187..199 & 201...211.
82. SCANLAN, R. H., State-of-the-art methods for calculating flutter, vortex-induced, and buffeting response of bridge structures. Report No. FHWA/RD-80/050, Federal Highway Administration, Offices of Research & Development Structures and Applied Mechanics Division, Washington, D. C. 1981, 108 p.
83. SCANLAN, R. H., Developments in low-speed aeroelasticity in the civil engineering field. *AIAA Journal*, **20**(1982)6, AIAA, pp. 839...844.
84. SCANLAN, R. H., Role of indicial functions in buffeting analysis of bridges. *Journal of Structural Engineering*, **110**(1984)7, ASCE, pp. 1433...1446.
85. SCANLAN, R. H., Interpreting aeroelastic models of cable-stayed bridges. *Journal of Engineering Mechanics*, **113**(1987)4, ASCE, pp. 555...575.
86. SCANLAN, R. H. and JONES, N. P., Aeroelastic analysis of cable-stayed bridges. *Journal of Structural Engineering*, **116**(1990)2, ASCE, s. 279...297.
87. SCANLAN, R. H., Bridge buffeting by skew winds in erection stage. *Journal of Engineering Mechanics*, **119**(1992)2, ASCE, pp. 251...269.
88. SCANLAN, R. H., Problematics in formulation of wind force models for bridge decks. *Journal of Engineering Mechanics*, **119**(1993)7, ASCE, pp. 1353...1373.
89. SCANLAN, R. H., Amplitude and turbulence effects on bridge flutter derivatives. *Journal of Structural Engineering*, **123**(1997)2, ASCE, pp. 232...236.
90. SCANLAN, R. H., Bridge flutter derivatives at vortex lock-in. *Journal of the Structural Engineering*, **124**(1998)4, ASCE, pp. 450...458.
91. SCRUTON, C. and FLINT, A. R., Wind-excited oscillations of structures. *Proceedings Institution of Civil Engineers*, **27**(1964), pp. 673...702.
92. SCRUTON, C., An experimental investigation of the aerodynamic stability of suspension bridges with special reference to the proposed Severn Bridge. *Proceedings Institution of Civil Engineers*, part I, March 1952, pp. 189...222.
93. SHINOZUKA, M., IMAI, H., ENAMI, Y. and TAKEMURA, K., Identification of aerodynamic characteristics of suspension bridge based on field data. Stochastic problems in dynamics, Clarkson, B. E. (Ed.), Pitman 1977, pp. 214...236.
94. SHIRAISHI, N, and MATSUMOTO, M., On classification of vortex-induced oscillations and its application to bridge structures. *Journal of Wind Engineering and Industrial Aerodynamics*, **14**(1938)1-3, pp. 419...430.
95. SIMIU, E. and SCANLAN, R. H., Wind effects on structures: an introduction to wind engineering, 2nd Edit. John Wiley & Sons, NewYork 1986, 589 p.
96. STROUHAL, V., Ueber eine besondere Art der Tonerregung. *Annalen der Physik und Chemie*, (1878), pp. 216...251.
97. Tables of indefinite integrals. BOIS, G. P. (Ed.), Dower Publications, inc., New York 1961, 150 p.
98. TANAKA, H. T. and DAVENPORT, A. G., Response of taut strip models to turbulent wind. *Journal of the Engineering Mechanics Division*, **108**(1982)1, ASCE, pp. 33...49.
99. TANAKA, H., LAROSE, G. L. and KIMURA, K., Aerodynamics of long-span bridges during

erection. Proc. of the international symposium on advances in bridge aerodynamics/Copenhagen/10-13 May 1998, Larsen, A. (Ed.) and Esdahl, S. (Ed). Balkema, Rotterdam 1998, pp. 119...127.

100. THEODORSEN, T., General theory of aerodynamic instability and the mechanism of flutter. NACA Technical Report 496, Aeronautics; Twentieth Annual Report of the National Advisory Committee for Aeronautics 1934, NACA 1935, pp. 413...433.
101. TOEBES, G. H., The unsteady flow and wake near an oscillating cylinder. *Journal of Basic Engineering*, **91**(1969)3, Transactions of the ASME Series D, pp. 493...502.
102. VICKERY, B. J. and CLARK, A. W., Lift or across-wind response of tapered stacks. *Journal of the Structural Division*, **92**(1972)1, pp. 1...20.
103. VICKERY, B. J. and BASU, R. I., Across-wind vibrations of structures of circular cross-section. Part I. Development of a mathematical model for two-dimensional conditions. *Journal of Wind Engineering and Industrial Aerodynamics*, **12**(1983)1, pp. 49...73.
104. WALL, F. J. and BUCHER, C. G., Probabilistic description of buffeting response of long-span bridges. I: basic concepts & II: extended analysis. *Journal of Engineering Mechanics*, **118**(1991)12, ASCE, pp. 2401...2420 & 2421...2441.
105. WALSHE, D. E., A résumé of the aerodynamic investigations for the Forth Road and the Severn Bridges. *Proceedings Institution of Civil Engineers*, **37**(1967), pp. 87...108.
106. WILKINSON, R. H., Fluctuation pressures on an oscillating square prism, part II: spanwise correlation and loading. *The Aeronautical Quarterly*, **32**(1981)2, pp. 111...125.
107. WOOTTON, L. R., The oscillations of large circular stacks in wind. *Proceedings Institution of Civil Engineers*, **43**(1969), pp. 573...598.
108. Wind effects on the Raippaluoto Bridge, Finland, in-service and construction stage tests, (confidential) report no. DMI 93165.01. Rev. B, Larose, G. L. (Aut.), Dannish Maritime Institute 1994, 95 p.
109. Wind tunnel tests of Kärkistensalmi Bridge, (confidential) research reports no. 941, 942 and 943. Helsinki University of Technology, Laboratory of Bridge Engineering, Otaniemi 1994, total 91 p.

Appendix A Correction for load lumping error due to imperfect spanwise correlation

If an uniformly distributed load with the imperfect spanwise correlation is lumped to typical node of a finite element model, a considerable error can occur. In general, this happens, if a nodal spacing is large in comparison to the decay characteristics of the associated correlation function. In most models related to buffeting, the decay is rapid at low wind velocities and at high frequencies necessitating special care in these cases.

By considering line-like structural member, the uncorrected spectral density, owing to two nodes A and B, can be given as

$$\tilde{S} = \iint \sqrt{S_A S_B}\; R(s_A - s_B)\; ds_A\, ds_B \approx \sqrt{S_A S_B}\; l_A\, l_B\; R(s_A - s_B)\;, \qquad \textbf{(A1)}$$

where S_i ($i = A$ or B) is the load spectral density per unit length, $R(s_A - s_B)$ is the normalized covariance function for the spanwise separation and the notation of *Fig. A1* is applied. Here, the integration is carried out "over the structure", i.e. over the interference lengths l_i.

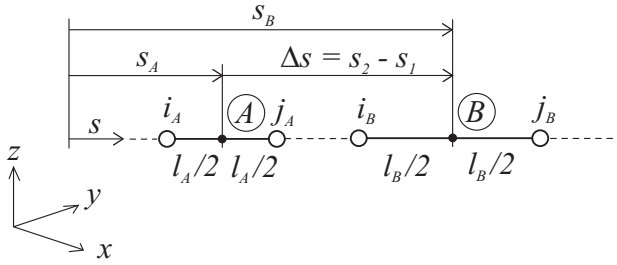

Fig. A1 Coordinate system for two nodes A and B having the spanwise separation Δs.

The approximation in Eq. (A1) implies the condition that nodal-loads are fully correlated along their interference lengths. To account for the imperfect correlation, the double integral of Eq. (A1) is divided into the components

$$\begin{cases} S \equiv S_{AA} + S_{BB} + S_{AB} + S_{BA} \\ S_{AA} = \int_{i_A}^{j_A}\int_{i_A}^{j_A} S_A e^{-c_{Eq}|r_1 - r_2|} dr_1 dr_2 \\ S_{BB} = \int_{i_B}^{j_B}\int_{i_B}^{j_B} S_B e^{-c_{Eq}|r_1 - r_2|} dr_1 dr_2 \\ S_{AB} = \int_{i_B}^{j_B}\int_{i_A}^{j_A} \sqrt{S_A S_B}\; e^{-c_{Eq}(r_2 - r_1)} dr_1 dr_2 \\ S_{BA} = \int_{i_B}^{j_B}\int_{i_A}^{j_A} \sqrt{S_A S_B}\; e^{c_{Eq}(r_1 - r_2)} dr_1 dr_2\;, \end{cases} \qquad \textbf{(A2)}$$

in which S is the corrected value of spectral density. Here, the normalized covariance function is approximated by means of the equivalent exponential covariance function as

$$R(s_A - s_B) \approx e^{-c_{Eq}|s_A - s_B|} , \qquad \textbf{(A3)}$$

where c_{Eq} is the equivalent decay coefficient. The solution for the first two components of Eqs (A2) has been given elsewhere [86] by

$$\begin{cases} S_{ii} \equiv S_i l_i^2 J_{ii} \\ J_{ii} \equiv \dfrac{2}{(c_{Eq} l_i)^2} \left(c_{Eq} l_i - 1 + e^{-c_{Eq} l_i} \right) , \qquad (i = A \text{ or } B) , \end{cases} \qquad \textbf{(A4)}$$

where J_{ii} is non-dimensional quantity accounting the imperfect load correlation (*Fig. A2*). The solution for the last two components can be obtained through elementary integration to yield

$$\begin{cases} S_{AB} = S_{BA} = \sqrt{S_A S_B}\, l_A l_B e^{-c_{Eq}|\Delta s|} J_{AB} \approx \sqrt{S_A S_B}\, l_A l_B R(s_A - s_B)\, J_{AB} \\ J_{AB} \equiv - \dfrac{e^{\frac{c_{Eq}(l_B - l_A)}{2}}}{c_{Eq}^2 l_A l_B} (e^{c_{Eq} l_A} - 1)(e^{-c_{Eq} l_B} - 1) . \end{cases} \qquad \textbf{(A5)}$$

Alternating schemes can be applied to derive relations for the equivalent decay coefficients. In the present study the equivalent decay coefficient is calculated as

$$c_{Eq} = - \frac{\ln R(s_A - s_B)}{|\Delta s|} . \qquad \textbf{(A6)}$$

Furthermore, when using Eqs (A4), the equivalent decay coefficient is calculated for unit separation. For a typical bridge span parallel to y-axis and coherence function given by Eq. (44), the exact value of the equivalent decay coefficient is given as $c_{Eq} = n\, c_y / U$, in which U is the reference wind speed associated with the coherence model. It can be noted that there is an obvious application for Eqs (A4) in section model experiments, if one is inspecting the effect of spanwise correlation to quantities like the RMS exciting coefficients or the normalized spectral densities.

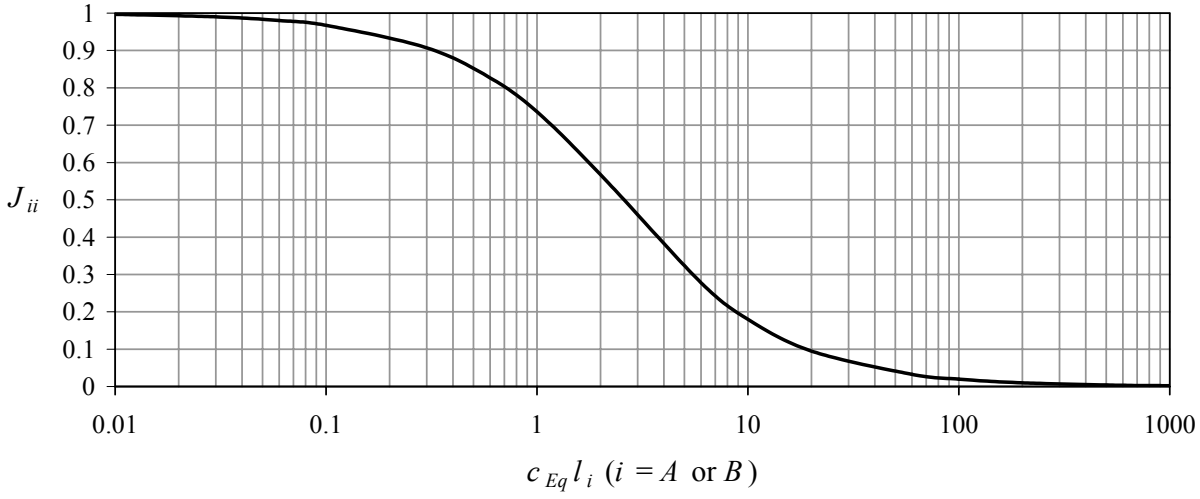

Fig. A2 The correction factor J_{ii} as function of dimensionless parameter $c_{Eq} l_i$.

Appendix B On-site measurements: signal filtering and postprocessing details

B.1 Turbulence characteristics

The Vaisala WAA15A cup anemometer used, generates digital voltage pulses with the rate proportional to the wind speed. These digital waveforms were sampled with the 1 kHz sampling frequency and converted to wind velocities by a computer code simulating a frequency counter. This allowed conversation to be done with mutually any averaging time. The turbulence intensities and mean wind velocities were based on 1 s (1 Hz) averaging while spectral densities were based on 0.2 s (5 Hz) averaging. Spectral densities were deduced by the following procedure:

- Spectrums for each 10 min samples containing 3000 numbers were prepared by the FFT-technique applying the array length of 2^{12}.
- Each spectrum was smoothed through the moving average of 3 adjacent spectrum values.
- The spectrums belonging to the same mean wind speed and direction regimes were averaged together. Number of spectrums corresponds to those given for turbulence intensities in *Table 4*.

The rough estimates for the integral length scales were obtained by normalizing the individual spectrums by variance and then averaging the spectrums belonging to the same wind direction regime. The estimate was then calculated from the resulting spectrum via Eq. (39). It can be noted that the auto-correlation functions were not needed or applied in the analysis.

B.2 Displacement measurements

The following filtering was conducted with the NOPTEL PSM90 laser optical device and the softwares:

- The receiver samples the channels containing horizontal and vertical displacement readings at the rate of 0.5 kHz.
- The data acquisition software averages 10 adjacent readings before recording them in a file. The sampling rate in the recorded data was approximately 50 Hz.
- 10 min recording periods were isolated from the data to match the sampling intervals of acceleration and wind speed data.
- The standard deviations were extracted from the time-scale data. Prior to this extraction, the moving averaging of 10 adjacent numbers was carried out. The recording periods containing vibrations caused by heavy vehicles passing the bridge were omitted.
- Each spectrum for ambient vibration study was prepared by the FFT-technique applying the unfiltered time-scale data. The array length involved was 2^{16} resulting the resolution of 0.0007 Hz.
- Each spectrum was soothed by taking the moving average of 3 adjacent spectrum values.
- Each spectrum was normalized to have the maximum value of unity. The resulting spectrums were averaged.

The displacement-based ambient vibration study results are shown only for the Kärkinen Bridge (*Fig. 28*). The resulting spectrum comprises data for 20 min (= 2 samples) recording period.

B.3 Acceleration measurements

The following filtering was applied for the acceleration signals:

- The analog first-order bandpass filtering with 3 dB attenuation points at 0.1 Hz and 2.1 kHz was conducted before sampling the signals.
- The analog-to-digital converter sampled three channels used (two acceleration signals & one anemometer signal) with the sampling rate approximately of 33 kHz per channel. The converter was programmed to take the average of 33 adjacent values before recording the data in the file with the sampling frequency of 1 kHz. One sample contained 600000 numbers per channel associated with the 10 min recording period.
- For time-scale responses, the digital ideal filtering involving the FFT-technique was applied to the sampled signals with the exact cutoff frequencies at 0.2 Hz and 5 Hz. The primary purpose of this filtering was to remove the low-frequency noise.
- The standard deviations were extracted by means of the time-scale data. The recording periods containing vibrations due to the heavy vehicles passing the bridge were omitted.
- Each spectrum for the ambient vibration study was prepared by the FFT-technique applying the unfiltered time-scale data. The array length invoked was 2^{20} resulting the resolution of 0.0009 Hz.
- Each spectrum was smoothed by taking the moving average of 3 adjacent spectrum values.
- Each spectrum was normalized to have the maximum value of unity. The resulting spectrums were averaged.

The acceleration-based ambient vibration study results are shown only for the Raippaluoto Bridge (*Fig. 28*). The resulting spectrum comprises data for the 80 min recording period (= 8 samples). Here, only the samples associated with the sufficient excitation of the bridge are chosen for the study. Through the resulting spectrum, the rough estimates of modal damping ratios are obtained by the half-power bandwidth method, i.e. with the formula $\zeta_i + \zeta_{Ai} = 0.5\Delta n/n_i$, in which Δn is the width of the mode related resonance peak at the half level of the peak height.